The Turbulent Jet in the Scale-Relativity Framework

Laurent Nottale, Thierry Lehner

The Turbulent Jet in the Scale-Relativity Framework

Laurent Nottale and Thierry Lehner
Laboratoire Univers et Théories, Observatoire de Paris
Université PSL, Université Paris Cité, CNRS
F-92195 Meudon Cedex, France

November 6, 2023

Abstract

We apply the scale-relativity theory of turbulence to the turbulent round jet problem. In this theory, the time derivative of the Navier-Stokes equations is integrated under the form of a macroscopic Schrödinger equation acting in velocity-space. In this equation, the constant $\hbar_v$ can be identified with the energy dissipation rate while the effect of pressure gradient manifests itself as an quantum harmonic oscillator (QHO) v-potential. This equation is solved in terms of a wave function whose modulus squared yields the probability density function (PDF) of velocities. The Reynolds stresses can then be derived from this PDF, so that the closure problem is solved in this case. This allows us to obtain a theoretical prediction for the turbulent intensity radial profile (and therefore for the pressure) which agrees with the experimental data. We also theoretically predict various purely numerical dimensionless invariants characterizing the turbulent jet. The ratio of axial over radial velocity fluctuations can be calculated from QHO properties: we find $R = 1.35 \pm 0.03$, in good agreement with its experimental values $1.3 - 1.4$; the jet opening parameter is predicted to be $\alpha = 1/2R^3 = 0.203 \pm 0.013$, which explains its well-known value $\alpha \approx 1/5$ observed in both laboratory and numerical experiments; the mean ratio $X = \sqrt{\mu\,\lambda}$, (where μ and λ are respectively the radial and axial ratios of turbulent intensity amplitudes over axial velocity on the jet centerline), is predicted to be $X = 19/80 = 0.2375 \pm 0.0013$, in good agreement with its universally measured value $\approx 1/4$; from X and R we derive $\mu = 0.202 \pm 0.013$, which agrees with the experimentally observed values $0.185 - 0.217$; finally, the correlation coefficient of velocities is predicted to be $\rho \approx 2\,\alpha = 1/R^3$, thus suggesting an explanation for the universal value ≈ 0.4 observed for the turbulent jet and for all free shear flows.

1 Introduction

Few turbulent flows have received more experimental and theoretical study than the simple free jet [1]. This is justified by its wide occurrence in nature and in many practical

applications, e.g., related to combustion, propulsion, mixing, and aeroacoustic. A jet is also important from a physical point of view because it represents a prototype of free turbulent flow. For these reasons it is frequently studied and modeled. The round jet shares also many common features with other free shear flows, such as plane jets, wakes and mixing layers. This both practical and fundamental importance of round jets is made clear by the large number of publications and reviews that have appeared on it (see e.g. [2, 3, 4] and references therein), involving either experimental, theoretical or numerical analysis [5, 6]. However, as remarked by Hussein et al [7], "the difficulties of predicting this flow with model constants determined from other flows has proved to be one of the more challenging problems faced by turbulence modellers".

Laboratory investigations of jets penetrating into a quiescent fluid of the same density consistently reveal that the envelope containing the turbulence caused by the jet adopts a nearly conical shape. In other words, the radius r of the jet is proportional to the distance x downstream from the discharge location [8].

When the jet remains laminar, as described by the Landau jet [9, p.115], which is an exact solution of the Navier-Stokes (NS) and continuity equations, [10, 11, 12], its opening angle decreases when the Reynolds number increases according to the jet strength.

But the turbulent jet is different and manifests one of the most puzzling mysteries of physics: laboratory observations reveal that its opening angle, although a dimensionless number, remains almost the same regardless of the nature of the fluid, of the orifice diameter and of the injection speed, (and therefore finally of the Reynolds number). As written by Landau about the turbulent round jet [9, p. 213], "the region of turbulence is a cone, the angle of which 2α is, *according to experimental data*, equal to about 25°". He adds [9, p. 217]: "The empirical value of the opening angle of a plane jet is close to that of the circular jet ($2\alpha = 25°$)". The corresponding value in rd is $\alpha_S = 0.218$ and its tangent $\eta_{\alpha_s} = r/x = 0.222$. As we shall see, this definition of $\alpha = \alpha_S$ from the spatial extension of the jet (i.e. from the turbulent-laminar transition) can be completed by a complementary definition from the edge of the axial velocity profile along the radial direction, fitted to $\alpha \approx 0.2$ (the ratio of the two definitions being $\alpha_S/\alpha = q \approx 1.1$). The puzzle is still there today, since there is, to our knowledge, no known analytical theoretical prediction for this value $\alpha \approx 0.2$.

The mystery of the turbulent jet is re-inforced by the existence of other quasi-universal structures such as the turbulent velocity radial profiles, and of dimensionless constants, such as the ratio $R \approx 1.3$ between the axial and radial turbulent intensities, the ratio $\approx 1/4$ of the standard deviations of the turbulent velocity fluctuations over the axial mean velocity on the centerline of the jet, and the correlation coefficient between the axial and radial velocity fluctuations $\rho \approx 0.4$ (a value which is common to all free shear flows [3, 2]). It is noticeable that these structures may not be universal in the sense of precise and unique numerical values [13], but as PDFs with well-defined peaks and small standard deviations, and/or narrow intervals of possible values. As we shall see, the solutions suggested in the present paper for their origin lead to just this kind of behavior.

The dimensionless character of this universal physical constant, $\alpha \approx 1/5$, makes the understanding of its value one of the most fascinating problems in physics. Moreover,

this question is clearly related to a more general problem in the theory of turbulence, namely, the closure problem: when jumping to a turbulent behavior, a fluid is described not only by its mean velocities which are solutions of the continuity and Navier-Stokes equations, but also by the velocity fluctuations. In today's theory there are no known first principle equations for the covariances of these fluctuations (Reynolds stress), which yet appear in the Reynolds-averaged Navier-Stokes (RANS) equations, so that the number of unknowns is larger than the number of equations. The closure is therefore obtained only using hypothetical models.

The scale-relativity approach to turbulence [14, 15, 16] is of a different nature. In its framework, the closing equations do not come from an assumed model. They just derive from a reformulation and an integration of the time derivative of the Navier-Stokes equations themselves, written in v-space and accounting for the non-differentiable and fractal nature of velocities in the turbulent regime (according to Kolmogorov K41 scaling). The main result of this approach is that these v-space NS-derivated (NSd) equations can be integrated under the form of a macroscopic Schrödinger equation [17, 18, 16].

Moreover, the potential entering this v-Schrödinger equation is, in an universal way, that of an harmonic oscillator, so that we can theoretically predict that the local velocity probability density functions (PDF) are that of quantized harmonic oscillators (QHO), possibly damped (QDHO). This theoretical expectation is well verified by experimental data analysis [16].

As a consequence, we can derive the PDF of the turbulent velocity fluctuations in terms of a combination of the PDFs of ground state and excited state QHOs, the probability distribution of their quantum numbers being given by statistical physics.

In the present paper, we first recall the various structures which are already accounted for by the current theory (RANS equations):

- self-similar scaling in terms of the variable traditionally denoted $\eta = r/x$, where r is the radial cylindrical coordinate and x the axial coordinate, with origin at the virtual top of the jet conic shape;
- profiles of the average velocities $U(x, \eta)$ and $V(x, \eta)$;
- profile of the Reynolds shear stress σ_{uv} (approximate, in integral form);
- relation between mean pressure and radial Reynolds stress: $\bar{p} = -\sigma_v^2$ (approximate).

Then we bring improvements to some of these results, by getting exact solutions to the RANS equations:

- more precise radial profiles $U(\eta)$ and $V(\eta)$;
- new scaling relation connecting the x and r derivatives;
- exact solution for the shear stress σ_{uv};
- exact relation between the mean pressure $\bar{p}$ and the radial Reynolds stress σ_v^2;
- theoretical prediction of the ratio $q = \alpha_S/\alpha$ between the spatial extent of the jet and its velocity extent.

In a second part of the paper, we briefly recall the principles which lead to integrating the time derivative of the NS equations into a macroscopic Schrödinger-type equation. Then we apply this equation to the case of the turbulent round jet, for an harmonic oscillator potential whose coefficients are given by r and x derivatives of the mean pressure.

This allows us to suggest new theoretical explanations for:

- the ratio of axial over radial turbulent intensities $R = \sigma_u/\sigma_v \approx 1.35$;
- the universal value of the jet opening parameter $\alpha = 1/2R^3 \approx 0.2$;
- the radial profile of the Reynolds stresses (and therefore of the mean pressure): we find an analytical solution given by $\sigma_v^2 = -p \propto \cos(\sqrt{3}\,\eta/\alpha)$ (plus a correction that fully agrees for the whole jet, including its boundary region);
- the constancy of the velocity correlation coefficient throughout the jet (except in its central region, where it is known to increase from zero to this constant value);
- the relative amplitude of the turbulent fluctuations, $\sqrt{\lambda\,\mu} = 19/80 \approx 1/4$);
- the value of the correlation coefficient, which we find equal to $\rho \approx 2\,\alpha = 1/R^3 \approx 0.4$, a value that is common to all shear flows [3].

2 Hydrodynamics equations for the turbulent jet

2.1 RANS equations

Let us write the velocities in cylindrical coordinates $(x,\, r,\, \theta)$ in terms of the Reynolds decomposition $U_t = U + u$, $V_t = V + v$ and $W_t = w$, where $U(x,r)$, $V(x,r)$, $W(x,r) = 0$ are their average values and u, v, w their turbulent fluctuations. The fluid mechanics equations for the turbulent jet consist of the continuity equation for the mean velocities,

$$\partial_x U + \frac{1}{r}\,\partial_r(r\,V) = 0, \tag{1}$$

of the continuity equation for the turbulent fluctuations,

$$\partial_x u + \frac{1}{r}\,\partial_r(r\,v) = 0, \tag{2}$$

and of the Reynolds averaged Navier-Stokes (RANS) equations.

One defines the Reynolds stresses as the variances and covariance of the fluctuating velocity components, $\langle u^2\rangle = \sigma_u^2$, $\langle v^2\rangle = \sigma_v^2$, $\langle w^2\rangle = \sigma_w^2$ and $\langle u\,v\rangle = \sigma_{uv}$. Experimental measurements from [19, 7] of the radial profiles of $\sigma_u(\eta)$ and $\sigma_v(\eta)$, where $\eta = r/x$, are shown in Fig. 2.

For any two velocities linked by the continuity equation (in particular $\{U, V\}$ and $\{u, v\}$), one has the transformation:

$$U\,\partial_x U + V\,\partial_r U = \partial_x\,U^2 + \frac{1}{r}\,\partial_r\,(rUV), \tag{3}$$

which allows to exhibit the energy and covariance terms. Neglecting the molecular viscosity contribution (which is vanishingly small with respect to the other terms in the turbulent case) and $\bar{p}$ being the mean pressure, this transformation allows one to write the RANS equations in cylindrical coordinates as [20, 21, 22]:

$$x-\text{RANS}: \quad U\,\partial_x U + V\,\partial_r U + \partial_x(\sigma_u^2 + \bar{p}) + \frac{1}{r}\,\partial_r(r\,\sigma_{uv}) = 0, \tag{4}$$

$$r-\text{RANS}: \quad U\,\partial_x V + V\,\partial_r V + \partial_r(\sigma_v^2+\bar{p}) - \frac{1}{r}(\sigma_v^2-\sigma_w^2) + \partial_x\sigma_{uv} = 0, \tag{5}$$

where we have set the fluid density $\varrho = 1$ for simplification owing to the incompressible character of the flow.

2.2 Exact solutions to the RANS equations for self-similar flows

2.2.1 Scaling relation

One of the main properties of the turbulent jet is its self-similar character [9, 2, 19, 7]. For the round jet, the velocities scale as $U = U_\eta(\eta)/x$, $V = V_\eta(\eta)/x$, $u = u_\eta(\eta)/x$, $v = v_\eta(\eta)/x$, and the pressure as $\bar{p} = \bar{p}_\eta(\eta)/x^2$, where x is the axial variable starting from the virtual origin of the conic shape of the jet and where the dimensionless radial variable is $\eta = r/x$.

This scaling allows one to relate the x and r partial derivatives, i.e., for a function $F(x,r) = f(\eta)/x^2$ one obtains:

$$x\,\partial_x F = -\frac{1}{r}\,\partial_r(r^2\,F). \tag{6}$$

This remarkable identity, since it applies for the round jet to U^2, V^2, σ_u^2, σ_v^2, σ_{uv} and $\bar{p}$, brings many simplifications to the equations and allows one to find explicit integral solutions.

2.2.2 Exact solution to the axial RANS equation

As regards the x-RANS equation, it can be integrated in a universal way thanks to this relation. Indeed, one finds that the x-RANS equation becomes proportional to the continuity equation, namely x-RANS$= -U\times$ CONT, and one obtains a solution which may be written in term of a general and exact expression for the shear stress:

$$\sigma_{uv} = -UV + \eta\,(U^2+\sigma_u^2+\bar{p}). \tag{7}$$

This is a new result to our knowledge, since up to now σ_{uv} was known only in a approximate way and in integral form.

2.2.3 Exact solution to the radial RANS equation

It is possible to also obtain an exact solution to the r-RANS equation. Such an exact solution may be useful in order to quantify more precisely the quality of this approximation and in situations which involve the first and second derivatives of the mean pressure (see hereafter), which may differ significantly from that of $-\sigma_v^2$.

This solution can be written under the form:

$$p = -\sigma_v^2 - V^2 - \varepsilon. \tag{8}$$

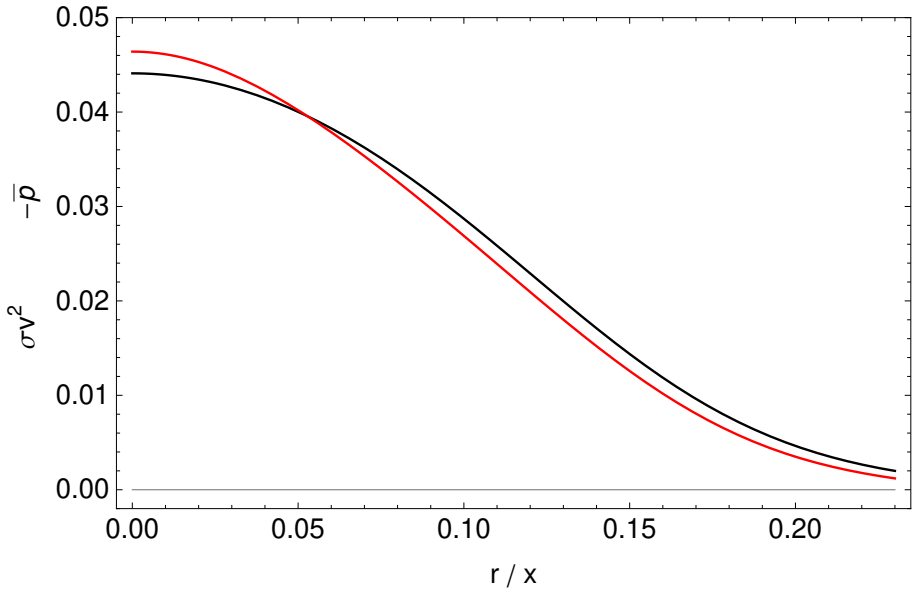

Figure 1: Exact solution to the r-RANS equation. Analytical expression for σ_v^2 (black curve) in function of the reduced radial distance $\eta = r/x$ to the jet centerline, compared with the exact pressure (red curve, $-p = \sigma_v^2 + V^2 + \varepsilon + c$), where ε is given by Eq. (12), here with the numerical constant $c = 0.002$.

We define, using the self-similarity of the velocities,

$$\mathcal{W} = (U^2 + \sigma_u^2) - (V^2 + \sigma_v^2) = \frac{\mathcal{W}_\eta}{x^2} = \frac{1}{x^2}\,(U_\eta^2 + \sigma_{u\eta}^2 - V_\eta^2 - \sigma_{v\eta}^2), \tag{9}$$

where $\sigma_{u\eta}$ and $\sigma_{v\eta}$ are respectively the radial parts of σ_u and σ_v (without their x dependance). Then we set

$$A(\eta) = \eta^2\,\partial_\eta \mathcal{W}_\eta + 3\,\eta\,\mathcal{W}_\eta - \frac{V_\eta^2}{\eta}. \tag{10}$$

We finds that $\varepsilon = \varepsilon_\eta / x^2$ is given by the simple differential equation:

$$(1-\eta^2)\,\partial_\eta \varepsilon_\eta - 3\,\eta\,\varepsilon + A(\eta) = 0. \tag{11}$$

This equation can finally be integrated to yield an exact solution of the r-RANS equation in function of the mean velocities and of the Reynolds stresses, that reads:

$$\varepsilon_\eta = \frac{1}{(1-\eta^2)^{3/2}} \left(c - \int A(\eta) \sqrt{1-\eta^2}\; d\eta \right), \tag{12}$$

It is defined only up to a numerical integration constant, as expected from the fact that only the pressure gradient has a physical meaning in the equations.

We show in Fig. 1 the effect of this correction to the approximate solution $p = -\sigma_v^2$ (radial part, without the x dependence). We find that, while it is vanishingly small as

regards its effect on σ_{uv}, its effect on the shape of the pressure is not totally negligible, in particular for the derivatives of the pressure (see Sec. 4.4). However, one should remark that this difference between $-p$ and σ_v^2 remains smaller than the differences observed between the various experimentally and numerically measured profiles (see Figs. 2 and 15).

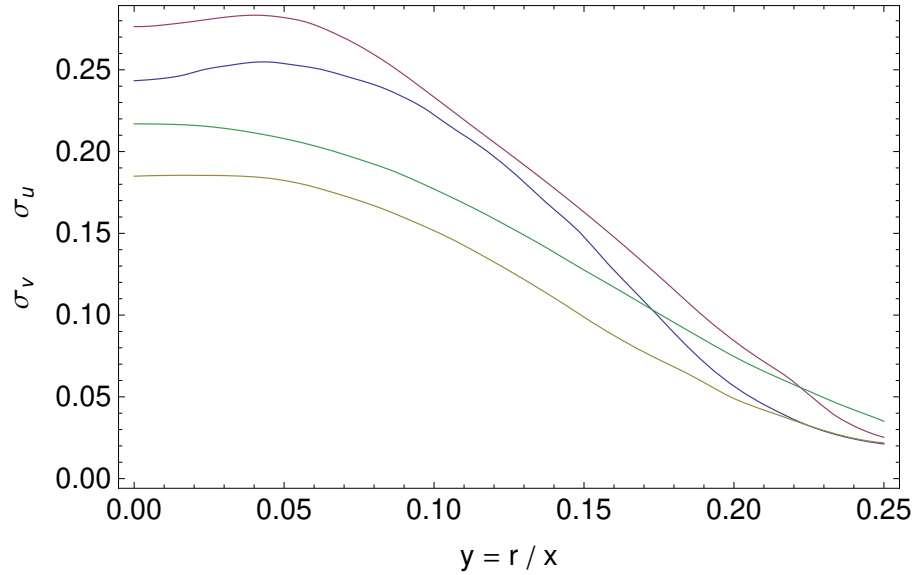

Figure 2: Experimentally observed standard deviations of turbulent velocity fluctuations ("turbulent intensities") in round jets, in function of the normalized radial distance to the jet centerline, $\eta = r/x$. Magenta top curve: σ_u from Panchapakesan and Lumley [19]; blue curve (second from top): σ_u from Hussein et al [7]; green curve (third from top): σ_v from [19]; brown down curve: σ_v from [7]. Laboratory and numerical experiments both show that the fluctuations become isotropic for $\eta > \approx 0.18$.

2.2.4 Boundary layer approximation

As regards the r-RANS equation, the usual approximate solution consists of neglecting the contributions $U\partial_x V + V\partial_r V$ and $\partial_x \sigma_{uv}$ and to account for the expectation $\sigma_v = \sigma_w$ for obtaining an expression for the mean pressure:

$$\bar{p} = -\sigma_v^2 + p_0(x), \tag{13}$$

where p_0 is the pressure at infinity and will be considered to vanish in what follows.

From this approximate solution, one obtains a new expression for σ_{uv} (no longer strictly exact):

$$\sigma_{uv} = -UV + \eta\,(U^2 + \sigma_u^2 - \sigma_v^2). \tag{14}$$

This relation can be simplified by accounting for the fact that $\sigma_u^2 - \sigma_v^2 \ll U^2$. Indeed, under the K41 hypothesis [23], the turbulence is expected to be locally isotropic, so that

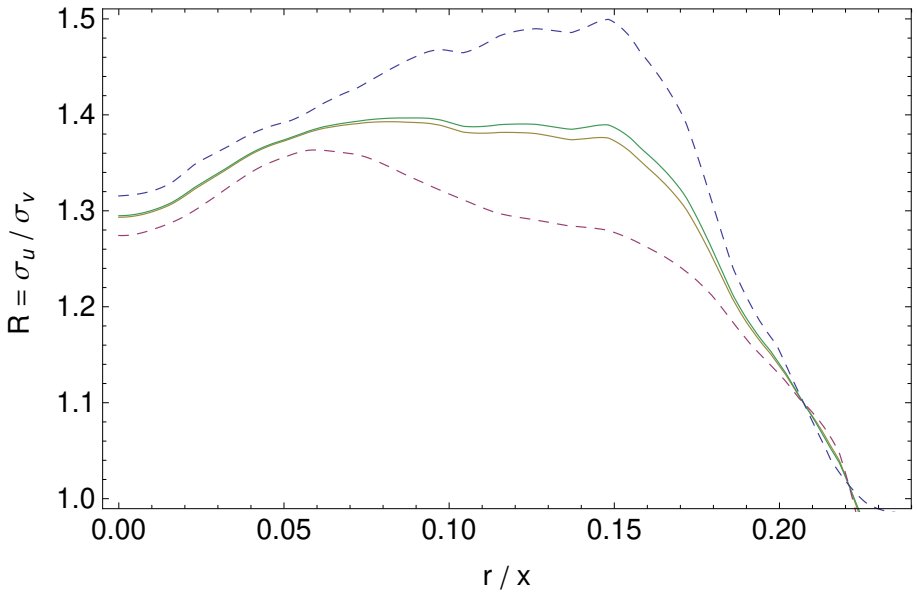

Figure 3: The experimentally observed ratio $R = \sigma_u/\sigma_v$ in function of the scaled radial distance, $\eta = r/x$. The green curve shows the mean R value $(R_H + R_P)/2$ from Hussein et al [7] and Panchapakesan and Lumley measurements [19], the beige curve shows $(\sigma_{uH} + \sigma_{uP})/(\sigma_{vH} + \sigma_{vP})$, while the dashed curves are the individual measurements (P: blue, H: magenta). They agree in the center of the jet and around its boundary while they show larger variations (± 0.1) in the middle region of the jet ($\eta = 0.06 - 0.18$).

$\sigma_u^2 \approx \sigma_v^2$. Experimental data on turbulent jets [19, 7, 2, 1, 24] confirm that they are of the same order, with $\sigma_u/\sigma_v = R \approx 1.3$ (only in one case [25], measurements have yielded exactly $\sigma_u^2 = \sigma_v^2$ inside the jet).

Tennekes and Lumley [3] argue that one expects $(\sigma_u^2 - \sigma_v^2)/(\sigma_u^2 + \sigma_v^2) = K$, where K is a constant independant from position. Their argument is that the major production term feeds energy along the axial direction, so that the energy must leak into v^2 by inertial interaction. The ratio of the supply rate to the leakage rate is expected to be constant because these two rates are determined by the same turbulence dynamics. As a consequence, the ratio $R = \sigma_u/\sigma_v$ should itself be constant. Experimental data are compatible with this result, yielding a constant of proportionality $K \approx 1/4$ in the interior of the jet (i.e. $R \approx 1.3$ as previoulsy stated, see Fig. 3), which falls abruptly to $K = 0$ at the jet boundary, i.e. $\sigma_u^2 = \sigma_v^2$ for $\eta = \alpha \approx 0.2$: this is expected from the fact that the turbulent fluctuations become far larger that the local mean velocities around the jet boundary, so that the K41 full isotropy becomes manifest.

Anyway, all experiments show that $U^2 >\approx 30(\sigma_u^2 - \sigma_v^2)$, thus supporting this approximation. One finally finds that the shear stress of the turbulent round jet can be expressed with a reasonable precision in terms of just the mean velocities:

$$\sigma_{uv} = \eta\, U^2 - UV. \tag{15}$$

Experimental data are in satisfying agreement with this relation (see Fig. 4).

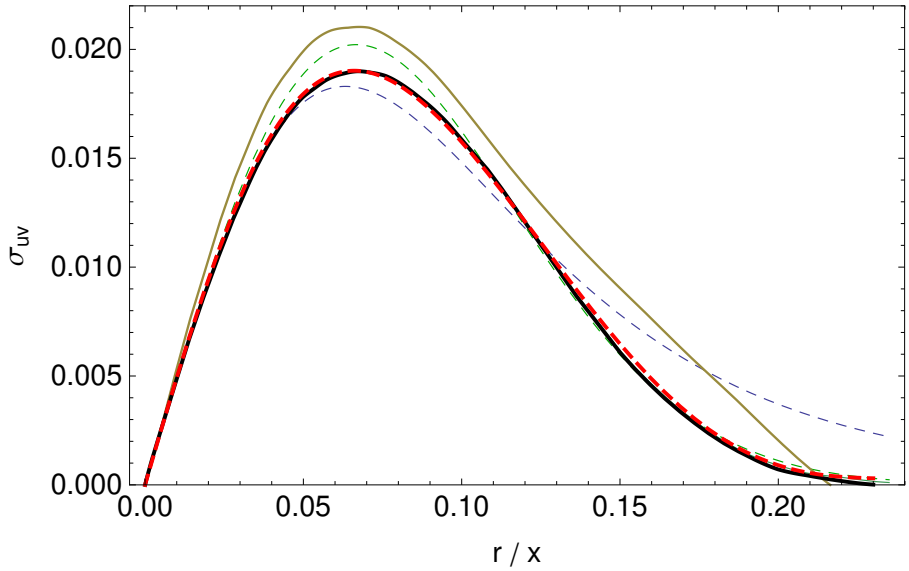

Figure 4: Comparison between experimental measurements of the Reynolds shear stress $\sigma_{uv} = \langle uv \rangle$ from Ref. [19] (black curve) and its theoretical expression, $\sigma_{uv} = U\,(\eta\,U - V)$ (Eq. (15), red dashed curve), in function of the normalized radial variable $\eta = r/x$. This last expression is calculated from a fit of U and V (where U was measured in the same experiment while V was deduced from the continuity equation [19]). The brown curve is the experimental measurement of Hussein et al [7]. The blue dashed curve is its expression for the constant turbulent viscosity solution, which is no longer valid at the edge of the jet. The green dashed curve is an exponential law $\frac{1}{2}\eta \exp[-\frac{1}{2}(\frac{\eta}{\alpha s})^2]$ for $\alpha = 0.2$ and $s = 1/3$.

2.3 Turbulent viscosity

The Boussinesq approach allows one to rely the Reynolds stress $\sigma_{uv} = \langle u\,v \rangle$ to the averaged axial velocity U by introducing a turbulent (or eddy) viscosity ν_T (see, e.g. [22],

$$\sigma_{uv} = -\nu_T\,\partial_r U. \tag{16}$$

Then the x-RANS equation takes the form:

$$U\,\partial_x U + V\,\partial_r U - \frac{1}{r}\,\partial_r(\nu_T\,r\,\partial_r U) = 0. \tag{17}$$

We see that, when ν_T is constant, this description allows indeed the shear stress to play a role similar to that of the molecular viscosity, since the RANS equation becomes

$$U\,\partial_x U + V\,\partial_r U - \nu_T\,\frac{1}{r}\,\partial_r(r\,\partial_r U) = 0. \tag{18}$$

Experimental data on turbulent jets fairly support such a description: the turbulent viscosity is found to remain almost constant in a large part of the jet, up to $\approx 60\%$ of its radius (see Fig. 6 and Sec. 3.1).

But it can also yield more general solutions of the RANS equations by allowing a varying turbulent viscosity. Thanks to our explicit integration of the shear stress Eq. (15), for any couple of velocities $\{U,\, V\}$, we know the turbulent viscosity which solves the NS equations:

$$\nu_T = \frac{U\,V - \eta\,U^2}{\partial_r U}. \tag{19}$$

It depends only on $\eta = r/x$ since the three functions $U\,V$, U^2 and $\partial_r U$ scale as x^{-2}.

This formula will be applied in what follows to deriving explicitly the turbulence viscosity from analytical expressions fitting the experimental data on jet velocities.

2.4 Deriving velocities from shear stress

Reversely, one can obtain new analytical solutions to the RANS equations from any expression fitting σ_{uv}. Let us set $\sigma_{uv}(\eta) = \eta\mathcal{F}(\eta)$. The velocities $U = (g/x)U_\eta$ and $V = (g/x)V_\eta$ are solutions of the continuity equation and of the above equation (15), which read (we make $g/x = 1$ in the full expressions in order to simplify, keeping only their η dependence):

$$(V + \eta\,\partial_\eta V) = \eta\,(U + \eta\,\partial_\eta U), \qquad \eta\,U^2 - UV = \eta\mathcal{F}(\eta). \tag{20}$$

After some calculations these two equations can be combined in terms of a differential equation for the function $\mathcal{G}(\eta) = (\mathcal{F}/U)^2$:

$$\partial_y \mathcal{G} = \frac{2}{\eta}\,(\mathcal{F} - 2\mathcal{G}). \tag{21}$$

Solving this differential equation for a given expression of $\mathcal{F}(\eta)$, one obtains $U = \mathcal{F}/\sqrt{\mathcal{G}}$ then $V = \eta(U - \mathcal{F}/U)$, from which one can also derive ν_T according to Eq. (19).

2.5 Deriving velocities from variable turbulent viscosity

It is also possible to derive the velocity profiles from a variable turbulent viscosity. We start from the expression of ν_T:

$$\nu_T = \frac{\sigma_{uv}}{\partial_r U} = \frac{U\,V - \eta\,U^2}{\partial_r U}. \tag{22}$$

Using the self-similarity we omit the x dependence of the various terms. We thus obtain a differential equation for U and V in function of the assumed known expression of $\nu_T = \nu_T(\eta)$:

$$\nu_T(\eta)\,\partial_\eta U + \eta\,U^2 - U\,V = 0. \tag{23}$$

It can be combined with the continuity equation, whose pure η form allows to connect the U and V profiles:

$$V + \partial_\eta V = \eta\,(U + \eta\,\partial_\eta U). \tag{24}$$

After some manipulations, we obtain a second order differential equation for U alone:

$$\eta\,\nu_T(\eta)\,(UU'' - U'^2) + [\nu_T(\eta) + \eta\,\partial_\eta \nu_T(\eta)]\,UU' + \eta\,U^3 = 0. \tag{25}$$

Once its solution is known, one can derive the v profile:

$$V = \eta\,U + \nu_T(\eta)\,\frac{\partial_\eta U}{U}. \tag{26}$$

A simplified form of the above differential equation can be obtained by keeping only the dominant terms, e.g. by suppressing the small contributions $\nu_T\,UU'$ and $\eta\,U^3$. Setting $G = \partial_\eta U/U$ and $F(\eta) = (\partial_\eta \nu_T)/\nu_T$, it writes:

$$\partial_\eta G + \eta F(\eta) G = 0. \tag{27}$$

A general solution is then found, which reads:

$$G = C_1 \exp \int -\eta F(\eta) d\eta, \quad U = C_2 \exp \int G(\eta) d\eta, \tag{28}$$

where C_1 and C_2 are integration constants.

In particular, this result can be applied around the jet edge, at the turbulent to laminar transition. Indeed, the axial velocity U is expected to become almost constant in the exterior laminar region [9], so that one expects $\partial_\eta U = 0$ at this transition. This implies a divergence of ν_T if σ_{uv} has itself not vanished.

Let us therefore look for the profile of the axial velocity derived from a linear turbulent velocity vanishing at the jet edge, $\nu_T(\eta) = b(\alpha_S - \eta)$. Such a behavior is supported by experimental data (see Fig. 6). In this case, the above solution can be explicitly integrated under the form:

$$U = A \exp[-B\Gamma(1 - \alpha_S, \alpha_S - \eta)], \tag{29}$$

where $\Gamma(a, x)$ is the incomplete Gamma function and A and B are integration constants which can be fixed from the values of U and its derivative at a given point. We have performed a numerical integration of the complete equation Eq. 25 and found it to be very close from this solution of the simplified equation (red curve in Fig. 5). The difference with a quadratic behavior remains small while the problem of divergence linked to $\partial_\eta U = 0$ is solved.

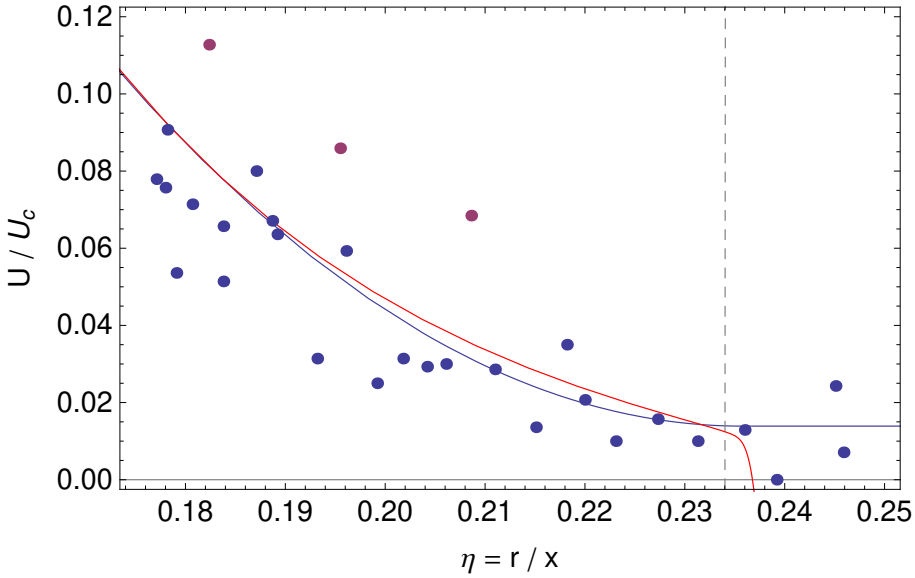

Figure 5: Radial profile of the mean axial velocity of a round turbulent jet around its edge. The points are experimental measurements [7, 19]. The blue curve is a quadratic solution matched to the laminar Landau solution at $\eta = \alpha_S = 0.235$. The red curve is the axial velocity derived from a linear turbulent viscosity vanishing at $\eta = \alpha_S$.

3 Solutions of the RANS equations for the turbulent round jet

3.1 Solution with constant turbulent viscosity in the central region

A first analytical approximation for the turbulent jet (which is solution of the RANS equations with constant turbulent viscosity and is valid in a large part of the inner region of the jet, $z = \eta/\alpha <\approx 0.6$), is given by the following expressions for the averaged velocities [26, 2]:

$$U = \frac{g}{x}\,\frac{1}{(1+\beta\,(\eta/\alpha)^2)^2}, \quad V = \frac{g}{x}\,\frac{\eta\,(1-\beta\,(\eta/\alpha)^2)}{2\,(1+\beta\,\eta/\alpha)^2)^2}, \tag{30}$$

where we recall that $\eta = r/x$.

A fit of experimental data by these expressions yields $\beta = 2$ with good precision at the origin: we find $\beta = 1.99 \pm 0.02$ from a fit of $U(z)$ for $z < 0.6$ (which is the limit of validity of this solution) using data from [19]. Values consistent with $\beta = 2$ are obtained with other sets of data [24, 7]. Actually, since β and α only appear together through their combination β/α^2 in these expressions, one is led to set $\beta = 2$ and to consider these velocity profiles as a definition of α. Recall that this parameter defines the radial extension of the jet in velocity space, and slightly differs from the jet opening angle in space which

can be defined as the turbulent-laminar transition, $\alpha_S = q\,\alpha$ with $q \approx 1.10 - 1.15$, see Sec. 3.2. A theoretical prediction for the value of this parameter will be obtained in what follows.

The constant g can be related to the jet velocity U_0 at the nozzle exit as

$$g = U_0\, a_0 = B\, U_0\, d, \tag{31}$$

where d is the nozzle diameter and $a_0 = Bd$ defines a virtual "origin" for the scaled velocity, i.e. a virtual point where the centerline velocity would be infinite. The empirical numerical constant B is found to be $B \approx 6$ according to experimental data [2, 19]. This value can be easily derived from the other parameters describing the flow. Indeed, another well-known approximate solution for the turbulent round jet flow is given by a Gaussian velocity profile $U(\eta) = \exp(-\eta^2/2\sigma^2)$. A fit of the experimental data [7, 2] yields $1/\sigma = 12.0 \pm 0.2$ and a fit of the above solution Eq. (30) with $\alpha = 1/5$ and $\beta = 2$ yields $1/\sigma = 12.1 \pm 0.1$. The standard error of the axial velocity profile therefore defines an opening angle $1/12$ which applies on the nozzle radius $d/2$, leading to a virtual point $a_0 = 6d$. Recall that this point is different from the virtual origin of the jet spatial extent, $x_0 = d/2\alpha \approx 5d/2$.

One can easily verify that this velocity field is solution of the continuity equation:

$$\partial_x U + \frac{1}{r}\,\partial_r(r\,V) = 0. \tag{32}$$

For the turbulent round jet, the RANS equations are given with a good approximation by their boundary layer form. The RANS axial equation writes:

$$U\,\partial_x U + V\,\partial_r U = -\frac{1}{r}\,\partial_r(r\langle u\,v\rangle), \tag{33}$$

while the radial equation reduces to $\bar{p} + \langle v^2\rangle = \text{cst}$, where $\bar{p}$ is the averaged pressure.

The Reynolds averaged Navier-Stokes-Boussinesq equations become :

$$U\,\partial_x U + V\,\partial_r U - \frac{1}{r}\,\partial_r(r\,\nu_T\,\partial_r U) = 0, \tag{34}$$

which, when $\nu_T = \text{constant}$, can be simplified to:

$$U\,\partial_x U + V\,\partial_r U - \nu_T\,\frac{1}{r}\,\partial_r(r\,\partial_r U) = 0. \tag{35}$$

Writing the velocities under the form:

$$U = \frac{g}{x} \times \frac{1}{(1+2\,z^2)^2}, \quad V = \frac{g}{x} \times \frac{\alpha\,z\,(1-2\,z^2)}{2(1+2\,z^2)^2}, \tag{36}$$

where $z = \eta/\alpha$, and applying the averaged axial NS equation Eq. (35) to these velocity profiles, one finds that this flow is indeed an exact solution of the RANS equations provided the turbulent viscosity takes the value:

$$\nu_T = g\,\frac{\alpha^2}{16}. \tag{37}$$

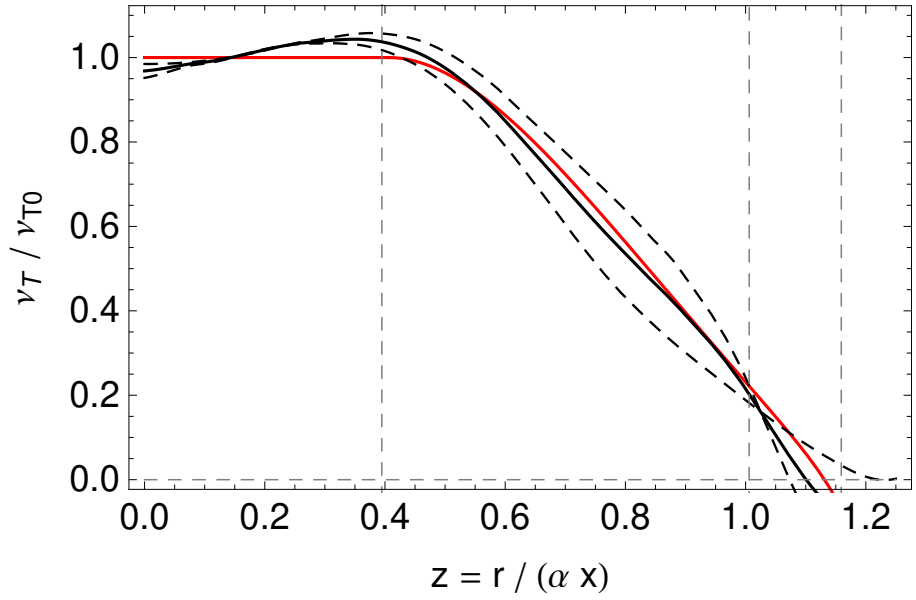

Figure 6: Normalized profile of the variable turbulent viscosity $16\nu_T/g\alpha^2$, where $\nu_T = -\sigma_{uv}/\partial_r U$, in function of the reduced and scaled radial distance, $z = r/(\alpha x)$. The dashed black curves are the turbulent viscosity derived from the experimental data of Panchapakesan and Lumley [19] and Hussein et al [7], and the black continuous curve is their mean. The red curve is its theoretical prediction from a matched solution of the RANS equations (Sec. 3.3 and Appendix B). All curves are normalized by the theoretical expectation derived from the NS axial equation, $\alpha^2/16 = 1/400$ for $\alpha = 0.2$. It is close to constant in the central region of the jet, up to $z \approx 0.6$, i.e. $\eta \approx 0.12$.

With the experimental values of the opening parameter $\alpha = 0.2$, one obtains $\alpha^2/16 = 1/400 = 0.0025$. This value of ν_T is in remarkable agreement with its direct measurement at the center of the jet [2]. As can be seen in Fig. 6, the turbulent viscosity is indeed experimentally observed to have this almost constant value 0.0025 in the inner 60% of the jet. Then it decreases and vanishes around the turbulent-laminar transition, as could be expected. This is a strong argument in support of the validity of the Boussinesq model for the central region of the turbulent round jet, and more generally for a description in terms of a variable turbulent viscosity.

3.2 Matched precise solution of RANS equations with variable turbulent viscosity

In what follows, we will need a precise solution for the radial profiles of the turbulent jet average velocities, including the boundary of the jet and beyond. The above constant viscosity solution is not enough, since it agrees with experimental data only in the central region of the jet, $\eta < 0.1$, while it departs strongly from them when approaching its frontier. Moreover, it relies on a simplifying assumption (model) while we need an exact

solution of the RANS equations. Such a solution can be expressed in terms of a variable turbulent viscosity. As we shall see, it leads to an almost constant value of ν_T in the center region of the jet, thus supporting the turbulent viscosity model in this region.

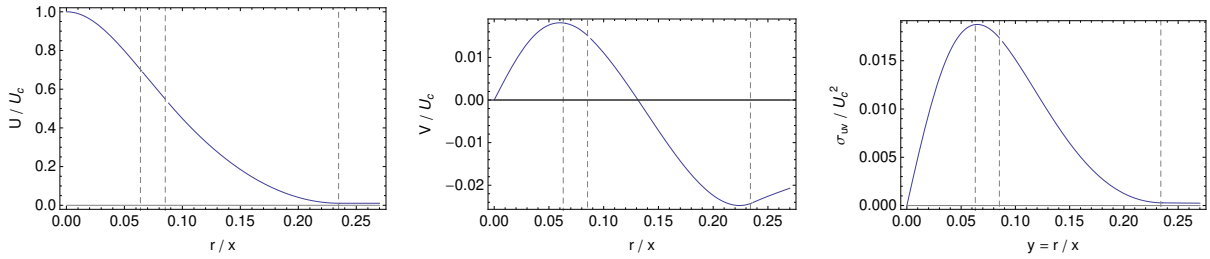

Figure 7: Radial profiles of $U_{tot}(\eta)$, $V_{tot}(\eta)$ and $\sigma_{uvtot}(\eta)$ in function of the scaled radial distance $\eta = r/x$. They are precise solutions of the RANS equations constructed by matching the velocities and their derivatives to the center solution (with constant turbulent viscosity) and to the exact solution of NS equations for the laminar flow exterior to the jet (see text and Appendix A).

Such a precise solution of the RANS equations can be constructed throughout the whole jet by matching local solutions for $U(\eta)$ and their derivatives to the central (constant ν_T) solution. Then $V(\eta)$ is derived from the continuity equation and the Reynolds shear stress from U and V.

We have achieved this in four steps: (1) central solution (a), ν_T =cst; (2) solution exterior to the jet (d) where the flow becomes laminar and irrotational; (3) quadratic solution (c) matched to the exterior solution; (4) linear solution (b) added between the central and quadratic solutions in order to match not only the velocities but also their derivatives.

In the central region of the jet, the solution is, as we have previously seen (omitting in the following for simplification the g/x scaling contribution which is in factor to all expressions):

$$U_a = \frac{1}{(1+2\,(\eta/\alpha)^2)^2}, \quad V_a = \frac{\eta\,(1-2\,(\eta/\alpha)^2)}{2\,(1+2\,(\eta/\alpha)^2)^2}. \tag{38}$$

The next law is a linear solution for $U(\eta)$. It can be matched to the central solution only at its inflexion point, which is given by $\eta_{ab} = \alpha/\sqrt{10} \approx 0.065$:

$$U_b = A_0 + A_1\frac{\eta}{\alpha}, \quad V_b = \frac{K_b}{\eta} + \eta\left(\frac{A_0}{2} + \frac{2A_1}{3}\,\frac{\eta}{\alpha}\right). \tag{39}$$

Then the profile of $U(\eta)$ can be very well fitted in the outer part of the jet by a parabolic profile:

$$U_c = \frac{\alpha^2}{4} + A_2\left(\frac{\eta}{\alpha} - q\right)^2, \quad V_c = \frac{K_c\,\alpha^2}{\eta} + \frac{\eta}{12}\left(\frac{3\,\alpha^2}{2} + A_2\left(6\,q^2 - 16\,q\,\frac{\eta}{\alpha} + 9\,\frac{\eta^2}{\alpha^2}\right)\right). \tag{40}$$

The matching point between U_b and U_c is $\eta_{bc} = -(A_3/2A_1)\,\alpha \approx 0.085$. Finally these profiles are matched to the velocity profiles of the exterior laminar flow. They have been determined by Landau [9] from their irrotational character, yielding the exact result:

$$U_d = \frac{\alpha_S^2}{4}\,\frac{1+\eta^2/2}{\sqrt{1+\eta^2}}, \quad V_d = \frac{\alpha_S^2}{4}\,\frac{1}{\eta}\left(K_d + 1 - \frac{1}{\sqrt{1+\eta^2}}\right), \tag{41}$$

where K_d is a matching constant whose value is given in Appendix A. To order $\mathcal{O}(\eta^2)$ (which is precise enough for our purpose), it is simplified as:

$$U_d = \frac{\alpha_S^2}{4}, \quad V_d = \frac{\alpha_S^2}{4\eta}\left(K_d + \frac{\eta^2}{2}\right). \tag{42}$$

The matching point between the interior and exterior regions of the jet is given by the turbulent-laminar transition, which we denote $\eta_{cd} = \alpha_S = q\,\alpha$. The value of q is experimentally found to be $q = 1.15$, i.e. the transition is observed to happen at $\eta = 0.235$ for $\alpha = 0.205$, which is the best fit for this transition in U, V and σ_{uv} from Hussein et al [HCG] [7] and Panchapakesan and Lumley [PL] [19] experimental data. It is noticeable that this value is also, as could be expected, just the limit experimentally found for the turbulent jet concentration profile [27]. The question of the theoretical prediction of this profile will be considered in a forthcoming paper [Nottale and Lehner, in preparation]. The detailed expressions for the various constants are given in Appendix A.

The resulting profiles are displayed in Fig. 7. We can see in Figs. 23, 24 and 25 of Appendix A that they provide an excellent account of experimental measurement results, the only fitted constants being the jet parameter α and the ratio $q = \alpha_S/\alpha$. Both parameters will be theoretically predicted in the following;

The theoretical profile of the variable turbulent viscosity can be derived from these relations as $\nu_T = -\sigma_{uv}/\partial_r U$, and is in satisfying agreement with the variable ν_T constructed from the experimental data (Fig. 6).

3.3 Theoretical prediction of the turbulent-laminar transition angle

The previous solution does not allow us to get a theoretical prediction for the parameter $q = \alpha_S/\alpha$, since we have constructed it by a priori matching the constant Landau velocity $U_S = \alpha_S^2/4$ of the exterior laminar flow to the inner turbulent solution.

3.3.1 A new matched global solution for mean velocity profiles

We have therefore constructed another solution by still matching the profile of the axial velocity $U(\eta)$ and its first derivative $U'(\eta)$, but now also its second derivative $U''(\eta)$, at a radial distance $\eta_k = k\alpha$ betwen the constant ν_T solution in the inner region and a quadratic solution in the outer region of the jet:

$$U_a = \frac{1}{(1+2\,z^2)^2}, \quad U_e = B_0 + B_1 z + B_2 z^2, \tag{43}$$

where $z = \eta/\alpha$. The resulting matched solution is given in more detail in Appendix B. We show in Fig. 8 the behavior of the velocity profile around the jet edge in function of the matching parameter k. The minimal value of U, $U_{\rm min} = B_0 - B_1^2/4B_2$ is given by

$$U_{\rm min} = \frac{6k^2 - 1}{1 + 2k^2)(10k^2 - 1)}. \tag{44}$$

We recognize in the divergent point $k = 1/\sqrt{10}$ of this expression a limit which corresponds to the inflexion point of the central region solution U_a. The minimal value of U is naturally constrained by $0 < U_{\rm min} < U_S$. This yields $\sqrt{1/6} < k < 0.411$, which corresponds to $1.1 < q < 1.2$. We can see in Fig. 8 that the matching with the range permitted for the laminar solution actually occurs between $q \approx 1.09$ and $q \approx 1.16$, in agreement with the experimentally observed values.

More precisely, the relation between k and q, given by the matching equation $U(q) = q^2\alpha^2/4$ at the turbulent-laminar transition, is well approximated by the simple linear law:

$$q = \frac{50}{3}k - 5.703, \tag{45}$$

thanks to a weak dependence in function of α. This relation correctly yields $k = (0.4082, 0.4097, 0.4112)$ for $q = (1.10, 1.125, 1.15)$.

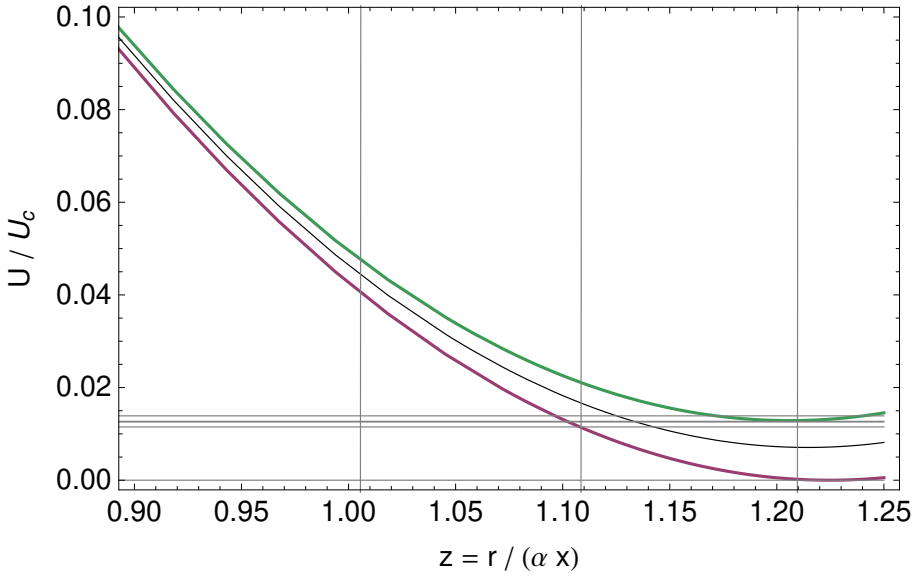

Figure 8: Axial velocity profile around the jet edge for solutions of the RANS equations matched at $\eta = k\alpha$. We show the resulting profile for three values of the matching parameter $k = \sqrt{1/6} = 0.40825$ (magenta curve), 0.410 (black curve), and 0.4115 (green curve). The horizontal gray lines give the range of possible values for the Landau laminar velocity $U_S = \alpha_S^2/4 = q^2\alpha^2/4$. We find that the parameter q is therefore constrained in the range $\approx (1.10 - 1.15)$.

3.3.2 Comparison with experimental and numerical data

Let us compare this theoretical prediction $q_{\rm th} = 1.125 \pm 0.025$ with estimates from data of laboratory and numerical experiments.

A first estimate of the ratio q is given by the Gaussian fits of the velocity, $U/U_0 = \exp(-K_U\,\eta^2)$ and concentration, $C/C_0 = \exp(-K_C\,\eta^2)$, profiles. Indeed, these expressions can be put under the standard form $\exp[-0.5(\eta/\eta_0)^2]$, defining a characteristic extent $\eta_0 \propto 1/\sqrt{K}$, so that $q = \sqrt{K_U/K_C}$. The spatial extent of the jet is well established to be larger than its velocity extent. One finds values of K_U around 75 [3] while $K_C \approx 60$ [27], yielding $q = \sqrt{K_U/K_C} = 1.12$. DNS and LES yield similar values [5, 6, 28]. We have fitted various combinations of experimental and numerical data and have confirmed these estimates: $K_U = 77.2 \pm 0.8$ (PL data); $K_U = 72.8 \pm 1.2$ (HCG data); $K_U = 75.9 \pm 0.7$ (joined HCG and PL data); $K_U = 76.1$ (DNS [5]); $K_U = 74.0 \pm 0.5$ (LES [28]).

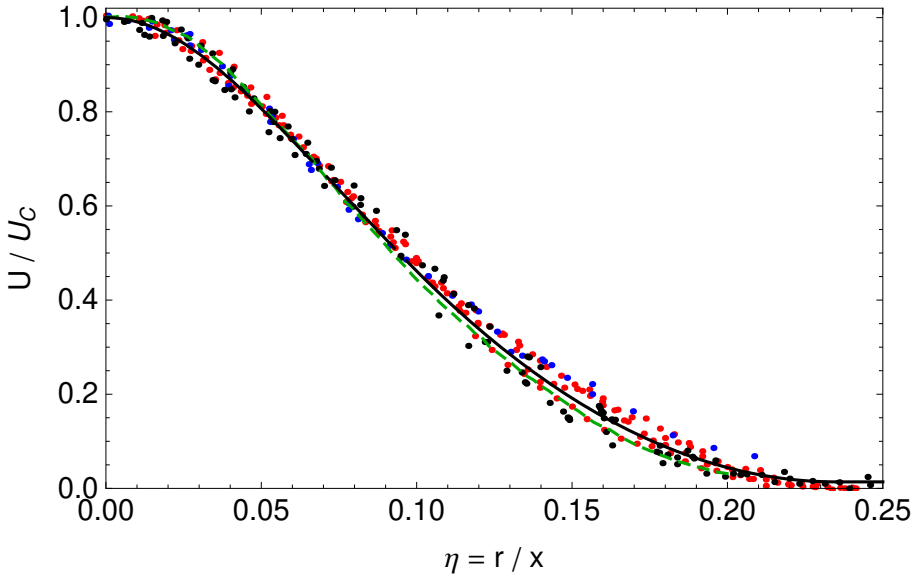

Figure 9: Axial mean velocity in a turbulent round jet. The black points are experimental data from PL [19], the blue points from HCG [7]; the red points are LES data from Aiyer and Meneveau [28]; the green dashed curve is the DNS from Boersma et al. [5]. The black curve is a fit of these data by the matched solution of the RANS equations of Sec. 3.2 with $\alpha = 0.21$ and $q = 1.12$, yielding $\alpha_S = 0.235$.

Another approach consists of comparing directly the experimental data with the theoretical expectation on the edge of the jet. It has been shown by Landau [9] that the value of U at the transition $\eta = \alpha_S$ between the turbulent and laminar regions is $U_S = \alpha_S^2/4$ and that it practically keeps this value in the laminar region. The mean value of U for $\eta \geq 0.22$ in PL data is $U_S = 0.014 \pm 0.002$, yielding a reasonable although imprecise estimate $\alpha_S = 0.235 \pm 0.030$.

Therefore, a far better way to obtain α_S and q consists of fitting the parabolic shape of the axial velocity in the outer part of the jet, $\eta >\approx 0.085$. We have performed such a

fit with various limits and found a stable and now precise result: $\alpha_S = 0.232 \pm 0.004$ from joined HCG and PL data.

On the other side, the value of α can be determined by fitting the center solution U_a (which actually yields its definition) in the inner part of the jet. The resulting values are rather stable in function of the chosen limit $\eta = 0.05$ to 0.12. One finds values ranging from (0.204 ± 0.005) in the very center, to (0.211 ± 0.002) up to $\eta = 0.12$, leading to a common final estimate $\alpha = 0.207 \pm 0.004$. With the previous value of α_S, we obtain $q = 0.121 \pm 0.029$, which agrees very well with our theoretical expectation.

We have finally directly performed a least-square fit of experimental and numerical data by the matched RANS solution of Sec. 3.2 and found a similar result: ($\alpha = 0.211$, $q = 1.12$, implying $\alpha_S = 0.236$) from HCG and PL data, and ($\alpha = 0.211$, $q = 1.15$) from LES data. We show in Fig. 9 that Laboratory and numerical experimental results compare remarkably well with our matched theoretical solution of the RANS equations for $\alpha = 0.21$ (for which we shall obtain a purely theoretical prediction in what follows) and the above theoretical prediction $q = 1.12$ of the ratio α_S/α.

4 Scale-relativity theory of turbulence: a short reminder

4.1 Principle of relativity of scales

The theory of scale-relativity and fractal space-time was initially constructed in order to obtain a geometric foundation of quantum mechanics (QM) from first principles [17, 29, 18]. This has been achieved by deriving all the QM postulates from the only principle of relativity, provided it is applied to position, orientation and motion (as in Galileo, Poincaré and Einstein theories of relativity), but also to scales, i.e. including resolution transformations of the coordinate system [29].

The theory is based on the relaxation of the hypothesis of space-time differentiability. One can prove that a continuous but non-differentiable space (more generally space-time) is fractal, under a general meaning going beyond mere self-similarity: namely, lengths become explicitly dependent on the resolution scale and divergent when the resolution interval tends to zero [17, 18].

This theorem is the basis for the scale-relativity method of dealing with non-differentiability: the various physical functions become fractal functions, i.e. explicitly scale-dependent functions $f = f(t, \tau)$, so that one can define a derivative at any given scale τ, $f'(t, \tau) = \partial_t f(t, \tau)$, even though it no longer exists at the limit $t \to 0$. In other words, while the standard differentiation method keeps only the limit $lim[f(t)]_{dt \to 0}$ and thus fails when this limit does not exist, the scale-relativity method keeps all the history of what happens when $dt \to 0$. We lose nothing in this way, since when the limit exists it is included in the description, while when it does not exist we still keep a description tool which is physically effective, i.e. which works at any finite resolution scale, as experimentally needed (while the null resolution interval is a mathematical concept which has actually

no physical meaning).

As we shall briefly recall in what follows, by constructing a scale-covariant derivative $\widehat{d}/dt$ which accounts for the geometric effects of a fractal space, we have written the equation of motion in such a space as a geodesics equation, i.e. under the form of Galilean free inertial motion, $\widehat{d}\mathcal{V}/dt = 0$. This equation can be generalized to the Newtonian form $\widehat{d}\mathcal{V}/dt = -\nabla\phi$ in the presence of an exterior potential (which can itself be the manifestation of an inner geometric property [30, 31, 32]) and then integrated under the form of a Schrödinger-type equation [17, 18].

4.2 Geodesics equations

The non-differentiability and fractality of coordinates implies at least three consequences [17, 18]:
(1) The number of geodesics is infinite. Their description naturally becomes non-deterministic and probabilistic. The ensemble of these paths therefore constitutes a (virtual) fluid, which is characterized by its velocity field.
(2) Each geodesic is itself fractal with fractal dimension $D_F = 2$ [33], corresponding to the Markovian nature of motion in a fractal space.
(3) The non-differentiability also implies a two-valuedness of the (scale-dependent) derivative of the coordinates, $(V_+,\ V_-)$,. Indeed, one needs one point to define a position, but two points to define a velocity, so that two definitions now exist (the second point being before or after the position point), which are no longer invariant under the reflexion transformation $|dt| \to -|dt|$ in the non-differentiable case [17].

These three properties of motion in a fractal space lead to describing the velocity field of geodesics in terms of a complex fractal function $\widetilde{\mathcal{V}} = (V_+ + V_-)/2 - i(V_+ - V_-)/2$. The $(+)$ and $(-)$ velocity fields can themselves be decomposed in terms of a differentiable part $v_\pm$ and of a fractal (divergent) fluctuation of zero mean $w_\pm$, i.e., $V_\pm = v_\pm + w_\pm$. Therefore the same is true for the full complex velocity field, $\widetilde{\mathcal{V}} = \mathcal{V}(x, y, z, t) + \mathcal{W}(x, y, z, t, dt)$.

The elementary displacements along these geodesics can be described in a stochastic way, $dX_\pm = d_\pm x + d\xi_\pm$, with

$$d_\pm x = v_\pm\, dt, \quad d\xi_\pm = \zeta_\pm \sqrt{2\mathcal{D}}\, |dt|^{1/2}. \tag{46}$$

Here $\zeta_\pm$ represents a dimensionless stochastic variable such that $<\zeta_\pm>= 0$ and $<\zeta_\pm^2>= 1$. The parameter $\mathcal{D}$ characterizes the amplitude of fractal fluctuations.

These various effects can be combined in terms of a total ("scale-covariant") derivative operator [17] which generalizes to a fractal space the Euler derivative $\partial_t + V.\nabla$, adding two imaginary terms to it:

$$\frac{\widehat{d}}{dt} = \frac{\partial}{\partial t} + \mathcal{V}.\nabla - i\,\mathcal{D}\Delta, \tag{47}$$

where $\mathcal{V} = V - i\,U$. Newton's fundamental equation of dynamics becomes, when it is written in terms of this operator

$$m\,\frac{\widehat{d}}{dt}\,\mathcal{V} = -\nabla\phi. \tag{48}$$

In the absence of an exterior field ϕ, this is a geodesic equation (i.e., a free inertial Galilean-type equation),

$$\frac{\widehat{d}}{dt}\,\mathcal{V} = \left(\frac{\partial}{\partial t} + \mathcal{V}.\nabla - i\mathcal{D}\Delta\right)\,\mathcal{V} = 0. \tag{49}$$

4.3 Macroscopic Schrödinger equation

The final step consists of making a change of variable in which one connects the velocity field $\mathcal{V} = V - i\,U$ to a complex function $\psi = e^{iS/S_0}$ (where S is the action, now complex because the velocity field is itself complex), according to the relation

$$m\mathcal{V} = -i\,S_0\,\nabla \ln \psi. \tag{50}$$

This equation is but the standard relation between momentum and action $P = \nabla S$, that provides a new expression (now exact) for the principle of correspondance. The parameter S_0 is a constant for the system considered ($S_0 = \hbar$ in standard quantum mechanics). This relation plays a fundamental role in the scale-relativity theory, since it translate the geometric description (left hand side, in terms of velocity field of geodesics of the fractal space-time) into the standard QM algebraic description (right hand side, wave function).

Thanks to this change of variables, the equation of motion can be integrated under the form of a Schrödinger equation [17, 18], generalized to a constant S_0 which may be different from $\hbar$,

$$\mathcal{D}^2\Delta\psi + i\mathcal{D}\frac{\partial}{\partial t}\psi - \frac{\phi}{2m}\psi = 0, \tag{51}$$

where $\mathcal{D}$ is another expression for S_0 according to the relation:

$$S_0 = 2m\mathcal{D}, \tag{52}$$

which is just another form for the Compton relation $\lambda_c = \hbar/mc$ in standard QM.

By setting finally $\psi = \sqrt{P} \times e^{i\theta}$, with $V = 2\mathcal{D}\nabla\theta$, one can show [29, 18] that $P = |\psi|^2$ gives the number density of virtual geodesics. This function becomes naturally a density of probability when the geodesics are manifested in terms of effective particles. The function ψ, being solution of the Schrödinger equation and subjected to the Born postulate and to the Compton relation, owns therefore all the properties of a wave function.

4.4 Application to turbulence in velocity-space

4.4.1 Conditions for Schrödinger equation

The transformation and integration of the fundamental equation of dynamics into a Schrödinger equation in nondifferentiable and continuous (therefore fractal) geometry is a general mathematical result which does not depend on the nature of the variables. It just relies on the properties of the derivative of a fractal variable (in the new sense defined hereabove) and on its dynamics described by its second order derivative.

In the case of turbulence, the *position* coordinates are, a priori, not fractal inside the relevant scale range, i.e. between the Kolmogorov dissipative scale and the integral scale. However, the *velocity* of fluid particles becomes fractal according to Komogorov K41 scaling law. This has led de Montera [14] to suggest applying the scale-relativity theory to turbulence in v-space, i.e. to the velocity v as coordinate and the acceleration a as its derivative.

This application relies on the fact that the various conditions on which the derivation of a Schrödinger equation is based are satisfied in the inertial range of a turbulent fluid [16]:
(1) The number of possible trajectories of a fluid particle (or of a reliable Lagrangian tracer) is infinite, due to the highly chaotic nature of turbulence.
(2) The Kolmogorov K41 scaling $\delta v \sim \delta t^{1/2}$ [23] in the inertial range means that the trajectories in v-space are fractal of dimension 2. There is no strict non-differentiability, since this range is lowerly limited by the Kolmogorov time-scale τ_η. But its effects are manifest through the recognized scale-dependence and divergence of accelerations toward small scales, $a \sim \tau^{-1/2}$ down to $\tau = \tau_\eta$.
(3) The non-differentiability also implies a two-valuedness of the (scale-dependent) derivative of the v-coordinates, i.e. of accelerations $(A_+,\ A_-)$, from which one constructs the complex variable $\mathcal{A} = (A_+ + A_-)/2 - i\,(A_+ - A_-)/2$. We have shown that this behavior is manifest in turbulence data [16], in which one finds that the accelerations a and their increments da are of the same order of size, contrarily to the basic assumption of differential calculus, $da \ll a$.
(4) The motion is Newtonian, i.e., the acceleration is proportional to the force applied (even though there are also non-Newtonian contributions like viscosity).
(5) The range of scales on which the effective fractal dimension is $D_F = 2$ should be large enough: this condition is fulfilled for large enough Reynolds numbers, since this range is simply given by $T_L/\tau_\eta = R_\lambda/2C_0$, where $R_\lambda = \sqrt{15 R_e}$ and $C_0 \approx 4 - 7$.

4.4.2 Scale-covariant derivative in velocity-space

The various effects of fractality and non-differentiability can therefore be combined in terms of a total derivative operator acting in v-space [14, 15, 16]:

$$\frac{\widehat{d}}{dt} = \frac{\partial}{\partial t} + \mathcal{A}.\nabla_v - i\,\mathcal{D}_v \Delta_v. \tag{53}$$

The Navier-Stokes equation (reduced to the Euler equation in the inertial range by neglecting for the moment the viscous term) writes in Lagrangian form $dv/dt = F = -\nabla p/\varrho$. In the incompressible case considered here, its derivative with respect to time reads (making $\varrho = 1$ for simplification of the writing):

$$\frac{da}{dt} = -\nabla \dot{p}. \tag{54}$$

In order to account for the various geometric effects of non-differentiability and fractality, one replaces d/dt by the new total derivative operator $\widehat{d}/dt$. One therefore obtains

a new form of the equation of dynamics in v-space:

$$\frac{\widehat{d}}{dt}\mathcal{A} = \left(\frac{\partial}{\partial t} + \mathcal{A}.\nabla_v - i\,\mathcal{D}_v\Delta_v\right)\mathcal{A} = \dot{F}, \tag{55}$$

where F contains the pressure gradient term and possibly any applied external force.

When the force is the v-gradient of a potential ϕ_v, we get the equation:

$$\frac{\widehat{d}}{dt}\mathcal{A} = -\nabla_v\phi_v. \tag{56}$$

Then we introduce a wave function ψ_v as a re-expression of the action $\mathcal{S}_v$ which is now complex (since the dynamical variables are complex), $\psi_v = e^{i\mathcal{S}_v/\hbar_v}$, that can be decomposed in terms of a modulus and a phase, $\psi_v = \sqrt{P_v} \times e^{i\theta_v/\hbar_v}$.

The main point here is that the PDF of velocities is given by the square of the modulus of the wave function, $P_v(v) = |\psi_v|^2$, while its phase is linked to the real part of the complex acceleration through the relation $A_R = \nabla_v\theta_v$. The constant $\hbar_v = 2\mathcal{D}_v$ is therefore the macroscopic equivalent in v-space of the constant $\hbar$ of standard quantum mechanics (more generally, when $m \neq 1$, one gets $\hbar_v = 2m\mathcal{D}_v$).

This new constant has the same dimensionality, $[\hbar_v] = [L^2T^{-3}]$, as $\varepsilon = \sigma_v^3/L$. We have suggested [16] that it can be identified with what is also the most fundamental constant of the classical description of turbulence [23], namely, the rate ε of transfered energy that is dissipated at the Kologorov scale (η, τ_η):

$$\hbar_v = \varepsilon. \tag{57}$$

4.4.3 Schrödinger equation in velocity-space

Finally, the time derivative of the Navier-Stokes equations of fluid dynamics takes, after integration on v, the form of a macroscopic Schrödinger equation in v-space [17, 31, 14, 15, 16]:

$$\mathcal{D}_v^2\,\Delta\psi_v + i\,\mathcal{D}_v\frac{\partial}{\partial t}\psi_v - \frac{1}{2}\phi_v\,\psi_v = 0, \tag{58}$$

with $\mathcal{D}_v = \hbar_v/2 = \varepsilon/2$ and with the PDF of velocities given by $P_v = |\psi_v|^2$.

4.4.4 New acceleration / force component

The complex acceleration field writes, in terms of the wave function,

$$\mathcal{A} = -2i\,\mathcal{D}_v\,\nabla_v \ln\psi_v, \tag{59}$$

so that we are now able to establish the expressions of A_+ and A_-:

$$A_+ = +\mathcal{D}_v\,\frac{\partial_v P_v}{P_v} + \partial_v\theta_v, \quad A_- = -\mathcal{D}_v\,\frac{\partial_v P_v}{P_v} + \partial_v\theta_v. \tag{60}$$

In many situations which may be relevant to the turbulence case (in particuler in an harmonic oscillator potential), the solutions of the Schrödinger equation are real [34], i.e. $\theta_v \approx$ cst and then $\partial_v \theta_v \approx 0$. Under this approximation (which is supported by the experimental data [16]), the new acceleration $A_q = (A_+ - A_-)/2$ reduces to:

$$A_q = \pm \mathcal{D}_v \, \partial_v \ln P_v(v), \tag{61}$$

and it is therefore divergent for the velocities v_i which defines the zeros of the local velocity PDF, $P_v = |\psi_v|^2$. As we have shown in [16], this acceleration/force component is responsible for the very large non-Gaussian tails of the acceleration PDF and for the various manifestations of intermittency in a turbulent fluid.

Let us indeed recall how one can derive in an universal way the turbulent acceleration PDF from the mere existence of these predicted null minima in the local velocity PDF [15]. In the present framework where velocity is the basic coordinate, the acceleration is some function $a = A(v)$ of the velocity. Then we can define the inverse of this function, $V(a) = A^{-1}(a)$. This inverse function may have multiple parts, defined on the various monotonic parts of $A(v)$. Let us call $V_k(a)$ these parts. The resulting probability distribution of acceleration is given by the inversion formula:

$$P_a(a) = \sum_k \frac{1}{|A'[V_k(a)]|} P_v[V_k(a)], \tag{62}$$

where the sum is done on each of the monotonic parts of the inverse function $V = A^{-1}$. In the simple case when there is only one part, this formula becomes:

$$P_a(a) = \frac{P_v[V(a)]}{|A'[V(a)]|}. \tag{63}$$

In the macroquantum-type approach advocated here, the velocity PDF is the square of the modulus of a wave function, $P_v(v) = |\psi_v(v)|^2$. This wave function may in general be positive or negative, and when it crosses $\psi_v = 0$ at some value of the velocity v_i, it will usually behave locally as $\psi_v(v_i) = k(v - v_i)$. Therefore the velocity PDF will generally behave in the minima as

$$P_v(v) \propto (v - v_i)^2. \tag{64}$$

We take $v_i = 0$ to simplify the argument, knowing that the final acceleration PDF does not depend on their values, but only on the parabolic shape of the local velocity PDF. From $P_v(v) = (v/v_0)^2$ and Eq. 61, one obtains $A(v) = \pm 2\mathcal{D}_v/v$, then $V(a) = \pm 2\mathcal{D}_v/a$. Therefore, applying Eq. 63 one derives the following asymptotic acceleration PDF [15]:

$$P_a(a) = \frac{(2\mathcal{D}_v)^3}{v_0^2} \frac{1}{a^4}. \tag{65}$$

We emphasize that this theoretical prediction of the basic form of the acceleration PDF is not the result of a model or of an hypothesis concerning the underlying statistics, but it is directly derived from the equations of fluid mechanics in which one has taken into

account the fundamental effects of turbulence. We have shown in Ref. [16] that this basic law can be improved by including the effects of the dissipative Kolmogorov scale and of parameter correlations leading to the emergence of an exponential cut-off in the tails, yielding a perfect fit to the experimental data.

4.4.5 Harmonic oscillator potential in velocity-space

The new formulation involving the derivative of the Navier-Stokes equations has introduced the time derivative of a force. It is therefore important to study in more details the nature of such a derivated force. We shall now prove that when the force in x-space derives from an x-potential, the force in v-space also derives, now, from a v-potential.

Let ϕ be the potential in x-space, with $F_i = -\partial_i \phi$ for $x_i = (x, y, z)$. The force in v-space is therefore

$$\dot{F}_i = -\frac{d}{dt}(\partial_i \phi) = -\partial_i \frac{d}{dt}\phi[x(t), y(t), z(t)], \tag{66}$$

Since $v_i = dx_i/dt$, we obtain for the first component of the force $\dot{F} = F_v$:

$$(F_v)_x = -\frac{\partial^2 \phi}{\partial x\, \partial t} - \frac{\partial^2 \phi}{\partial x^2}\, v_x - \frac{\partial^2 \phi}{\partial x\, \partial y}\, v_y - \frac{\partial^2 \phi}{\partial x\, \partial z}\, v_z, \tag{67}$$

and similar expressions for the two other components.

Therefore we find that this v-force derives in a universal way from a v-potential, which reads (adopting Einstein's notation about indices summation)

$$\phi_v = (\partial_t \partial_i \phi)\, v_i + \frac{1}{2}(\partial_i \partial_j \phi)\, v_i\, v_j. \tag{68}$$

In a more explicit way, it writes in dimension 2:

$$\phi_v(v_x, v_y) = \left(\frac{\partial^2 \phi}{\partial x\, \partial t}\, v_x + \frac{\partial^2 \phi}{\partial y\, \partial t}\, v_y\right) + \frac{1}{2}\left(\frac{\partial^2 \phi}{\partial x^2}\, v_x^2 + 2\frac{\partial^2 \phi}{\partial x\, \partial y}\, v_x\, v_y + \frac{\partial^2 \phi}{\partial y^2}\, v_y^2\right), \tag{69}$$

with similar terms involving the third coordinate in dimension 3.

This is in particular true for the pressure gradient in the NS equation, in which the pressure itself plays the role of a potential energy in the incompressible case (while this role is played by the enthalpy when the fluid is compressible). The pressure can be decomposed, under the Reynolds method, in terms of a mean pressure $\bar{p}$, which is differentiable and of a turbulent fluctuation δp which is non-differentiable and of zero mean. In the derivated Navier-Stokes equations, we obtain a force $-\nabla_v p_v$ in terms of v-potential p_v coming from the mean pressure $\bar{p}$, which writes in 2D:

$$\phi_v(v_x, v_y) = \left(\frac{\partial^2 \bar{p}}{\partial x\, \partial t}\, v_x + \frac{\partial^2 \bar{p}}{\partial y\, \partial t}\, v_y\right) + \frac{1}{2}\left(\frac{\partial^2 \bar{p}}{\partial x^2}\, v_x^2 + 2\frac{\partial^2 \bar{p}}{\partial x\, \partial y}\, v_x\, v_y + \frac{\partial^2 \bar{p}}{\partial y^2}\, v_y^2\right), \tag{70}$$

with similar z terms in 3D.

In the stationary case the mean pressure is independant of time, and the potential energy reduces to its pure harmonic oscillator form.

Another approch consists in taking solutions which are only local. As concerns the specific question considered here, namely, the shape of the potential which will appear in the macroscopic Schrödinger equation, the main point is that the Schrödinger equation Eq. (58) is written and holds at the integral scale and beyond, since its very construction relies on the cascade of eddies of the K41 inertial regime which plays the role of a microscopic theory for these (relatively) large scales. The potential ϕ_v which appears in it is therefore defined at this scale, which means that its coefficients are averaged over the scale $\sim T_L$ for the time coordinate and $\sim L$ for the space coordinates and can therefore be considered as constant over these space and time scales.

A final question to be discussed is the fact that the force expression from which we started, $F = -\nabla p/\varrho$ is valid in Eulerian coordinates, while its expression in Lagrangian coordinates has a more complicated form involving a Jacobian transform. However, our final result in v-space can be expressed in terms of the velocity components V_i alone, which now play the role of primary coordinates. Such a force depending just on the coordinates therefore applies both to the Eulerian and Lagrangian form of the Navier-Stokes equations (and their derivative).

4.5 Solution in principle of the closure problem

The completion in the scale-relativity theory framework of the classical fluid mechanics equations by a macroscopic Schrödinger equation (which is just a prime integral of the derivated NS equations under turbulent conditions) solves in principle the closure problem.

Indeed, there are six unknown functions in the RANS equations, U, V, $\bar{p}$, σ_{uv}, σ_u and σ_v. Three of them can be derived from the two RANS equations and the continuity equation, e.g. U, V and $\bar{p}$. The v-Schrödinger equation is solved in terms of a wave function ψ_v, whose squared modulus yields the PDF of turbulent velocity fluctuations, $|\psi_v|^2 = P(u, v)$. From this PDF, the Reynolds stresses can then be calculated as integrals $\langle u^2 \rangle$, $\langle u\, v \rangle$ and $\langle v^2 \rangle$.

In practice, the situation is somewhat more complicated for the turbulent round jet. Thanks to its self-similar character, the RANS and continuity equations yield solutions for U, V and σ_{uv} and imply the relation $\bar{p} = -\sigma_v^2$ (up to small correction terms that we have calculated hereabove). But, despite this relation, the pressure remains unknown in itself, while it is the main ingredient entering in the v-Schrödinger equation (since the potential energy is given by second order derivatives of pressure). As a consequence, the Reynolds stresses cannot be directly calculated.

The problem can nevertheless be solved thanks to the relation $\bar{p} = -\sigma_v^2$. Owing to this identification, the Reynolds stress σ_v^2 enters in the left-hand-side of the v-Schrödinger equation as an unknown whose derivatives define the potential energy. Then it can also be derived from the solutions of this Schrödinger equation. Namely, the wave functions of the various (ground and excited) states, $\psi_{vs}(u, v)$, yield the probability density of velocity fluctuations for each state, $P_{vs}(u, v) = |\psi_{vs}(u, v)|^2$, from which the corresponding

variances σ_{vs}^2 can be calculated as:

$$\sigma_{vs}^2 = \int_{-\infty}^{+\infty} \int_{-\infty}^{+\infty} u^2 \, P_{vs}(u,v) \, du \, dv, \tag{71}$$

$$\sigma_{uvs} = \int_{-\infty}^{+\infty} \int_{-\infty}^{+\infty} u \, v \, P_{vs}(u,v) \, du \, dv, \tag{72}$$

$$\sigma_{us}^2 = \int_{-\infty}^{+\infty} \int_{-\infty}^{+\infty} v^2 \, P_{vs}(u,v) \, du \, dv, \tag{73}$$

where $P_{vs}(u,v)$ is normalized to one.

Then the final variance is the sum of these variances, e.g, $\sigma_v^2 = \Sigma_s \, p_s \, \sigma_{vs}^2$, weighted by the probability rate p_s of each state (s) as given by statistical physics (possibly corrected for the existence of offsets, i.e. of a fluctuating non null mean velocity). In practice we shall simply use in the present paper the fact that the potential is of the harmonic oscillator type for relating the final variance to the ground state variance. This is rendered possible by the fact that the QHO solutions are given by products of Hermite polynomials by the ground state Gaussian wave function. This allows us to write differental equations of which the Reynolds stress is solution (and therefore also the pressure).

Finally, thanks to this method, we shall actually obtain a solution of the closure problem for the turbulent round jet, at least in its central region. Some problems remain in its edge region, which we aim to study in more detail in a forthcoming work.

5 Scale-relativity theory of the turbulent jet in velocity-space

5.1 Method

Let us now apply the scale-relativity theory to the turbulent jet. The total velocity (mean plus fluctuations) is given by $U_t = U + u$, $V_t = V + v$ and $W_t = w$. The mean velocities U and V are fixed at a given spatial point (x, r) and $W = 0$, in the same way as the covariances $\langle uw \rangle = \langle vw \rangle = 0$. In a plane $x = \text{cst}$, there is full isotropy of the motion so that one expects $\langle w^2 \rangle = \langle v^2 \rangle$, which is fairly supported by experimental measurements [2, 7, 19]. We can therefore write an equation for the only variables u and v, from which the full covariance matrix can be derived.

The time-derivated Navier-Stokes equations are transformed into a Schrödinger-type equation which reads in its stationary form (in Cartesian coordinates):

$$\partial_u \partial_u \, \psi_v + \partial_v \partial_v \, \psi_v + \frac{2}{\hbar_V^2} \left(E_v - \phi_v \right) \psi_v = 0, \tag{74}$$

where $\hbar_V = \varepsilon$ is the macroscopic equivalent of the Planck constant in v-space. As we have previously seen, it can be identified with the turbulent K41 energy dissipation rate [16]. The plane and the round jet share the same equation under this description mode, where

v is here a 2D radial velocity in the round turbulent jet while in the case of the plane jet, v is the 1D velocity fluctuation perpendicular to the slit.

In order to obtain solutions of this v-Schrödinger equation for the turbulent jet, we need to know the v-potential ϕ_v. It is given, as we have proved hereabove, by second order derivatives of the mean pressure, namely,

$$\phi_v = \frac{1}{2}\,(k_u u^2 + 2k_{uv} u\, v + k_v v^2), \tag{75}$$

where

$$k_u = \partial_x \partial_x \bar{p}, \quad k_{uv} = \partial_x \partial_r \bar{p}, \quad k_v = \partial_r \partial_r \bar{p}, \tag{76}$$

since $\bar{p}$ is time-independent. We assume in what follows that the flow is incompressible, which allows us to simplify the writing by taking a density $\varrho = 1$.

The three coefficients are functions of x and r, i.e., of x and the variable $\eta = r/x$ which accounts for the scaling properties of the jet. For a given position (x, η) inside the jet, they are constant and the Schrödinger equation yields the PDF $P_v = |\psi_v|^2$ of the velocity fluctuations (u, v) at that point.

The mean pressure of the turbulent jet is given by the solution of the r-RANS equation, which reduces to $\partial_r(\bar{p} + \sigma_v^2) = 0$, i.e.:

$$\bar{p} = \bar{p}_0(x) - \sigma_v^2. \tag{77}$$

From the general scaling laws of the jet we know that p_0 and σ_v^2 vary in terms of the axial coordinate x (defined from the virtual origin of the conic shape of the jet) as $1/x^2$, so that we can write the mean pressure under the form:

$$\bar{p}(x, \eta) = \frac{g^2}{x^2}\,(\bar{p}_0 + p_\eta(\eta)) = \frac{g^2}{x^2}\,(p_0\,\mu^2 - \sigma_{v_\eta}(\eta)^2), \tag{78}$$

where p_0 is a purely numerical constant, σ_{v_η} is the scaling part of the radial Reynolds stress (without its x dependence) which depends only on $\eta = r/x$, and μ is its amplitude on the centerline of the jet $\eta = 0$. From now on we shall consider only the η-dependent parts of the various quantities (velocities, Reynolds stresses, pressure,..), which amounts to make $g/x = 1$ in their expressions.

The potential in the v-Schrödinger equation is that of two correlated quantum harmonic oscillators. The excited solutions of these QHOs are given by the product of a Gaussian function and of Hermite polynomials. They are characterized by the existence of velocity values v_i where the probability density is null, $P_v(v_i) = |\psi_v|^2(v_i) = 0$. These zeros create a divergent acceleration $A_q = \pm \mathcal{D}_v\, \partial_v \ln P_v$ which, as we have recalled hereabove, yields an explanation for intermittency and for the very large non-Gaussian tails $\sim a^{-4}$ observed in the acceleration PDF of turbulent fluids [16]. The ground state is given by the same Gaussian function that is involved in the excited state solutions (multiplied by Hermite polynomials).

Owing to the QHO nature of the potential, the ground state solution is given by a normal distribution (in the case when it is attractive for both v and u), which can be

written under the form:

$$\psi_v = \exp\left(-\frac{1}{4}\frac{u^2}{s_u^2} + \frac{\rho}{2}\frac{u}{s_u}\frac{v}{s_v} - \frac{1}{4}\frac{v^2}{s_v^2}\right), \tag{79}$$

times a normalization factor. From the probability density $P_v = |\psi_v|^2$ we can calculate the velocity variances and covariance:

$$\sigma_u^2 = \frac{s_u^2}{1-\rho^2}, \quad \sigma_v^2 = \frac{s_v^2}{1-\rho^2}, \quad \rho = \frac{\sigma_{uv}}{\sigma_u \sigma_v}. \tag{80}$$

Expressing the coefficients $\{k_u,\ k_{uv},\ k_v\}$ in terms of the η part $p_\eta(\eta)$ of the mean pressure $[\bar{p} = (g/x)^2 p_\eta]$, and adding the subscript F in order to specify that we deal here with the fundamental level (ground state) solution, we find :

$$k_v = \partial_\eta \partial_\eta p_\eta = \frac{1}{4\,\sigma_{vF}^2\,(1-\rho_F^2)^2}\left(\frac{\hbar_v^2}{\sigma_{vF}^2} + \rho_F^2 \frac{\hbar_u^2}{\sigma_{uF}^2}\right), \tag{81}$$

$$k_{uv} = -(3\,\partial_\eta p_\eta + \eta\,\partial_\eta \partial_\eta p_\eta) = -\frac{\rho_F}{4\,\sigma_{uF}\,\sigma_{vF}\,(1-\rho_F^2)^2}\left(\frac{\hbar_u^2}{\sigma_{uF}^2} + \frac{\hbar_v^2}{\sigma_{vF}^2}\right), \tag{82}$$

$$k_u = 6(\bar{p}_0 + p_\eta) + 6\,\eta\,\partial_\eta p_\eta + \eta^2\,\partial_\eta \partial_\eta p_\eta = \frac{1}{4\,\sigma_{uF}^2\,(1-\rho_F^2)^2}\left(\frac{\hbar_u^2}{\sigma_{uF}^2} + \rho_F^2 \frac{\hbar_v^2}{\sigma_{vF}^2}\right), \tag{83}$$

where ρ_F is the correlation coefficient of the ground, and where we have temporarily introduced two constants $\hbar_u$ and $\hbar_v$ for generality. As we shall see in the following, the unicity of this macroscopic Planck-type constant, $\hbar_V = \hbar_v = \hbar_u$, plays a leading role in our demonstration, since it allows us to relate the space and velocity anisotropies of the jet.

One can recombine these equations and simplify them under the form:

$$\partial_\eta \partial_\eta \sigma_v^2 = -k_v, \quad \partial_\eta \sigma_v^2 = \frac{1}{3}(k_{uv} + \eta\,k_v), \quad \sigma_v^2 = \bar{p}_0 - \frac{1}{6}(k_u + 2\,\eta\,k_{uv} + \eta^2 k_v). \tag{84}$$

5.2 Theoretical prediction of the ratio between axial and radial Reynolds stresses

We know that the macroscopic Planck-type constant in v-space is $\hbar_V \propto \varepsilon$, where ε is the kinetic energy dissipation rate and we have moreover suggested that they are actually identical. Two different forms can be given to this constant along the axial and radial directions, according to the standard K41 relation between the standard deviation of velocity fluctuations and length scales:

$$\hbar_u = \frac{\sigma_u^3}{L_u}, \quad \hbar_v = \frac{\sigma_v^3}{L_v}, \tag{85}$$

where L_u and L_v are characteristic length-scales respectively along the x and r directions. If $\hbar_V = \varepsilon$, they are just the integral correlation lengths. However this identification is not

necessary in what follows since only their ratio will be used. It is therefore sufficient to know that they are proportional to the integral length-scales. Let us set:

$$R = \sigma_u/\sigma_v, \quad f = L_u/L_v. \tag{86}$$

We have recalled in Sec. 2.2.4 that the ratio R between the axial and radial turbulent velocity dispersions is expected to be almost constant according to Tennekes and Lumley [3] (see Fig. 3). Experimental data supports this expectation, yielding $R \approx 1.3 - 1.4$.

The Schrödinger equation has been obtained under the K41 scaling, corresponding to universal fractal dimension $D_F = 2$ in v-space, so that we expect the v-Planck macroscopic constant to be unique, i.e., $\hbar_V = \hbar_u = \hbar_v$. Therefore the anisotropy ratio $f = L_u/L_v$ is related to the turbulent intensity ratio $R = \sigma_u/\sigma_v$ as:

$$f = \frac{L_u}{L_v} = \left(\frac{\sigma_u}{\sigma_v}\right)^3 = R^3. \tag{87}$$

We know that the jet is fundamentally anisotropic: its full extension along the radial r coordinate is 2α times its length along the axial x coordinate, and we therefore expect the constant f to manifest this anisotropy, i.e.,

$$f = \frac{1}{2\alpha} \approx 2.5. \tag{88}$$

This expectation is very well verified by experimental data, according to the measurements of Wygnanski and Fieldler [24] (see Fig. 10).

This allows us to derive a theoretical estimate for the velocity dispersion ratio:

$$R = (2\alpha)^{-1/3}, \tag{89}$$

which yields $R = \{1.31, 1.38\}$ for the observed range of opening angles $\alpha = \{0.19, 0.22\}$, in excellent agreement with the experimental data (see Fig. 3). Therefore the small difference between the axial and radial turbulent velocities with respect to the K41 prediction of full isotropy can be attributed to the strong anisotropy of the turbulent round jet.

Reversely, when we shall obtain a theoretical prediction for the R ratio (see next section 5.4), the expected value of α will be derived as:

$$\alpha = \frac{1}{2R^3}. \tag{90}$$

5.3 Relation between the radial Reynolds stress and the velocity variance of the normal state

In the scale-relativity picture, the local velocity PDF of a turbulent fluid is expected to be given by $P_v = |\psi_v|^2$, where the ψ_v's are solutions of the QHO Schrödinger equation written in v-space. We have given experimental proofs of such a theoretical prediction

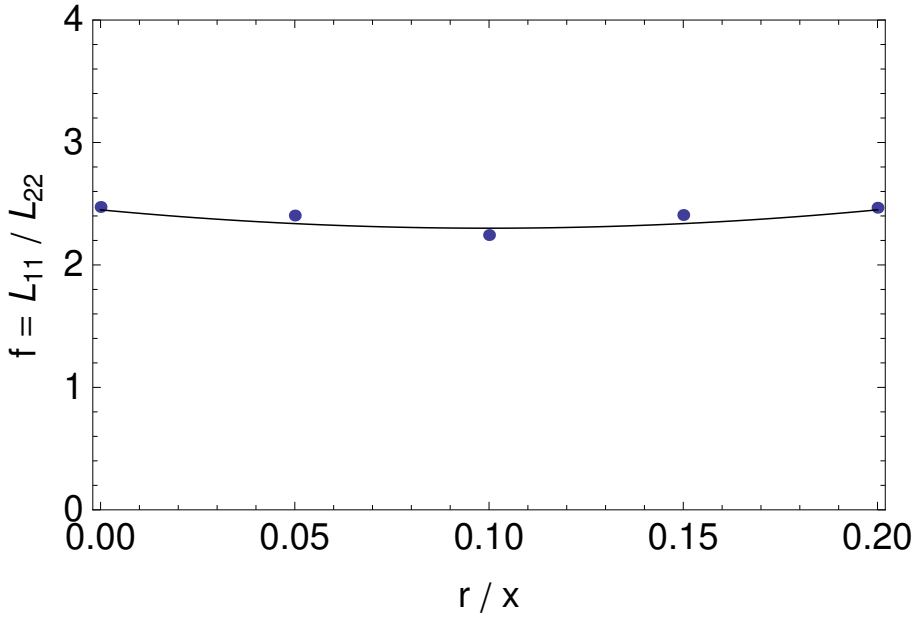

Figure 10: Measurement of the ratio of integral scales along the axial and radial directions according to Wygnanski and Fieldler [24]. This ratio is remarkably constant over the entire jet section and equal to $1/2\alpha = 2.5$ as expected.

in Ref. [16] from analysis of data acquired in contra-rotating von Karman flows at high Reynolds numbers [35].

It is actually possible to decompose any trajectory into sub-trajectories identifiable to QHOs with well-defined quantum numbers and parameters, and jumping from one set of parameters to another set. We give in Figs 11 and 12 two examples of trajectories from Mordant et al. data [35, 36, 37, 38]. We can clearly identify *both* quantum-like behavior and mean corresponding classical behavior in these trajectories, as can be expected from Ehrenfest theorem. The velocity averaged over time-scales $\tau > \approx T_L$ (at which the acceleration PDF itself becomes Gaussian [35]) is given by a classical harmonic oscillator (CHO), while its full PDF (for $|a| < \sigma_a$) including fluctuations is clearly given by a quantum harmonic oscillator PDF (QHO), respectively with quantum numbers $n = 2$ and $n = 3$ (with also damping in the second example). This coexistence of the classical and quantum HO's allows one to identify the various constants (in particular $\hbar_v$) and parameters (ω_v, the offset v_0 etc.) describing locally the trajectory. We complete the proof by another example, now of 2D trajectory (Fig. 13) compared to a simulation of trajectory in a 2D QHO with quantum numbers $(n_x,\, n_y) = (1,\, 1)$.

The probability to have a given excited state is given, according to the principles of statistical physics, by a Gibbs distribution. In the QHO case, this leads to a global Gaussian velocity PDF given by the Bloch formula [40]:

$$dw = \exp\left[-\frac{\omega_v}{\hbar_v}\tanh\left(\frac{\hbar_v\omega_v}{2T_v}\right)v^2\right]dv \tag{91}$$

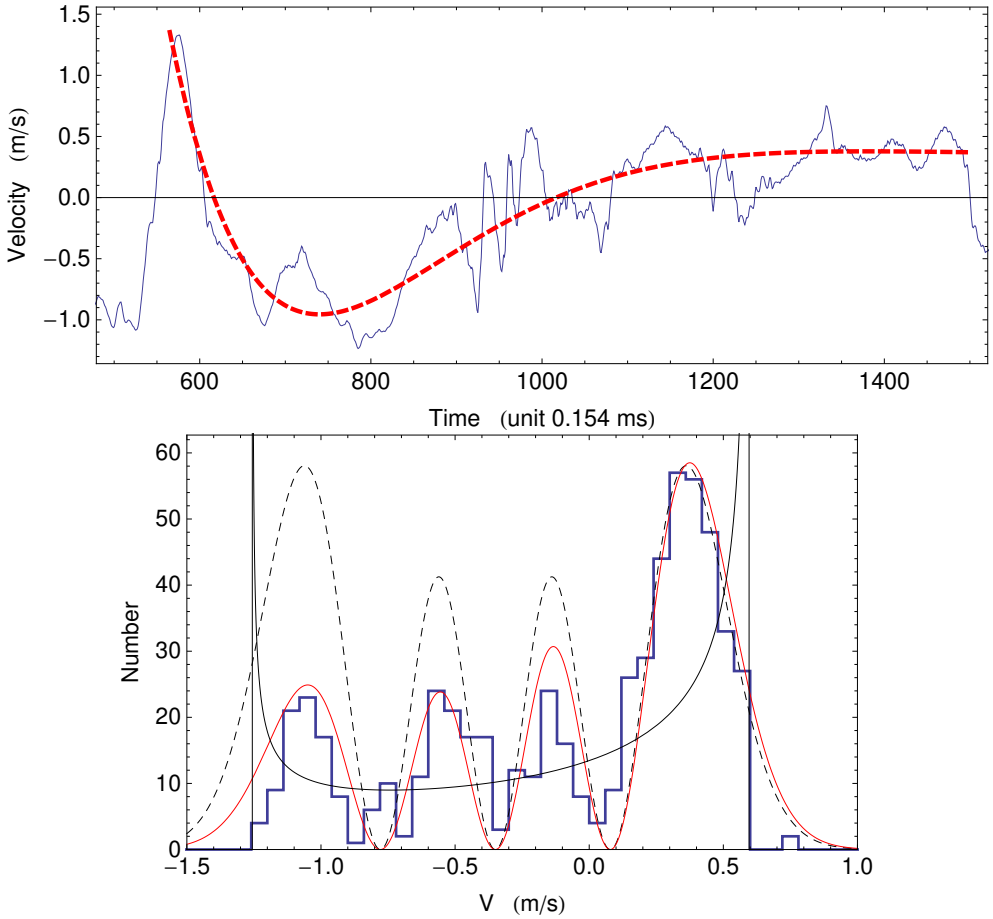

Figure 11: Example of both classical and macroquantum motion of a seed particle in a turbulent flow (Mordant's experiment man290501, part of segment Seg3398 [35, 38]). Top figure: velocity in function of time. The red dashed curve is the fit of the mean velocity (averaged over time-scales $\delta T = 2T_L$) by a classical damped harmonic oscillator (CDHO). Down figure: observed PDF of velocities (blue histogram), for $a < \sigma_a$. It is compared to the expected PDF for a quantum damped harmonic oscillator (QDHO) with $n = 3$ (red curve); the PDF of the corresponding quantum undamped HO (black dashed curve); and the PDF of the underlying (mean) CDHO (thin black curve).

(times a normalization factor). Here T_v is the equivalent of a temperature, but now defined in v-space, so that we expect it to be proportional to the acceleration variance, $T_v = k_B\, \sigma_a^2$.

This result yields an explanation for the known Gaussian global distribution of turbulent velocities [39, 38], which strongly contrasts with its highly non-Gaussian character at the local level [16].

When the v-temperature $T_v \gg \hbar_v \omega_v$ (i.e. for a large R_λ), one recovers the classical Gaussian law with a variance $\sigma_v^2 = T_v/\omega_v^2$. When the temperature is small, $T_v \ll \hbar_v \omega_v$,

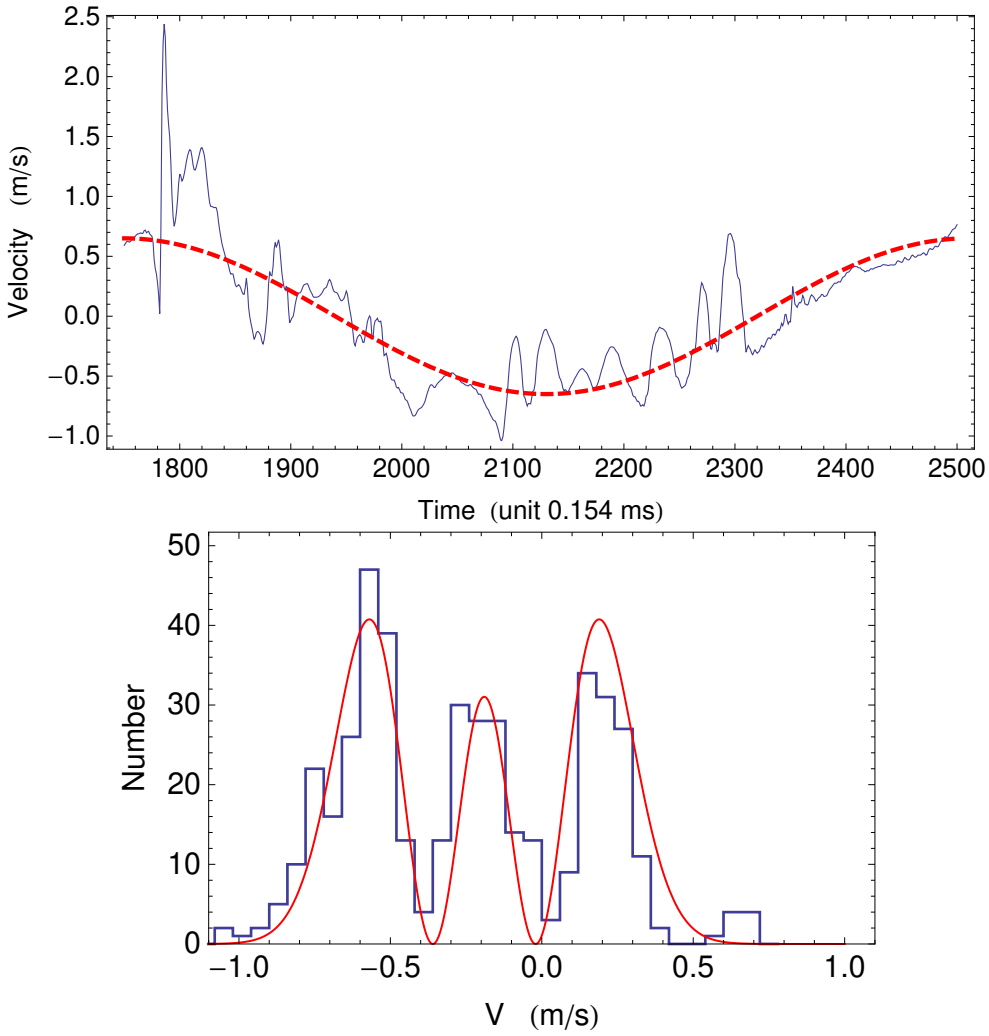

Figure 12: Another example of turbulent trajectory (of duration $5\,T_L$, extract from segment Seg3398 of Mordant's experiment #3-man290501 [35, 38]) well described by a QHO. Top figure: velocity in function of time (blue curve). The velocity averaged over $\tau \approx T_L$ is given by a classical HO (red dashed curve). Down figure: velocity PDF for the same turbulent trajectory, for accelerations $|a| < \sigma_a$ (recall that one expects a macroquantum to classical transition for accelerations larger than their standard error σ_a [16]). It is remarkably well fitted by a QHO PDF with quantum number $n = 2$, $\hbar_v = 4.5 \pm 0.5$ and $\omega_v = 53$. This value of $\hbar_v$ is compatible with $\varepsilon = 21$ [38] once taking account of the large particle size $d = 250\,\mu$m.

the oscillator is no longer excited and it therefore remains in its Gaussian normal state. This means that there are no zero of P_v in this case and therefore no divergence of the acceleration A_q, no intermittency and no large tails of the acceleration PDF. This case can be understood as the transition to turbulence. Therefore the fully developed turbulent case corresponds to $T_v = \sigma_a^2 \gg \hbar_v \omega_v$ and to $\sigma_v^2 \approx T_v/\omega_v^2$.

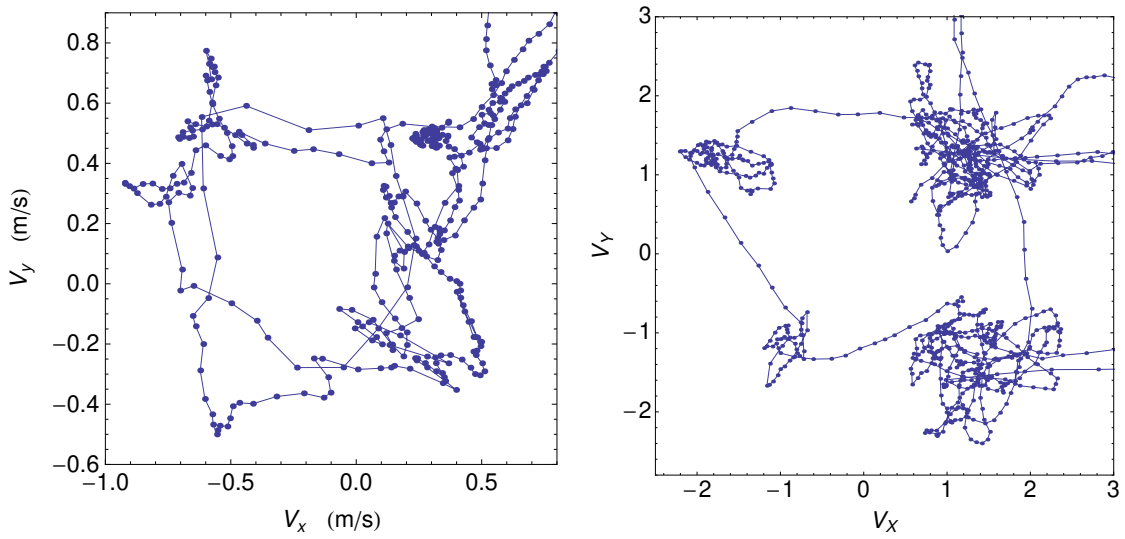

Figure 13: Example of 2D trajectory in Mordant [35, 38] data (extract from Seg2D-193 in experiment man290501-2D) (left figure), compared with a simulation of trajectory in a 2D quantum harmonic oscillator potential with quantum numbers $(n_x,\, n_y) = (1,\, 1)$ (right figure).

5.4 Theoretical prediction of the turbulent jet opening parameter

As reminded hereabove, Tennekes and Lumley [3] have argued that the energy in the u component differs from that in the v component because the major production term feeds energy into σ_u^2 (along the axial direction), so that the energy must leak into σ_v^2 (along the radial direction) by inertial interaction. Since the two effects (axial supply and radial leakage) are determined by the same turbulence dynamics, they conclude that $K = (\sigma_u^2 - \sigma_v^2)/(\sigma_u^2 + \sigma_v^2) \approx$ cst and that it should be less than unity. This implies that $R = \sigma_u/\sigma_v \approx$ cst and that $R > 1$.

In what follows, we shall derive the theoretically expected possible values of R by only using a self-evident property of the turbulent jet which appears clearly in this analysis and in the governing equations, the mere fact that $K \geq 0$, i.e. $\sigma_u \geq \sigma_v$.

Let us now apply this inequality in the scale-relativity framework, where the derivative of the Navier-Stokes equations take a (macroscopic) quantum form. We have decomposed the global Gaussian turbulent velocity fluctuations variances σ_u^2 and σ_v^2 in terms of two-dimensional quantized harrmonic oscillators (QHOs), which are known to be defined by quantum numbers $\{n_u,\, n_v\}$.

The above inequality, applied on the various excited states of a 2D QHO, simply becomes $n_u \geq n_v$. As this level of the analysis we take $R =$ cst, in agreement with Tennekes and Lumley's argument and with its observed relative variation $< \pm 10\%$ except on its edge (see Fig. 3). This allows us to consider only the centerline of the jet, where

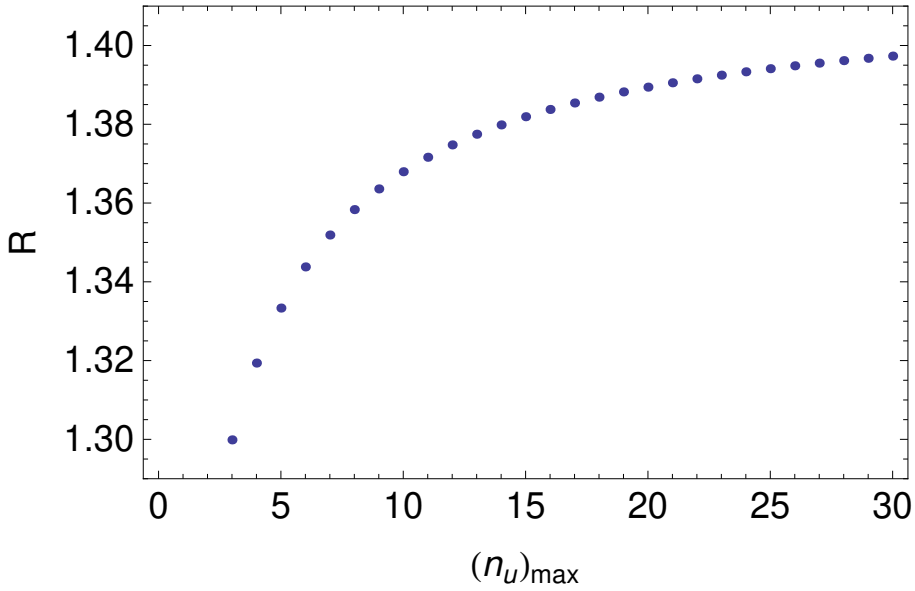

Figure 14: Expected distribution of values for the ratio $R = \sigma_u/\sigma_v$, derived from the decomposition of the turbulent fluctuation velocities into QHOs, for a maximum quantum number $n_u = 30$. The density of points increases for higher R values ~ 1.4 but the probability of smaller values ~ 1.3 is larger according to Gibbs distribution, yielding an average $R \approx 1.34$.

the correlation coefficient is null, so that the variances of each of these QHOs is given by

$$\sigma_{n_u}^2 = (2n_u + 1)\,\sigma_{uF}^2, \quad \sigma_{n_v}^2 = (2n_v + 1)\,\sigma_{vF}^2, \tag{92}$$

where $\sigma_{uF}^2 = \hbar_v/2\omega_u$ and $\sigma_{vF}^2 = \hbar_v/2\omega_v$ are the variances of the normal (ground) state for the u and v coordinates (the PDFs of which are Gaussian).

Toward the centerline of the jet ($\eta \to 0$), one has $\rho_F = 2\eta \to 0$, the ground state becomes isotropic and one obtains $\sigma_{uF} = \sigma_{vF}$.

The global variances will therefore be $\sigma_u^2 = \langle\sigma_{ui}^2\rangle$ and $\sigma_{vu}^2 = \langle\sigma_{vi}^2\rangle$, where the mean is taken on all the QHOs with fluctuating quantum numbers. We find finally:

$$R^2 = \frac{\sigma_u^2}{\sigma_v^2} = \frac{\langle 2n_u + 1\rangle}{\langle 2n_v + 1\rangle} \tag{93}$$

for the PDF of n_u given by the Gibbs distribution and $n_v = \{0,\, 1,\, 2,\, ...,\, n_u\}$. This result corresponds to Cartesian coordinates, and it strictly applies to the plane jet. For the round jet, one jumps to cylindrical coordinates and on gets a hardly different result, $R^2 = \langle 2n_u + 1\rangle/\langle 2n_v + 2\rangle$. We therefore from now on obtain an explanation for the quasi identity of the plane jet and turbulent jet opening angles [9].

When the Reynolds number is large enough, this distribution is almost flat (as a first approximation) and we can take the direct average.

Let us first consider some selected given value of n_u. From statistical physics, one expects only small quantum numbers to play a leading role. For $n_u = 2$, $\langle n_v\rangle = 1$ then

$R = \sqrt{5/3} = 1.29$; for $n_u = 3$, $R = \sqrt{7/4} = 1.32$; for $n_u = 4$, $R = \sqrt{9/5} = 1.34$. These are just the typical values experimentally obtained in the central region of the jet (see Fig. 3).

More generally, taking all the values of n_u between 1 and $(n_u)_{max}$, we find the R values given in Fig. 14. They are distributed between $R = 1.29$ and $R = 1.41$, which is compatible with the experimental data (see [19, 7] and Fig. 3). Identifying this interval with $\pm 2\,\sigma$, we obtain $R_{\rm th} = 1.35 \pm 0.03$, to be compared to the mean experimental value from Panchapakesan and Lumley [19] and Hussein et al. [7] data (for $\eta < 0.18$, since R falls down to $R = 1$ at the edge of the jet where full isotropy is recovered), $R_{\rm exp} = 1.36 \pm 0.04$.

From this result and the previous relation $R = (2\alpha)^{-1/3}$, we derive a theoretical prediction for the turbulent jet opening parameter α:

$$\alpha = \frac{1}{2R^3} = 0.203 \pm 0.013, \tag{94}$$

which agrees with the experimentally obtained value $\alpha \approx 0.2 - 0.21$. The opening angle α_S of the jet in space (defined from the concentration profile) is close to this value (which characterizes the axial velocity radial profile). As already noticed, their ratio can be obtained from the turbulent to laminar transition, which yields a factor $\alpha_S/\alpha = 1.15$, or from Gaussian fits of the concentration and velocity profiles $C = \exp(-K_C\eta^2)$ and $U = \exp(-K_U\eta^2)$ with $K_C \approx 75$ [19] and $K_C \approx 60$ [27] yielding a compatible value $\alpha_S/\alpha = \sqrt{K_U/K_C}$=1.12.

Note that the "classical" prediction $R = \sqrt{2}$ would have given a too low value, $\alpha = 0.177$, so that the quantized nature of the energy (and therefore of the local Reynolds stresses) plays an essential role in this solution of the turbulent jet puzzle.

This result is still reinforced by accounting for the expected Gibbs distribution of the QHOs, which favor smaller values of the quantum numbers. The probability for a QHO to be in a given state of quantum number n can be written as [40]:

$$w(n) = e^{-\frac{1}{2}(2n+1)\frac{\hbar_v \omega}{T_v}}, \tag{95}$$

where $T_v = k_B a^2$ is the equivalent of temperature in v-space, $\hbar_v = \varepsilon = \sigma_v^3/L$, $\omega = 2\pi/T$. We have found from Mordant data that $T = NT_L$, with $N \approx 6$, so that $\omega \approx 1/T_L$. We can now relate all these constants to $R_\lambda = \sqrt{15L\sigma_v/\nu}$, since $\sigma_v \sim R_\lambda^2$, $\sigma_a^2 \sim R_\lambda^9$ and $T_L \sim R_\lambda^{-2}$. One finally finds:

$$\frac{\hbar_v \omega}{T_v} = \frac{\sqrt{15}\,\pi\, C_0}{k_B A_0 N R_\lambda}, \tag{96}$$

where C_0 and A_0 are the two Kolmogorov constants (having values $\approx 4 - 6$), $C_0 = 2\sigma_v^2/\varepsilon T_L$ and $A_0 = \sigma_a^2 \tau_\eta/\varepsilon$. Finally, we find that the constant in the Gibbs distribution in proportional to $1/R_\lambda$. This means, as could be expected, that higher quantum numbers n contribute more for higher Reynolds numbers. Finally the probability can be written under the form:

$$w(n) = \exp\left(-\frac{R_{\lambda_0}}{R_\lambda}\left(n + \frac{1}{2}\right)\right), \tag{97}$$

where the constant $R_{\lambda_0} \approx 100$ from an analysis of Mordant's data.

We find with this value, for a fully developed turbulent jet with $R_\lambda = 1000$ and maximum quantum numbers respectively $n_{max} = (10,\ 20,\ 30)$, $\langle R \rangle = (1.31,\ 1.33,\ 1.335)$. For larger values $n_{max} \leq 50$ the mean value of R stabilizes at $\langle R \rangle = 1.34$. This is just the mean value observed in the center region of the jet. The peak value of its probability density, combining the density of points, see Fig. 14, with the Gibbs probability w, is $R_{peak} = 1.38$, which is the mean value observed in the middle region of the jet, $\eta = 0.05 - 0.16$, see Fig. 3. These improved values agree with the previous rough estimate and yield α in the interval $0.19 - 0.21$.

The experimental value 12.5 deg quoted by Landau [9] corresponds to an angle of 0.218 rad and therefore its tangent is $\alpha_S = r/x = 0.222$. This corresponds to the jet opening angle in space, which is related, as we have seen previously, to the parameter α defined from velocities by $\alpha_S = q\,\alpha$, with $q = 1.10 - 1.15$. This yields an experimental value $\alpha = 0.193 - 0.202$, which is compatible with our theoretical prediction.

It is remarkable that the solution for the value of R, though remaining in the range $1.3 - 1.4$ (and therefore α in the range $0.185 - 0.225$), depends on many different conditions, in particular the maximum level of quantized states attained and the effective distribution of these states for a given experiment, the Reynolds number, the precise values of the parameters in the Gibbs distribution, etc. We therefore do not expect precise values to emerge for R and α, but different values for different experiments fluctuating in a somewhat uncontrolable way. They however remain in a well defined narrow interval of relative width $<\approx 10\%$, a result that experimental and numerical measurements tend to support.

5.5 Theoretical prediction of the pressure / radial stress profile

It is known that the radial Reynolds stress has zero slope at the origin [1, 19, 7, 2]. Therefore the power series expansion of σ_v to order η^2 (in the core of the jet) may be written as:

$$\sigma_v = \frac{g}{x}\,\mu\,\left(1 - a\,\frac{\eta^2}{\alpha^2}\right), \tag{98}$$

where a is a purely numerical constant and $\mu \approx 0.2$ is the centerline value of the radial turbulent intensity, while we recall that $g = U_0 a_0 \approx 6\,R_e\,\nu$.

We find an excellent fit of Hussein et al. [7] data by this function in the inner part of the jet ($\eta <\approx 0.15$) with $a = 0.745 \pm 0.005$ (see Fig. 17). This agrees with other sources [19, 24] which globally yield $a = 0.75 \pm 0.05$, i.e. $a = 3/4$. Actually, since a and α do not appear separately in this expression, we can set $a = 3/4$ and consider it as a new *definition* of α, which fully agrees with that coming from U and V.

The pressure, or equivalently the radial Reynolds stress $\sigma_v^2 = -\bar{p}$, is solution of the k_v equation (81), which may be written under the form:

$$k_v = -\partial_\eta \partial_\eta\,\sigma_v^2 = H_0\,\sigma_v^2\,\frac{(1 + \rho_F^2/R_F^2)}{(1+h)^2\,(1-\rho_F^2)^2}, \tag{99}$$

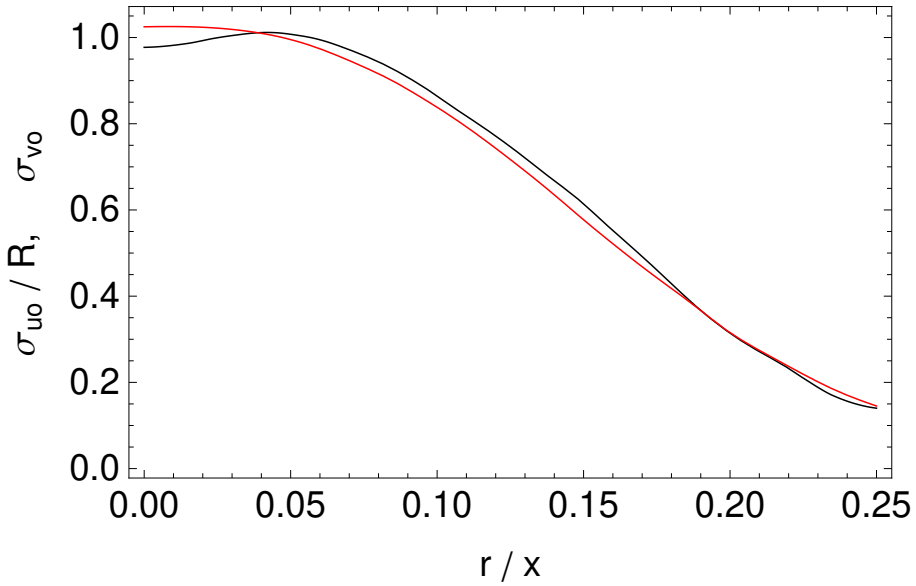

Figure 15: Pure radial profiles of the turbulent velocity intensities in turbulent round jets, in function of the scaled variable $\eta = r/x$. The curves show the average of experimental measurements by Hussein et al [7] and Panchapakesan and Lumley [19]. The black curve gives the mean profile of σ_u/λ and the red curve of σ_v/μ (λ and μ being respectively the σ_u and σ_v amplitudes on the centerline of the jet – besides the g/x dependence, see text).

where ρ_F and R_F are respectively the velocity correlation coefficient of the ground state and the velocity dispersion ratio $R_F = \sigma_{uF}/\sigma_{vF}$ of the ground state. We have written the η dependence of $H = 1/4 g_v^4 L_v^2$ as $H(\eta) = H_0[1 + h(\eta)]^{-2}$, with H_0 its value on the jet centerline.

We know that $\rho_F(\eta) \to 0$, $h(\eta) \to 0$ and $R_F(\eta) \to 1$ when $\eta \to 0$, so that we obtain a first approximation for the solution of this equation by neglecting the perturbative terms. Such a solution is expected to be valid in the central region of the jet. The equation becomes a mere harmonic oscillator differential equation:

$$\partial_\eta \partial_\eta \, \sigma_v^2 + H_0 \, \sigma_v^2 = 0. \tag{100}$$

The general solution of this equation is a linear combination of cosine and sine solution. However, the constraint of zero slope at the origin implies the vanishing of the sine term. The same conclusion can also be obtained from the second (k_{uv}) equation. Then we find a theoretical solution for the profile of the jet radial turbulent velocity variance, $\sigma_v^2 = \mu^2 \cos(\sqrt{H_0}\ \eta/\alpha)$, valid in the center region of the jet, i.e. for small η values. A power series of this solution, compared with Eq. (98) with $a = 3/4$, yields $H_0 = 3/\alpha^2$ and finally (re-introducing the x scaling dependence):

$$\sigma_v^2 = \frac{g^2}{x^2}\, \mu^2 \, \cos\left(\sqrt{3}\, \frac{\eta}{\alpha}\right). \tag{101}$$

The amplitude μ remains unpredicted at this level of the analysis (we shall obtain a theoretical prediction for it in the following), i.e., only the pure profile $\sigma_{vo}(\eta) = \sigma_v(\eta)/\mu$ is theoretically predicted up to now. This theoretical solution is in very good agreement with the shape of σ_v^2 known from experimental data and from DNS in the inner 3/4th of the jet (see Fig. 17). Moreover, this solution allows one to obtain the η profile of the velocity correlation coefficient: one finds it to be constant throughout the main part of the jet ($\eta = 0.05 - 0.15$). The value of this constant (≈ 0.4) will be determined in the following, once the value of the Reynolds stress amplitude is theroretically predicted.

The corresponding radial profiles across the jet of k_u, k_{uv} and k_v for this cosine solution are shown in Fig. 16.

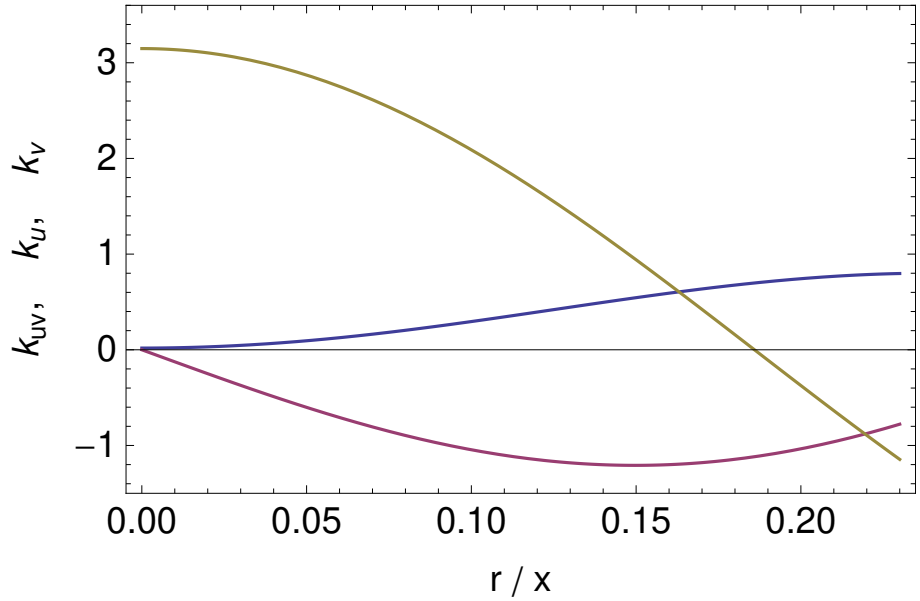

Figure 16: Profiles of k_u (blue curve), k_{uv} (magenta curve) and k_v (brown curve) in function of the scaled radial distance $\eta = r/x$, calculated for $\sigma_v^2 = \mu^2 \cos(\sqrt{3}\,(\eta/\alpha)$ (without the x dependence), with $\mu = 0.217$ and $\alpha = 0.205$. We have taken here $\bar{p}_0 = \mu^2$ in Eq. (83), which allows k_u to remain positive, then ensuring an attractive harmonic oscillator potential in the axial direction.

5.6 Generalized solution for the pressure and radial Reynolds stress profile valid up to the jet boundary

5.6.1 Corrective term in the radial stress equation equation

Let us now derive an improved solution accounting for the perturbative terms, that we expect to be valid throughout the whole jet. Setting $z = \eta/\alpha$, we now write the exact k_v equation as:

$$\partial_z \partial_z \, \sigma_v^2 + H_0 \, (1 + w(z)) \, \sigma_v^2 = 0, \tag{102}$$

where $H_0 = 3/\alpha^2$. The corrective term writes:

$$1 + w = \frac{(1 + \rho_F^2/R_F^2)}{(1+h)^2(1-\rho_F^2)^2}, \tag{103}$$

where we recall that $\rho_F(z)$ is the radial profile of the correlation coefficient in the ground state, $R_F(z)$ is the ground state ratio σ_{uF}/σ_{vF} and $H = 1/(4g_v^4 L_v^2) = H_0(1+h(z))^{-2}$.

As explained in Appendix C, we find that $w(z) = 1 + w_2 z^2 + w_4 z^4$ with $w_2 = 0$, so that the full Reynolds stress differential equation writes:

$$\partial_z \partial_z \sigma_v^2 + 3\,\sigma_v^2\,(1 + w_4\, z^4) = 0. \tag{104}$$

The solution of this equation amounts to a stretching of the cosine solution toward the jet edge:

$$\sigma_v^2 = \mu^2\ \cos\left(\frac{\sqrt{3}\,z}{1 + a_4\, z^4}\right). \tag{105}$$

where $a_4 = -w_4/30$ (see Appendix C) and where the coefficient a_2 of the z^2 contribution is found to vanish.

5.6.2 Comparison with experimental data

Hussein et al [7] experimental data are well fitted on the whole jet by this stretched cosine solution for $a_4 = 0.178 \pm 0.003$ (Fig. 17), which corresponds to a corrective term in the k_v equation given by $w_4 = -5.4$ (with the linear relation) and $w_4 = -7.5$ (with the non linear correction, see Appendix C). Taking the mean data from HCG [7] and PL [19], one finds compatible values $a_2 = 0.001 \pm 0.017$ and $a_4 = 0.167 \pm 0.014$. DNS data [5] yield similar results .

As we shall see in the following Sec.6, the value of a_4 can be theoretically predicted from the second (k_{uv}) differential equation obtained from the v-Schrödinger equation and is found to be just the experimentally observed value $a_4 = 0.18$.

6 Theoretical prediction of the turbulent fluctuation amplitudes

6.1 Statement of the problem

Up to now we have just obtained a theoretical prediction for the turbulent intensity pure profile $\sigma_v(\eta)/\mu$ and therefore of the pressure profile across the jet. But its amplitude μ remained undefined from the only k_v equation.

This amplitude should be predictable from the second differential equation involving $k_{uv} = \partial_x \partial_r \bar{p}$ and the Reynolds shear stress σ_{uv}, since the mean pressure $\bar{p}$ depends on μ while σ_{uv} does not.

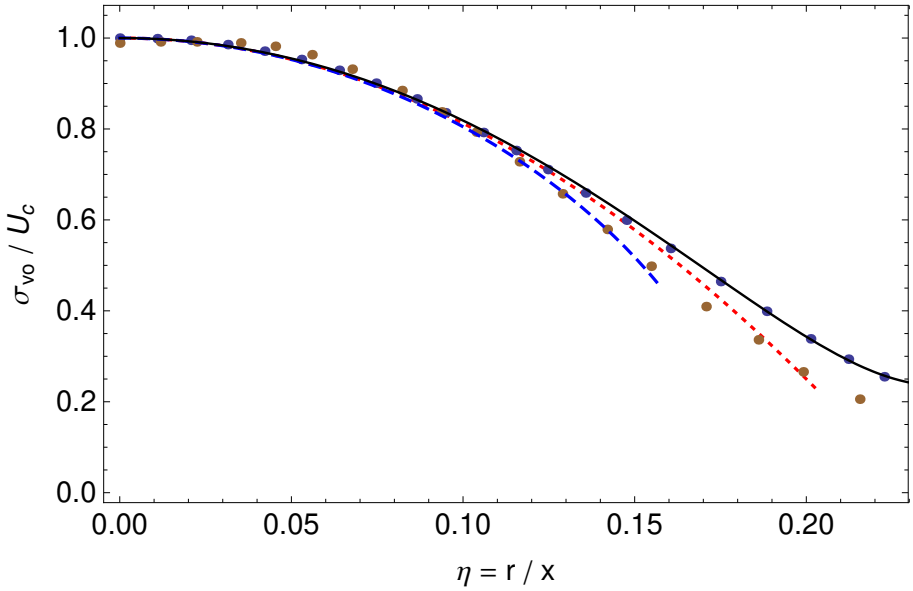

Figure 17: Experimental normalized profile of the radial turbulent velocity dispersion from Hussein et al. data [7, 2] (blue points) and Panchapakesan and Lumley [19] (brown points) compared with: (1) a fit of the inner part of the jet by the function $\sigma_v = \mu\,(1 - 3\eta^2/4\alpha^2)$ (red dotted curve, $\alpha = 0.2$); (2) our analytical solution to the macroscopic Schrödinger equation in the center region, $\sigma_{vo} = \cos\left(\sqrt{3}\,\eta/\alpha\right)^{1/2}$ (blue dashed curve, $\alpha = 0.2$); (3) our theoretical full stretched cosine solution accounting for perturbative terms (Eq. 105 with $\alpha = 0.205$ and $a_4 = 0.18$, black curve). The experimental (brown) points [19] are well fitted by a slightly smaller value of $\alpha = 0.195$.

Practically, this means that we can use our knowledge of σ_{uv} for deriving a second expression for $\sigma_v^2 = -\bar{p}$ from the second differential equation involving k_{uv}. Then the solution we are looking for will be obtained by identifying the two expressions.

In order to proceed further, let us separate the σ_v pure profile (i.e. normalized to 1 on the jet centerline) from its amplitude by writing:

$$\sigma_v = \mu\,\sigma_{vo}, \tag{106}$$

where the pure profile has been found to be $\sigma_{vo} = \cos(\sqrt{3}\,\eta/\alpha)$, corrected by a stretching term when approaching the jet boundary. In the same way, we define $\bar{p} = \mu^2\,p_o$, where p_o is the pure pressure profile. We obtain the equation:

$$\mu^2\,(3\,\partial_\eta p_o + \eta\,\partial_\eta\partial_\eta p_o) = H\,B\,\frac{\sigma_{uv}}{(1-\rho_F^2)^2}. \tag{107}$$

We express a possible variation of H across the jet by writing it as $H = H_0/(1+h(\eta))^2$, where $h \ll 1$ in the inner 3/4th of the jet and may increase around the jet boundary. We have found that $H_0 = 3/\alpha^2$ on the centerline of the jet.

We also introduce the ratio $R_F = \sigma_{uF}/\sigma_{vF}$ of the velocity variances in the ground state: we know that $R_F = 1$ at the origin $\eta = 0$ and on the jet boundary. The parameter B can be written as:

$$B = \frac{\rho_F}{\rho} \frac{1 + R_F^2}{R_F^3 \, R}. \tag{108}$$

Defining $k_{uvo} = -(3 \, \partial_\eta p_o + \eta \, \partial_\eta \partial_\eta p_o)$ and setting $X = \mu\sqrt{R} = \sqrt{\lambda \, \mu}$, where λ is the amplitude of σ_u, we can therefore write the equation for the Reynolds stress amplitude under the form:

$$X^2 = \frac{6 \, \sigma_{uv}}{\alpha^2 k_{uvo}} \times \frac{\rho_F}{\rho \, (1 - \rho_F^2)^2 (1 + h)^2} \frac{1 + R_F^2}{2 \, R_F^3}. \tag{109}$$

Solving this equation for X would yield the value of μ owing to the theoretical knowledge of the turbulent intensities ratio $R = \sigma_u/\sigma_v \approx 1.35$ that we have previously achieved. However, this solution is expressed in terms of unknown functions of η, $\rho(\eta)$, $\rho_F(\eta)$, $R_F(\eta)$ and possibly $R(\eta)$ (which is almost constant across the jet, but is expected to fall down to $R = 1$ on the jet edge where full isotropy is recovered).

Nevertheless, we know the values of these functions on the jet centerline ($\eta = 0$) and we can infer their behavior when η tends toward the turbulent-laminar transition, in the following way.

6.2 A characteristic function

In our scale-relativity description of turbulence, we have seen that the velocity evolution over time is given by QHOs with quantum numbers which vary according to the energy fluctuations in a probabilistic way determined by the laws of statistical physics. The intermittency signature of turbulence (such as the alternation of calm behavior and strong bursts, the large non-Gaussian tails of the acceleration PDF, etc.) is understood in this framework as due to the zeros of the velocity PDF, $P_v(v_i) = 0$, which exist for all excited states and lead to the emergence of a force / acceleration $A_q = \pm\frac{1}{2}\hbar_v(\partial_v P_v)/P_v$ which is divergent around the points $v = v_i$ [15, 16].

On the other hand, the laminar flow (which is reached beyond the turbulent-laminar transition $\alpha_S = q \, \alpha$, with $q \approx 1.15$) corresponds to the full disappearance of all these effects: the K41 scaling $\delta v^2 \sim \delta t$ vanishes, so that the derivative of the NS equations remains classical and there is no longer any macroscopic Schrödinger equation.

But, between the fully turbulent domain inner to the jet ($\eta <\approx \alpha$) and the laminar flow $\eta > \alpha_S$, there should exist an intermediate regime in which the Schrödinger equation is still active while the energy is low, so that excited states do not occur and only the Gaussian ground state manifests itself. Moreover, in this region the axial and radial Reynolds stresses become equal, i.e. $\sigma_{uF} = \sigma_{vF}$ (full isotropy).

Let us therefore define the function:

$$F(\eta) = \sqrt{\frac{6 \, \sigma_{uv}}{\alpha^2 \, k_{uvo}}} = X \sqrt{\frac{\rho}{\rho_F}} \, (1 - \rho_F^2) \left(\frac{2 \, R_F^3}{1 + R_F^2} \right)^{1/2} (1 + h). \tag{110}$$

Consider first the behaviour of this function in the central region of the jet. When $\eta \to 0$, $R_F \to 1$, $\sigma_{uv} \to \eta/2$, so that $\rho = \sigma_{uv}/(R\mu^2\sigma_{vo}^2) \to \eta/2X^2$, $\rho_F \to 2\eta$ so that $\sqrt{\rho/\rho_F} \to 1/2X$. Finally, with $h \to 0$, we find that when $\eta \to 0$, $F(\eta) \to 1/2$.

Consider now the behavior of $F(\eta)$ when $\eta \to \alpha_S = q\,\alpha$, the turbulent-laminar transition. We have seen that $\rho \to \rho_F$ with $\rho \to 0$ and $R_F \to 1$. Therefore the function $F/(1+h)$, which is identical to $F(\eta)$ in the inner region of the jet, tends asymptotically toward the numerical constant X that we are looking for.

This leads us to define the function:

$$G(\eta) = \frac{F(\eta) - X}{\frac{1}{2} - X}, \tag{111}$$

resulting from a translation and a dilation of $F(\eta)$, i.e., to describe the profile of $F(\eta)$ as:

$$F(\eta) = \frac{1}{\alpha}\sqrt{\frac{6\,\sigma_{uv}}{k_{uvo}}} = X + G(\eta)\left(\frac{1}{2} - X\right). \tag{112}$$

The function $G(\eta)$ is expected to be theoretically given by some expression $G_s(\eta)$ having the following properties:

- Its value on the centerline of the jet is $G(0) = 1$, then it decreases. We can therefore write its power series expansion around the origin as: $G(\eta) = 1 - \eta^2/(2s^2\alpha^2)$ when $\eta \to 0$.

- It tends asymptotically to 0 when η approaches the turbulent-laminar transition $\alpha_S = q\,\alpha$.

As we shall now show, $G_s(\eta)$ is very precisely a Gaussian function that yields a second expression for the solution to the pressure profile across the jet.

6.3 Theoretical prediction of the stress amplitude in the jet central region

Let us define a Gaussian function of variance s^2 for the variable $z = \eta/\alpha$:

$$G_s(z) = \exp\left(-\frac{1}{2}\,\frac{z^2}{s^2}\right). \tag{113}$$

Recall that in the central region of the jet ($\eta \leq \alpha/\sqrt{10}$), we have obtained from the RANS equations and the v-Schrödinger equation the following quasi-exact solutions:

$$\sigma_{uv} = \frac{1}{2}\,\frac{\eta}{(1 + 2\,(\eta/\alpha)^2)^3}, \qquad -p_o = \sigma_{vo}^2 = \cos\left(\sqrt{3}\,\frac{\eta}{\alpha}\right). \tag{114}$$

From these solutions of the hydrodynamics equations, we can calculate the expression of G in the central region of the jet (setting $z = \eta/\alpha$ and $Q = \frac{1}{2} - X$ in order to simplify its writing):

$$G = 1 + \frac{1}{Q}\left(\frac{1}{(1+2z^2)^{3/2}\,(\cos(\sqrt{3}z) + \sqrt{3}\,\sin(\sqrt{3}z)/z)^{1/2}} - \frac{1}{2}\right). \tag{115}$$

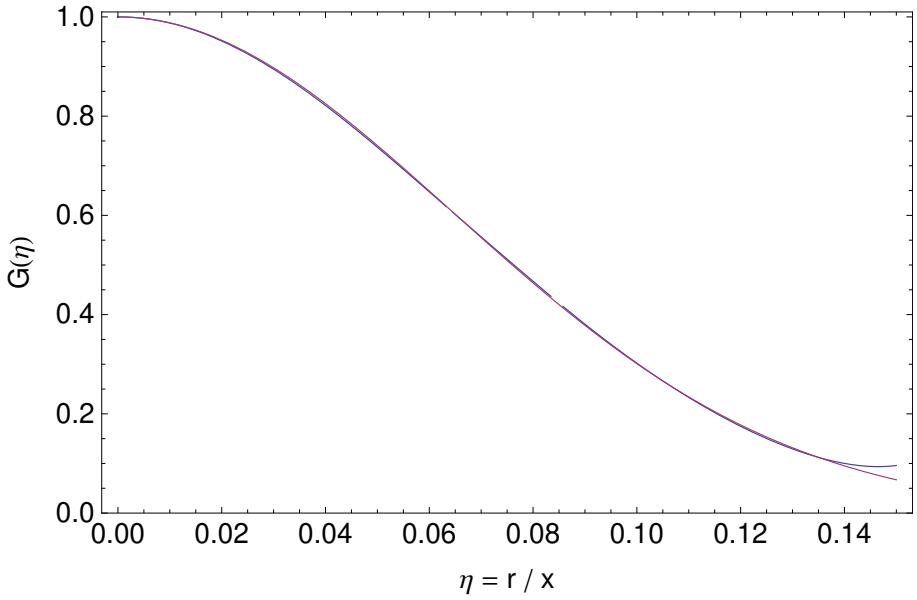

Figure 18: Comparison between the function $G(\eta)$ (Eq. (111), blue curve), and the Gaussian function $G_s(\eta)$ (Eq. (113), magenta curve). The function $G(\eta)$ is established from σ_{uvtot} (defined in Sec. 3.2 and Appendix A) and the stretched cosine profile solution for p_o. The two functions agree remarkably well up to the $\approx 3/4$th of the jet, within which they are clearly indistinguishable. They begin to depart one from another only for $\eta > 0.14$, as expected. The standard deviation of their differences is only 2.3×10^{-3}, as illustrated in Fig. 19.

The power series expansion of $G(z)$ to order z^4 writes:

$$G(z) = 1 - \frac{21}{16\,Q}\,z^2 + \frac{4167}{1280\,Q}\,z^4 + \mathcal{O}[z^6], \tag{116}$$

while for a Gaussian function it writes:

$$G(z) = 1 - \frac{z^2}{2\,s^2} + \frac{z^4}{8\,s^4} + \mathcal{O}[z^6]. \tag{117}$$

The identification of the z^2 terms of the power series of G and G_s yields a first relation $Q = \frac{21}{8}s^2$ and therefore:

$$X = \frac{1}{2} - \frac{21}{8}s^2. \tag{118}$$

The identification of the z^4 term of G with that of the Gaussian function G_s yields a second relation:

$$\frac{1}{8\,s^4} = \frac{4167}{1280\,Q}, \tag{119}$$

from which we obtain $Q = 4167/160s^4$ and therefore:

$$s^2 = \frac{140}{1389} = 0.1008, \quad X = \frac{109}{463} = 0.2354, \tag{120}$$

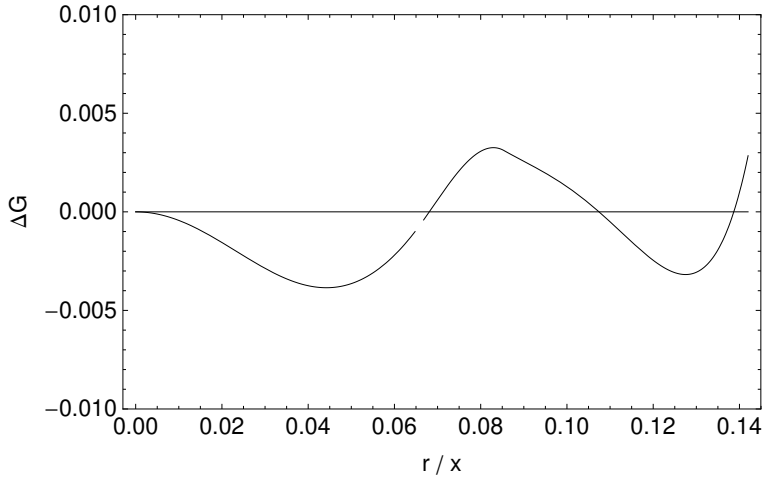

Figure 19: Optimized difference between the function $G(\eta)$ (Eq. (111), $\eta \leq 0.14$), calculated from the precise solution σ_{uvtot} of the RANS equations – see Sec. 3.2 and Appendix A – and the stretched cosine solution of the v-Schrödinger equation, and the Gaussian function $G_s(\eta)$ (Eq. 113), which are directly compared in Fig. 18. The standard deviation of the residuals is only 0.002. The small gap corresponds to the first matching point ($\eta = \alpha/\sqrt{10} \approx 0.065\alpha$) of the precise solution for U, V, from which we derive $\sigma_{uv} = UV - \eta U^2$.

very close to the inflection point $s = 1/\sqrt{10}$ which would yield $X = 19/80 = 0.2375 \approx 1/4$. It is noticeable that this solution is independant from α.

6.4 New pressure analytical solution of the Schrödinger equation

We can also combine the two k_v and k_{uv} equations to obtain a first order differential equation for the pressure profile (in the central region approximation $h \to 0$ and $\rho_F \to 0$):

$$\alpha^2\, \partial_\eta p_o(\eta) = \eta\, p_o(\eta) + M(\eta). \tag{121}$$

where

$$M(\eta) = \frac{2\,\sigma_{uv}(\eta)}{(X + (1/2 - X)\, G_s(\eta))^2}. \tag{122}$$

Setting as before $z = \eta/\alpha$ in order to simplify the writing, this equation can be analytically solved under the form:

$$p_o(z) = e^{z^2/2} \left(-1 + \int e^{-z^2/2} M(z) dz \right). \tag{123}$$

Let us show that it indeed provides a new complementary solution for the pressure in the central region of the jet. Its power series expansion up to order z^6 writes:

$$-\,p_o = 1 - \frac{3}{2} z^2 + \frac{3}{8} z^4 - \frac{279 s^2 - 28}{32 s^2} z^6, \tag{124}$$

to be compared with the power series expansion of our previous k_v equation solution, $p_o = -\cos(\sqrt{3}\,z)$,

$$-p_o = 1 - \frac{3}{2}z^2 + \frac{3}{8}z^4 - \frac{3}{80}z^6. \tag{125}$$

It is remarkable that the two solutions fully coincide up to order z^4. Moreover, the identification of the z^6 coefficient provides us with a solution for the numerical value of the constant s:

$$s = \sqrt{\frac{140}{1389}} = 0.3175, \tag{126}$$

which is just the previously obtained value. This quasi perfect identification of the two functions in the central region of the jet (up to $\eta \approx 0.1$, i.e. $z \approx 0.5$) proves that the new solution Eq. (123) solves both the k_v and k_{uv} equations, which fully justifies the Gaussian character of $G = G_s$.

As already remarked, the resulting dispersion $s \approx 1/\sqrt{10}$ is just the peak position of σ_{uv} and the inflection point of $a(\eta)$, i.e. the first matching point of our precise solution U_{tot} (see Sec. 3.2 and Appendix A). From this approximation $s^2 = 1/10$, we find the simple solution $X = 19/80 \approx 1/4$.

This means that we have finally obtained a theoretical understanding, from the scale-relativity approach, of the typical value $X = \sqrt{\lambda\,\mu} \approx 1/4$ measured by laboratory and numerical experiments, which was one of the main mysteries of the turbulent jet.

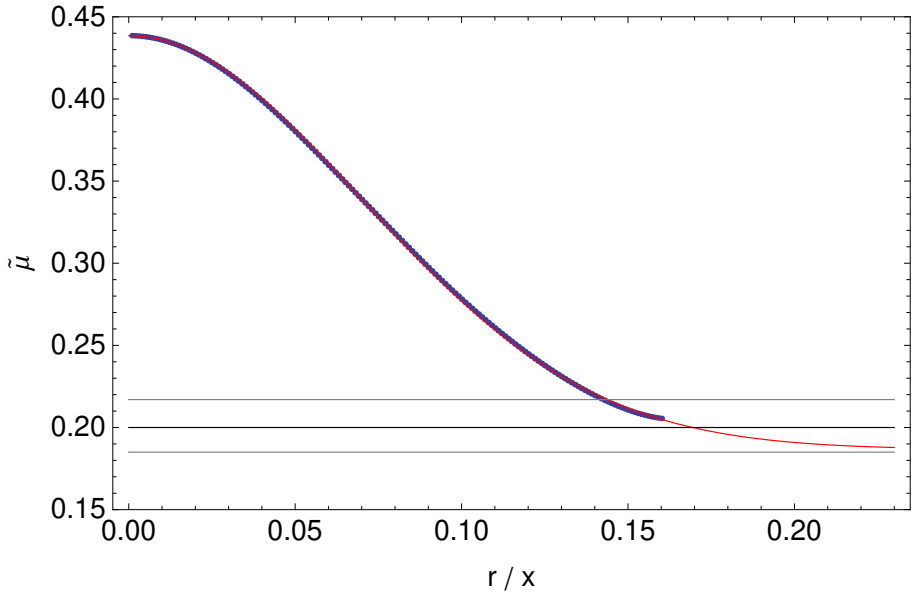

Figure 20: Comparison between the theoretical function $F(\eta)/\sqrt{R}$ (Eq. (112), blue thick curve, $\eta \leq 0.16$, $R = 1.3$) and the function $\tilde{\mu} = \mu + \left(\frac{1}{2} - X\right) G_s(\eta)/\sqrt{R}$, where G_s is the Gaussian function Eq. (113) (red curve, which tends to μ asymptotically). The two horizontal gray lines are the experimentally observed range for the values of the radial turbulent intensity amplitude on the jet centerline, $\mu = \sigma_v(0)$.

We can still improve this result by using better solutions for σ_{uv} and for the p_o profile in the calculation of the function $G(\eta)$. We take σ_{uvtot}, obtained from matching precise solutions of the RANS equations (see Sec. 3.2 and Appendix A) and p_{os}, the stretched cosine solution to the k_v QHO equation. We are then able to theoretically predict the free parameters of these functions, X, s and a_4, by finding, through least-square optimization, a numerical solution of the equation $G(\eta) = G_s(\eta)$. The α dependence is found to be very small, in agreement with our previous central region solution which was indeed independent of *alpha*. We get for $\eta \leq 0.14$ (see Appendix D and Figs. 27 and 28):

$$X = 0.2370 \pm 0.0003, \quad s = 0.3225 \pm 0.0004, \quad a_4 = 0.180 \pm 0.003, \tag{127}$$

where the residual fluctuation takes the very small value $\sigma_\xi = 0.0023$ (compared with functions normalized to unity).

The values of X and s found here remain very close to the analytical solution obtained in the central region of the jet (well approximated by $X = 19/80 = 0.2375$ and $s^2 = 1/10$) and, remarkably, the predicted value of a_4 is the same as that previously derived from the stretching of the cosine solution for p_o.

6.5 Theoretical prediction of the turbulent intensity amplitudes

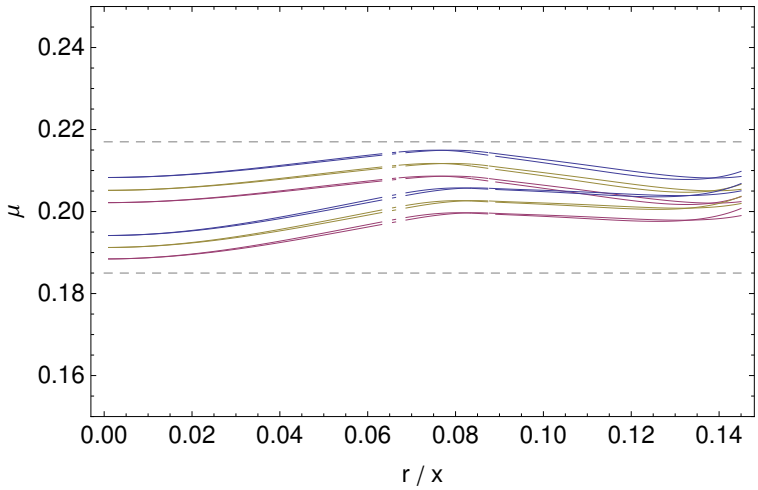

Figure 21: The running value across the jet of the amplitude μ of the turbulent fluctuation σ_v in function of the scaled radial distance $\eta = r/x$, as given by Eq. (128). It remains globally constant over the inner 3/4th of the jet and agrees with the experimentally observed range (dashed lines). The various curves are calculated for $\alpha = (0.20, 0.21)$ (small differences), $s = (1/\sqrt{10} = 0.316, 0.326)$ (largest differences) and $R = (1.30, 1.34, 1.38)$ (blue, beige and magenta curves).

Finally, from our results $X = (0.2350 - 0.2375)$ and $R = (1.30 - 1.38)$, we can derive the range of possible values for the turbulent intensity amplitude $\mu = X/\sqrt{R}$ (see Fig. 21),

and therefore of $\lambda = R\,\mu$:

$$\mu = \frac{1}{2\sqrt{R}}\,\frac{2F(\eta) - G_s(\eta)}{1 - G_s(\eta)} = 0.202 \pm 0.013. \tag{128}$$

This result is in full agreement with the measured values from laboratory and numerical experiments, which lie in the range $(0.185 - 0.217)$ [7, 19, 5]. It is in particular remarkable that the theoretically obtained value for μ, Eq. (128), seems to be a running function of $\eta = r/x$ from its expression, but that it is found to be practically unvarying, as expected from its nature of constant parameter, as can be seen in Fig. 21.

7 Theoretical prediction of the velocity correlation coefficient

The correlation coefficient of velocities is universally found to be $\rho \approx 0.4$ for all free shear flows [2, 3]. This is one of the main mysteries of turbulent flows, for which we are now able to suggest a solution, at least in the turbulent jet case.

In function of the various variables we have introduced, the correlation coefficient may be successively written as:

$$\rho = \frac{\sigma_{uv}}{\sigma_u \sigma_v} = \frac{\sigma_{uv}}{R\,\sigma_v^2} = \frac{\sigma_{uv}}{R\,\mu^2\,\sigma_{vo}^2} = -\frac{\sigma_{uv}}{X^2\,p_o}, \tag{129}$$

where we recall that $X^2 = R\,\mu^2$ and that p_o is the mean pressure profile normalized to unit amplitude on the jet centerline.

As a first order approximation, the Reynolds shear stress writes $\sigma_{uv} = -UV + \eta\,U^2$, and it is given by the solutions U and V of the RANS equations,. Another more complete expression involves our theoretical solutions for R and σ_v^2 (with $\sigma_u = R\,\sigma_v$), $\sigma_{uv} = -UV + \eta(U^2 + (R^2 - 1)\sigma_v^2)$.

From the known expression of σ_{uv} and the pression pure profile, we have already reached the conclusion (Sec. 5.5) that the correlation coefficient profile is almost constant in the middle part of the jet, but without knowing the value of this constant at this level of the analysis. Since we have now at our disposal theoretical predictions for all parameters (α, q, R and μ), we can construct a theoretical radial profile for ρ. It is given as the continuous black curve in Fig. 22 and is shown to be in excellent agreement with the profiles derived from experimental data.

We have now a theoretical prediction for the value of X and we can therefore derive that of the correlation coefficient. From the shear stress expression obtained in the jet central region, $\sigma_{uv} = \frac{1}{2}\,\eta(1 + 2\eta/\alpha)^3$ and the power series expansion of the cosine solution of the v-Schrödinger equation, $\sigma_{ov} = 1 - \frac{3}{4}\,(\eta/\alpha)^2$, we obtain the following radial variation of the correlation coefficient:

$$\rho(\eta) = \frac{\eta}{2X^2\,\left(1 - \frac{3}{4}\,\frac{\eta^2}{\alpha^2}\right)^2\,\left(1 + 2\,\frac{\eta^2}{\alpha^2}\right)^3}\,. \tag{130}$$

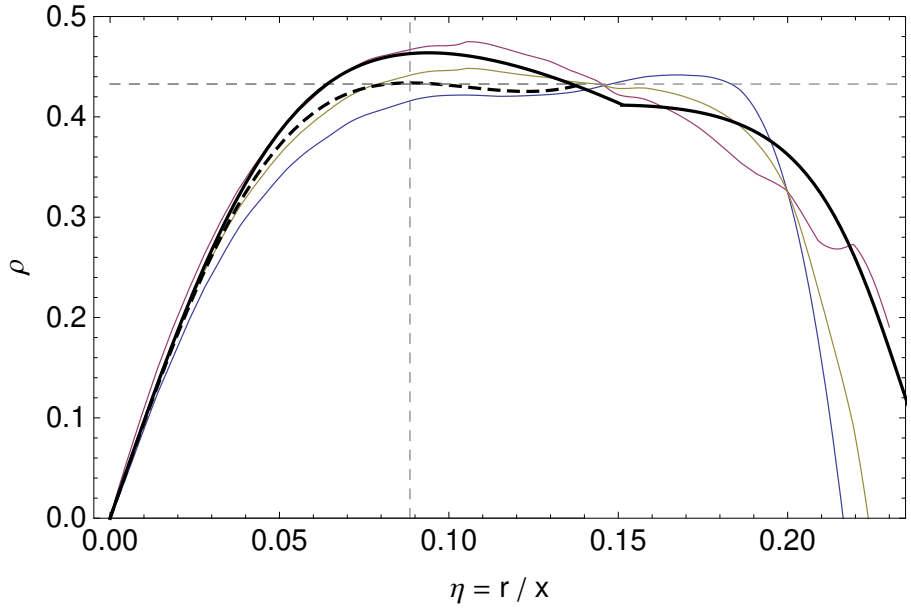

Figure 22: Theoretically predicted radial profile of the velocity correlation coefficient, compared with the experimentally observed profiles (blue curve from HCG data [7], magenta curve from PL data [19] and their mean, beige curve). The black dashed curve is the theoretical prediction for σ_{uv} given by the constant turbulent viscosity solution (valid in the central region of the jet). The continuous black curve is the prediction for $\rho(\eta)$ from the more complete matched solution of Sec. 3.3 and Appendix B (with $\alpha = 0.21$, $k = 0.408$, $a_4 = 0.18$ and $\mu = 0.195$), in which we have taken the Reynolds stress profile $\sigma_v^2(\eta)$ given by our stretched cosine solution and, for the R ratio, our predicted constant value $R = 1.35$ up to $\eta = 0.15$, then a decreasing linear behavior down to its expected value $R = 1$ on the jet edge.

The derivative of this function yields the position of its peak at $\eta_p = \alpha\sqrt{(31-\sqrt{97})/108} \approx 0.4425\,\alpha$ and its height (which is also the constant value we are looking for, see Fig. 22):

$$\rho_p = \frac{90699264\sqrt{93-3\sqrt{97}}}{\left(85-\sqrt{97}\right)^3\left(113+\sqrt{97}\right)^2}\,\frac{\alpha}{X^2} \approx \frac{15}{133}\,\frac{\alpha}{X^2} \approx 0.1128\,\frac{\alpha}{X^2}, \tag{131}$$

which is well approximated (to within 1 %) by $\rho = \alpha/(9X^2)$.

From the theoretically predicted value $X = \sqrt{R}\,\mu = 109/463 = 0.2354$ in the jet central region, we finally derive the value of the correlation coefficient in the middle region of the round jet ($\eta = 0.06 \to 0.15$):

$$\rho = 2.035\,\alpha. \tag{132}$$

With the optimized value $X = 19/80 = 0.2375$ for $\eta \leq 0.15$, we get exactly $\rho = 2.0\,\alpha$. The theoretically predicted value $X = 109/463 = 0.2354$ is very well approximated by $X = 1/3\sqrt{2} = 0.2357$; with $\rho = \alpha/(9X^2)$, it yields exactly the same simple result, $\rho = 2\,\alpha$.

From the predicted range $\alpha = (0.20 - 0.21)$, one gets $\alpha/X^2 = (3.55 - 3.79)$ and finally $\rho = (0.40 - 0.43)$, in excellent agreement with the experimentally observed values (see Fig. 22). A similar result is obtained with the more precise (and valid farther) solutions we have derived for σ_{uv} and σ_v.

Under this form, the predicted value of ρ remains specific of the turbulent jet and of its opening parameter α. However, we have found that this parameter is given by $2\alpha = 1/R^3$ and therefore that it is itself related to the more general quantity $R = \sigma_u/\sigma_v$, which describes the velocity anisotropy. These last quantities characterize all shear flows. In their terms, the correlation coefficient reads:

$$\rho = \frac{1}{R^3} = \frac{\sigma_v^3}{\sigma_u^3} \approx 0.4, \tag{133}$$

which could therefore be valid for all shear flows. We shall study this conjecture in future works.

8 Discussion

8.1 Summary of method and results

We have obtained here a solution for the various characteristics of the turbulent round jet, but in a somewhat complicated way. This comes in a large part from the fact that the new feature brought by the scale-relativity approach is a macroscopic Schrödinger equation in v-space, in which the potential is given by second order derivatives of the pressure, while the pressure is itself one of the unknowns. This situation is improved by one of the solutions of the RANS equations for the turbulent jet, which links the mean pressure to the radial Reynolds stress. It is however also itself one of the unknowns. We have therefore been led to get around this difficulty by using specific methods in order to reveal the otherwise hidden information.

It should however be stressed again that the SR approach to turbulence is not an empirical model but instead a genuine fluid mechanics theory, since the SR-Schrödinger [SRS] equation is but a reformulation of the Navier-Stokes equations (derivated in time then integrated on velocity) under the (K41) fractal and nondifferentiable conditions implied by turbulence [16]. The various results obtained, even if some of them are acquired by numerical integration due to the complexity of some of the equations, are nevertheless solutions of these purely theoretical equations, not fits of experimental data nor fitted parameters of hypothetical closure models.

Let us trace back the origin of these results.

We use two sets of governing equations, the RANS equations for averaged quantities (plus the continuity equation) and a v-Schrödinger equation for the PDF of turbulent fluctuations. Both equations are constructed from the Navier-Stokes equations. The RANS equations result from averaging of the NS equations. The macroscopic v-Schrödinger equation results from time-derivating the NS equations written in v-space, then v-integrating

it in terms of an universal prime integral of motion equations (of the Hamilton-Jacobi type), after having taken into account the scale-relativity effects on differential calculus of the fractality (in v-space) of turbulent fluid particle trajectories. The stationarity of the jet is accounted for by the existence of the time-independent Schrödinger equation.

(1) Our first result is the range of possible values for the parameter $R = \sigma_u/\sigma_v$. It is derived from the identification of the global PDF of turbulent velocity fluctuations as resulting from a combination of harmonic oscillator solutions to the SRS equation. This combination includes the ground level and various excited levels according to the laws of statistical physics. The range of values theoretically obtained, $R = (1.3-1.4)$, results from the mere condition $\sigma_u \geq \sigma_v$ and from the quantization involved by the macroquantum nature of the scale-relativity description.

(2) The value of the jet opening angle is one of the main mysteries of the turbulent jet. It has been remarked by Landau [9, p. 212] that not only one does not know how to calculate the angles emerging in shear flows such as mixing layers and jets, but that "one *cannot* calculate them theoretically".

The scale-relativity solution to this puzzle relies on the existence of a unique constant $\hbar_v$ in the Schrödinger equation and on the fact that it has the same dimensionality as ε, the rate of dissipated energy (also transferred along scales in the turbulent cascade). This energy rate is also just the most fundamental constant in Kolmogorov theory of turbulence. This means that $\hbar_V = k\,\varepsilon$, while we actually expect $k = 1$ [16]. From the well-known expression for ε in terms of velocity dispersion and integral scale, one obtains $\hbar_V = \sigma_v^3/L_v = \sigma_u^3/L_u$, which relates the ratio of axial and radial Reynolds stresses to the spatial anisotropy of the jet.

This results in the relation $2\alpha = 1/R^3$, from which typical values of the jet opening angle $0.2 - 0.22$ are obtained, in agreement with the universally observed ones.

(3) We have theoretically derived an expression for the profile $\sigma_{vo}(\eta)$ of the radial turbulent intensity (and therefore of the pressure). This profile is given by the square root of a cosine function with stretching correction on the edge of the jet. It is a solution of the SRS equation, in which the pressure has been replaced by $-\sigma_v^2$ according to the RANS equation solutions.

(4) The amplitude of the radial turbulent intensity is derived from the second equation coming from the SRS equation. It involves σ_{uv} (derived from the RANS equations) and k_{uvo}, deduced from the pressure profile, which is itself derived from RANS and SRS equations. One obtains $X = \sqrt{\lambda\,\mu} = 19/80$, close to the universal value $\approx 1/4$ measured in numerical and laboratory experiments.

(5) The correlation coefficient of velocities involves σ_{uv}, derived from the RANS equations, and $X = \sqrt{\lambda\,\mu}$, derived from the SRS equation. We theoretically obtain the relation $\rho = 2\alpha$, which yields the value $\rho \approx 0.4$ universlly observed in all shear flows.

It is noticeable that all these results have been obtained without being directly related to turbulent jet trajectory data. The various quantum-type properties predicted by the scale-relativity theory of turbulence have been already validated from data analysis of turbulent flows [16], although it was in counter-rotating von Karman type experiments [35]. This means that our claims concerning the turbulent round jet could be put to the test in

the future from data analysis of trajectories of valid tracers, provided these trajectories be long enough for being able to evidence the predicted quantum-type structures.

8.2 Drawbacks and remaining problems

The theoretical predictions of all these dimensionless parameters have been obtained from solutions of the RANS and v-Schrödinger equations valid in the inner region of the jet, $\eta <\approx 0.12 - 0.16$ and which show full self-consistency.

However, the edge region of the jet ($\eta \approx 0.18 - 0.235$) was more badly known both theoretically and experimentally with "classical" methods. This difficulty partly remains even though adding the scale-relativity approach to the description of the turbulent jet. The k_v equation could be made self-consistent on the jet edge only by using a transformation from coordinates along the mean virtual conic shape of the jet toward curvilinear coordinates describing its true shape (including fluctuations). But, even in this case, the $k_u v$ equation remained contradictory around the jet edge. This could be due to the fact that the basic relation $\bar{p} = -\sigma_v^2$ upon which we rely throughout our whole study becomes wrong around the jet edge, as clearly shown by the experimental measurements of Miller and Comings [1] (for the plane jet). Another possibility would be that the pressure fluctuations become non negligible around the jet edge.

We have not made use of the k_u equation, which depends on an additional unknown constant and was itself not fully consistent. Without a source axial term, it corresponds to a repulsive harmonic oscillator potential, which seems to contradict the experimental evidence.

These problems point out toward the fact that, while our description seems to be fully correct along the radial direction (where $\sigma_v \gg V$), our description of the axial direction (x, U and u), where $U > \sigma_u$ except at the edge, remains partly incomplete or possibly inadequate. The Schrödinger equation in velocity space that we have written seems to be not fully adapted to the axial direction, probably due to its time-dependant character.

Another drawback is the expected existence of offsets in the velocity PDF: namely, the mean velocity of each QHO state is generally not null, as can be seen in Mordant's [35] data (see [16] and Figs. 11, 12, 13). We have given in Eq. (153) the new form taken by the k_v equation when offsets are taken into account. They do not change fundamentally the description, just adding a new corrective terms to the previouly identified ones. Another element which should also be accounted for in a more detailed study to come is the existence of damping on some of the harmonic oscillators (see Fig. 11).

Some open problems remain to be solved: (i) the shape of the axial Reynolds stress profile σ_u differs slightly from the radial one, showing a bump around $\eta \approx 0.05$, i.e. $z = \eta/\alpha \approx 1/4$, which is confirmed in every laboratory and numerical experimental measurements. The origin of this bump (which would be well described by a phase term in the cosine solution), is still unkown; (ii) this question is directly related and equivalent to that of the R radial profile. We have taken R =cst throughout the whole paper, but it shows clearly small variations of order $\pm 10\%$ which are to be understood. (iii) The border of the jet is not an abrupt limit: there is an interface between the typical angle $\alpha \approx 0.2$ and

the turbulent-laminar transition which is found to lie at $\alpha_S = q\,\alpha$ with $q \approx 1.15$. We have suggested a theoretical prediction for this value. Experimental measurements of the jet extension in space [27] yield an end of the jet around this transition, although numerical simulations [6, 28] seem to favor an unlimited Gaussian behavior. This question of the precise concentration profile of turbulent jets in space and of its theoretical prediction will be considered in a forthcoming paper II (Nottale and Lehner, in preparation).

9 Conclusion

We have obtained theoretical solutions of the Navier-Stokes equations for the turbulent round jet, which agree with its experimentally observed properties. This has been achieved in the framework of the theory of scale-relativity [17, 18], applied to turbulence in velocity space [14, 16] .

This theory, which relies on the fact that scales are defined only through their ratios and never in an absolute way, consists of constructing a scale-covariant derivative which accounts for the geometric effects of the non-differentiability of trajectories (and therefore of their explicit scale-dependance) in a fractal medium or space. The first effect is loss of determinism: there is an infinite family of virtual trajectories instead of only one, so that one jumps to a probabilistic description. The second effect is fractality of trajectories: their length becomes explicitly scale-dependent and divergent when the scale-interval tends to zero. The third effect is two-valuedness of derivatives (here of accelerations): this leads one to jump to a theoretical description made in terms of complex numbers.

The equation of dynamics, written as a geodesics equation expressed in terms of this scale-covariant derivative, is then spontaneously integrated under the form of a Schrödinger equation [17, 30]. We have shown [16] that a fully developed turbulent flow satisfies these three conditions in velocity space, as suggested by L. de Montera [14], so that the Navier-Stokes equations can be integrated as a Schrödinger equation acting in v-space. The solution of this v-Schrödinger equation is a wave function whose squared amplitude yields the PDF of velocity fluctuations, from which the velocity variances, i.e. the Reynolds stresses, can be deduced. In other words, this approach solves the closure problem of turbulence, at least in principle.

In the present paper, we have put this new method to the test by applying it to an effective problem, that of the turbulent round jet. The avantages of this choice are that this flow has been widely studied since years and that it has evidenced universal structures characterized in particular by dimensionless numbers, which have been recovered in numerical experiments but were not understood up to now.

The application of the scale-relativity approach to the round turbulent jet has given encouraging results. A theoretical solution has been obtained for the radial Reynolds stress profile which fairly agrees with experimetal data in the central region of the jet. Dimensionless parameters such as the jet opening angle, the relative amplitude of turbulent intensities, the ratio of axial to radial turbulent intensities and the velocity correlation coefficient have been recovered from theory, in a way that is fully consistent with experi-

mental results. Namely, one does not observe precise values, but rather narrow intervals of possible values, corresponding to an approximative universallity [13]. This is exactly what is theoretically expected, since the final result depends on the effective repartition of the macroquantum states, which may vary according to the conditions, among which in particular the Reynolds number.

Appendix A: precise matched solution of the RANS equations for the turbulent jet velocities

The expressions for the $U(\eta)$ and $V(\eta)$ velocity normalized profiles of the matched solution of Sec. 3.2 are:

$$U_a = \frac{1}{(1+2\,(\eta/\alpha)^2)^2}, \quad V_a = \frac{\eta\,(1-2\,(\eta/\alpha)^2)}{2\,(1+2\,(\eta/\alpha)^2)^2}. \tag{134}$$

$$U_b = A_0 + A_1\frac{\eta}{\alpha}, \quad V_b = \frac{K_b}{\eta} + \eta\left(\frac{A_0}{2} + \frac{2A_1}{3}\,\frac{\eta}{\alpha}\right). \tag{135}$$

$$U_c = \frac{\alpha^2}{4} + A_2\left(\frac{\eta}{\alpha} - q\right)^2, \quad V_c = \frac{K_c\,\alpha^2}{\eta} + \frac{\eta}{12}\left(\frac{3\,\alpha^2}{2} + A_2\left(6\,q^2 - 16\,q\,\frac{\eta}{\alpha} + 9\,\frac{\eta^2}{\alpha^2}\right)\right). \tag{136}$$

$$U_d = \frac{\alpha_S^2}{4}, \quad V_d = \frac{\alpha_S^2}{4\eta}\left(K_d + \frac{\eta^2}{2}\right). \tag{137}$$

The matching parameters for this matched solution are given by:

$$A_0 = \frac{125}{108}, \quad A_1 = -\frac{25}{27}\sqrt{\frac{5}{2}}, \quad A2 = -\frac{A_1^2}{4A_0 + 4A_1 q - q^2\alpha^2}, \quad A3 = 4A_0 + 2A_1 q - q^2\alpha^2, \tag{138}$$

$$y_{ab} = \frac{\alpha}{\sqrt{10}}, \quad y_{bc} = -\frac{A_3}{2A_1}\alpha, \quad y_{cd} = \alpha_S = q\,\alpha, \tag{139}$$

$$K_c = -\frac{1}{192A_1^4}(A_1^2A_3^2A_4 - 9A_2A_3^4 + 192A_1^4K_b - 32A_1A_2A_3^3q), \tag{140}$$

where

$$A_4 = 24A_0 - 16A_3 - 24A_2q^2 - 6q^2\alpha^2. \tag{141}$$

$$K_b = \frac{1}{6^4}, \quad K_d = \frac{12K_c - A_2q^4}{3q^2}. \tag{142}$$

The resulting functions are compared to experimental data in Figs. 23, 24 and 25.

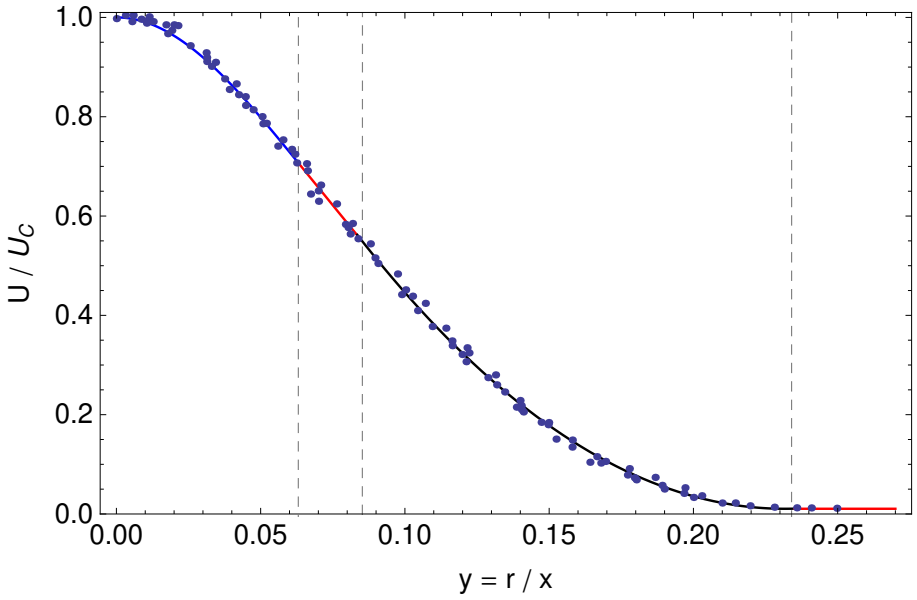

Figure 23: Precise solution of the RANS equations for the mean axial velocity profile $U(\eta)$ (where $\eta = r/x$ is the scaled radial distance) normalized to the centerline velocity U_C (continuous curve). This solution is obtained by matching the central solution and its derivative to intermediate and boundary solutions, then to the exact solution of the NS equations for the exterior laminar flow (see Sec. 3.2). The vertical dashed lines show the matching points between the different solutions. This theoretical profile is compared with renormalized fits of experimental data (points) from Hussein et al [7] and Panchapakesan and Lumley [19].

Appendix B: second matched solution of the RANS equations

This new solution (Sec. 3.3) is made of the central solution with constant turbulent viscosity already given in Sec. 3.2 and Appendix A, i.e. U_a, V_a, $\sigma_{uva} = -U_a V_a + \alpha z\, U_a^2$ (where $z = \eta/\alpha$). We give here only the pure radial profiles, normalized by the centerline axial velocity U_C, without the axial g/x dependence:

$$U_a = \frac{1}{(1+2\,z^2)^2}, \quad V_a = \alpha \frac{z\,(1-2\,z^2)}{2\,(1+2\,z^2)^2}, \quad \nu_{Ta} = \alpha^2/4. \tag{143}$$

It is matched at $\eta_k = k\,\alpha$ with a quadratic solution:

$$U_e = B_0 + B_1 z + B_2 z^2, \quad V_e = \alpha \left(\frac{K_e \alpha}{z} + \frac{B_0}{2} z + \frac{2B_1}{3} z^2 + \frac{3B_2}{4} z^3 \right), \tag{144}$$

$$\nu_{Te} = -\alpha^2 \, \frac{(B_0 + B_1 z + B_2 z^2)(-12K_e + 6B_0 z^2 + 4B_1 z^3 + 3B_2 z^4)}{12 z (B_1 + 2B_2 z)}, \tag{145}$$

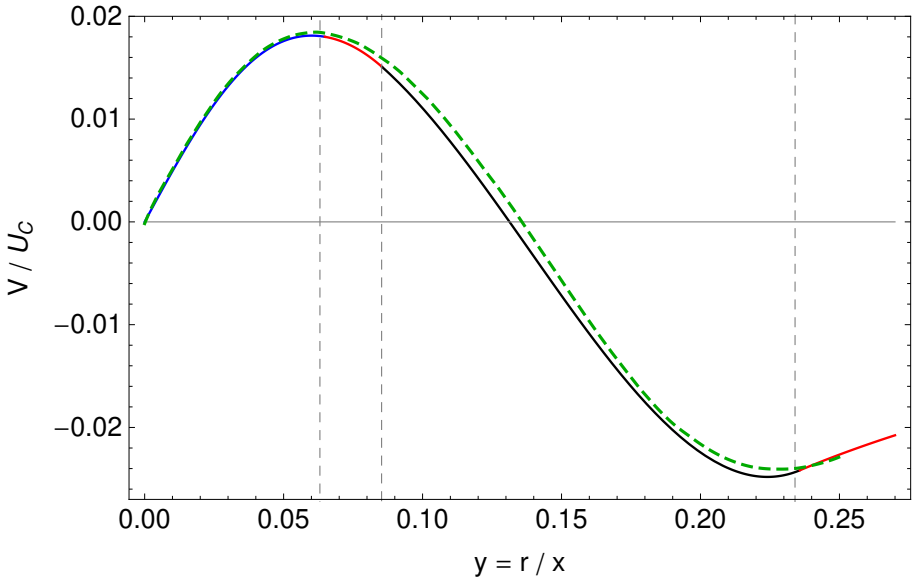

Figure 24: Precise solution of the RANS equations for the mean radial velocity profile $V(\eta)$ normalized to the centerline velocity U_C (continuous curve), derived from $U(\eta)$ (Fig. 23) and the continuity equation. The vertical dashed lines show the matching points between the different solutions. This profile is compared with the mean experimental data (green curve) from Hussein et al [7] and Panchapakesan and Lumley [19].

The matching is now performed by ensuring the continuity of U, U' and now also U'', so that the quadratic solution is fully determined from the mere inner solution. This allows us to obtain a theoretical prediction for the behavior of the velocity profile at the edge of the jet and to compare it with the laminar flow exterior to the jet.

The matching parameters of this solution are:

$$B_0 = \frac{1+8k^2+60k^4}{(1+2k^2)^4},\ B_1 = -\frac{96k^3}{(1+2k^2)^4},\ B_2 = \frac{4(10k^2-1)}{(1+2k^2)^4},\ K_e = \frac{2k^6(1-2k^2)}{(1+2k^2)^4}. \quad (146)$$

The corresponding predicted radial profile of the turbulent viscosity is shown in Fig. 6 and compared with those derived from HCG and PL experimental data.

Appendix C: improved solution for pressure and Reynolds stress

Stretched cosine solution The corrective term in the differential equation for mean pressure $\bar{p}$ and radial Reynolds stress $\sigma_v^2 = -\bar{p}$ can be written in terms of a power series $w(z) = 1 + w_2 z^2 + w_4 z^4 + \mathcal{O}[z^6]$. Since the cosine solution holds when $z \to 0$, we are led

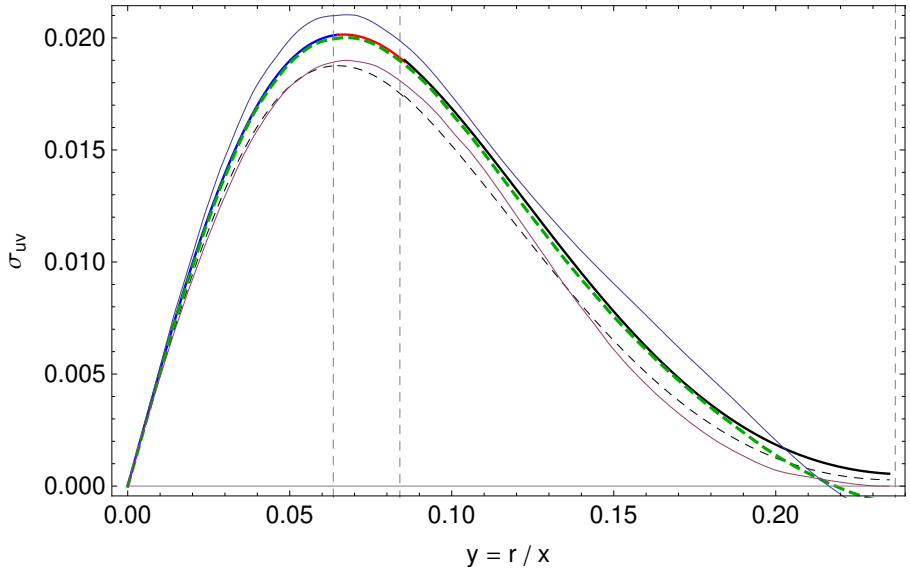

Figure 25: Precise solution of the RANS equations for the Reynolds shear stress profile $\sigma_{uv}(\eta)$ normalized by the centerline velocity U_C^2 (continuous curve), derived from $U(\eta)$ (Fig. 23) and $V(\eta)$ (Fig. 24) by the equation $\sigma_{uv} = -U\,V + \eta\,(U^2 + \sigma_u^2 - \sigma_v^2)$. The vertical dashed lines show the matching points between the different solutions. This profile is compared with experimental data from Hussein et al [7] and Panchapakesan and Lumley [19] (thin curves) and their mean (green dashed curve). The black dashed curve shows the shear stress approximation $\sigma_{uv} = -U\,V + \eta\,U^2$.

to look for an improved solution of the form:

$$\sigma_v^2 = \mu^2\,\cos\left(\frac{\sqrt{3}\,z}{1 + a_2\,z^2 + a_4 z^4}\right). \tag{147}$$

The identification of the z^2 and z^4 coefficients yields:

$$w_2 = -12\,a_2, \quad w_4 = -30\,a_4 - 6\,a_2 + 45\,a_2^2. \tag{148}$$

We have seen that the pure cosine solution remains valid up to the 3/4th of the jet, so that $a_2 = 0$, yielding $w_2 = 0$. This leads us to write the pressure / Reynolds stress equation as:

$$\partial_z \partial_z \sigma_v^2 + 3\,\sigma_v^2\,(1 + w_4\,z^4) = 0. \tag{149}$$

We have constructed an analytical solution to this equation by numerically solving it, then by showing that the corresponding order z^4 expression (which is a stretching of the cosine solution toward the jet edge) is an excellent approximation of this solution across the whole jet:

$$\sigma_v^2 = \mu^2\,\cos\left(\frac{\sqrt{3}\,z}{1 + a_4\,z^4}\right). \tag{150}$$

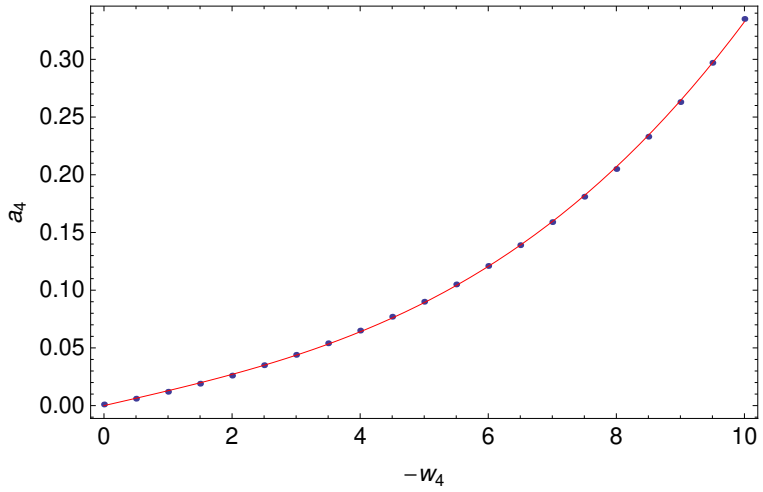

Figure 26: Relation between the coefficient w_4 describing the z^4 corrective term in the k_v equation and the coefficient a_4 in its stretched cosine solution, obtained by optimization of the difference between the numerical and analytical solutions over the whole jet ($z = 0$ to 1.2). The red line is the least-square fit of this relation by a cubic polynomial (Eq. 152), which is statistically highly significant (Student variable $t_{St} = 140$). The predicted value is $a_4 = 0.18$ (see Sec. 6), corresponding to $w_4 = -7.5$.

From the above relations between coefficients, we find

$$w_4 = -30\, a_4. \tag{151}$$

Actually this stretched cos solution remains excellent, not only in the central region, but also for the whole jet (see Fig. 17), provided the relation between a_4 and w_4 includes a non-linear contribution. We have established this relation by least-square optimization of the difference between the analytical and numerical solution to the k_v equation (Fig. 26). We find the following fit:

$$a_4 = -(0.0127 \pm 0.0001)\, w_4 \left(1 + \left(\frac{w_4}{7.86}\right)^2\right). \tag{152}$$

The standard error of the difference between the numerical and analytical solutions is less that 0.01. The theoretical prediction $a_4 = 0.18$ (see Sec. 6) corresponds to $w_4 = -7.5$.

Stretching from curvilinear coordinates There is however a drawback to this result. The function $-(\partial_z \partial_z \sigma_v^2)/\sigma_v^2$ computed from this stretched cosine solution becomes negative for $z >\approx 0.6$ while its expression from the corrective terms, $(1+\rho_F^2/R_F^2)(1+h)^{-2}(1-\rho_F^2)^{-2}$ is always positive. One can also generalize this expression by accounting for possible non negligible offsets of the quantum harmonic oscillator PDFs, which are not always centered on $v = 0$ (see [16] and Figs. 11, 12, 13). This results in a new contribution σ_v^c additional to the purely quantum contribution to the velocity fluctuation σ_v^Q, yielding $\sigma_v^2 = \sigma_v^{Q2} + \sigma_v^{c2}$.

Setting $m = \sigma_v^c/\sigma_v$ (which remains ≤ 1), the full corrective term in the k_v equation becomes

$$1 + w = \frac{(1 + \rho_F^2/R_F^2)}{(1+h)^2(1-\rho_F^2)^2(1-m^2)^2}, \tag{153}$$

and it remains positive. We conclude that the stretched cosine solution is valid only for $z <\approx 0.6$, i.e. $\eta <\approx 0.12$ in the theoretical description used up to now although it fits the experimental data down to the jet edge.

The origin of the fair agreement of experimental data with the stretched cosine solution in the outer part of the jet must therefore be searched for, at least partly, in another mechanism. We suggest that it is linked to the true shape of the turbulent jet boundary. Its conic shape is only a virtual average, while the true jet shows important fluctuations with respect to this cone. Therefore, the dimensionless variable $\eta = r/x$, in function of which the pressure and Reynolds stress profiles are expressed, does not fully account for the effective, more complicated shape of the jet, particularly around its edge.

The suggestion to use transformed variables for better implementing the self-similarity of the turbulent jet has already been made by Batchelor [41]. He has defined a compensated time and a compensated Lagrangian velocity which exhibits statistically stationary Lagrangian dynamics. The idea of this stationarisation is to compensate the effect of Eulerian inhomogeneity on the Lagrangian variables to retrieve a Lagrangian dynamics which becomes independent of the initial position and statistically stationary [42].

Let $X_a = \sqrt{x^2 + r^2}$ be the axial coordinate in a spherical coordinate system and $\tilde{X}_a$ the corresponding curvilinear coordinate along the true shape of the jet , which accounts for the turbulent fluctuations. From it one can define $\tilde{x}^2 = \tilde{X_a}^2 - r^2$. Strictly speaking, $\tilde{X}_a$ fluctuates in a time dependent way, but we are interested here only in the mean increase $\tilde{x}/x \approx \tilde{X}_a/X_a$, which is stationary. We suggest that the transformation $\eta \to Y = \eta/(1 + a_4\,(\eta/\alpha)^4)$ is just the result of replacing $\eta = r/x$ by $Y = r/\tilde{x} = \eta \times (x/\tilde{x})$ in order to account for the true shape of the jet.

This suggestion is supported by the variation in function of η of the rate of axial velocities going backward due to the turbulent fluctuations. It depends on the ratio σ_u/U, which is observed to vary as $\sigma_u/U \approx \lambda(1 + 10z^4)$. This rate is found to be

$$\tau = \frac{1}{2}\left(1 + \mathrm{erf}\left(\frac{U}{\sigma_u\sqrt{2}}\right)\right) \tag{154}$$

and the length increase can be approximated by

$$\tilde{x}/x = (1+\tau)^{1/2}. \tag{155}$$

We find an excellent fit of the radial profile of this quantity by the function $(1+\tau)^{1/2} = 1 + 0.175\,z^4$ down to $\eta \approx 0.21$, which clearly supports our interpretation of the stretching origin.

Appendix D: improved solution for the Reynolds stress amplitude

Stress amplitude from solutions valid up to larger radial distance An improved solution for the turbulent fluctuation amplitude can be obtained from the equation $G(\eta) = G_s(\eta)$, where we recall that $G_s(z) = \exp(-0.5z^2/s^2)$ and

$$G(z) = \frac{F(z) - X}{1/2 - X}, \tag{156}$$

with

$$F(z) = \frac{1}{\alpha}\sqrt{\frac{6\sigma_{uvo}}{k_{uvo}}}. \tag{157}$$

The improved function $F(z)$ is constructed from using $\sigma_{uv} = \sigma_{uvtot}$, obtained from matching precise solutions of the RANS equations (see Sec. 3.2 and Appendix A); and $p_o = p_{os}$, the stretched cosine solution to the k_v QHO equation, inserted in $k_{uvo} = -(3\partial_z p_o + z\partial_z\partial_z p_o)$.

The free parameters of these functions, X, s and a_4, are obtained as numerical solutions of the equation $G(\eta) = G_s(\eta)$ by a least-square optimization (while the α dependence is found to be very small). We get for $\eta \leq 0.14$:

$$X = 0.2370 \pm 0.0003, \quad s = 0.3225 \pm 0.0004, \quad a_4 = 0.180 \pm 0.003, \tag{158}$$

where the residual fluctuation takes the very small value $\sigma_\xi = 0.0023$.

From this theoretical prediction of $a_4 = 0.18$, we deduce the value of the parameter w_4 in the z^4 correction to the k_v equation (see Sec. 5.6), $w_4 = -7.5$. This result can be used for obtaining a more complete estimate of the various corrective terms in the k_v and k_{uv} equations (see Appendix E).

The standard deviation σ_ξ of the residual differences between G and G_s is extremely small, only 0.2% of their amplitude (they vary from 0 to 1), which means that the function $G(\eta)$ is indeed totally indiscernable from a Gaussian function, as can be seen in Fig. 18. Such a remarkable agreement may be a consequence of the central limit theorem or, equivalently, result from the laws of statistical physics.

Actually, with slightly different optimized parameters, the fully Gaussian character of $G(\eta)$ can be established beyond the 3/4th of the jet, up to $\eta = 0.162$. In this case, the function $F(\eta)$ has even entered into the experimentally observed range for μ, $(0.185 - 0.217)$ [19, 7], as can be seen in Fig. 20.

We compare in Fig. 27 the two successive approximations to the function $F(\eta)$ that we have obtained. The two optimized Gaussian laws and the two asymptotic limits which define $X = \sqrt{\lambda\,\mu} \approx 0.2375$ are very close one to each other, which supports the validity of this analysis. Beyond $\eta = 0.16$, one enters in the edge region of the jet, which is more badly defined, both experimentally and theoretically, and in which the function $F(\eta)$ is multiplied by the unknown function $1 + h(\eta)$, where, contrarily to what happens in the jet center case, $h(\eta)$ is no longer vanishing.

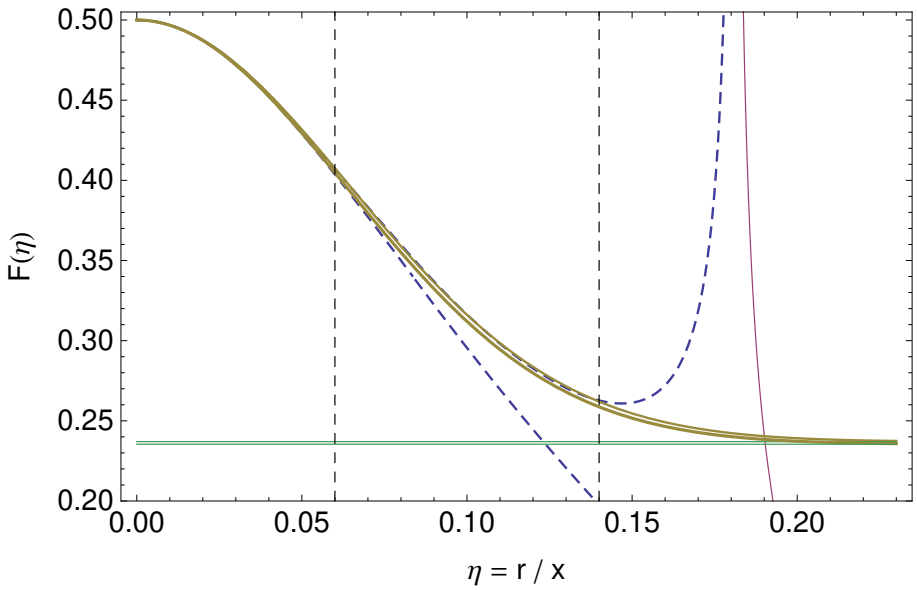

Figure 27: Successive approximations of the function $F(\eta) = \sqrt{6\,\sigma_{uv}/k_{uvo}}/\alpha$ (blue dashed curves), compared to the Gaussian law optimized for each of them. The two laws are calculated with $\sigma_{uv} = \sigma_{uvtot}$. The first function F is computed using the theoretical solution $p_o = -\cos(\sqrt{3}\,\eta/\alpha)$ valid in the central region of the jet and yields a Gaussian law up to $\eta \approx \alpha/\sqrt{10}$ (dashed vertical line to the left). The second function F is computed using the better solution $p_o = -\cos(\sqrt{3}\,Y/\alpha)$, with $Y = \eta/(1 + 0.18(\eta/\alpha)^4)$ and yields a pure Gaussian law up to $\eta \approx 0.14$ (second vertical dashed line). These solutions yield very close values for the final (asymptotic) values of X (green horizontal lines).

Solution for the pressure profile valid up to the jet edge One can see in Fig. 27 that beyond their domain of validity, the two approximative functions $F(\eta)$ depart from the Gaussian law with a negative then positive difference. This is typical of what happens when comparing a function to its successive power series approximations, and suggests that the Gaussian law may still be correct up to even larger radial distances.

In a previous section, we have obtained an analytical solution for the pressure in the central region of the jet, using a combination of the k_v and k_{uv} equations and the centre solution $\sigma_{uv} = \sigma_{uva}$ (corresponding to constant turbulent viscosity). We shall now use the full k_{uv} second order differential equation:

$$3\,\partial_\eta\, p_o + \eta\,\partial_\eta\partial_\eta\, p_o = \frac{6\,\sigma_{uv}}{\alpha^2\,(X + G_s(\eta)\,(\frac{1}{2} - X))^2}. \tag{159}$$

We have solved numerically this equation for the precise solution $\sigma_{uv} = \sigma_{uvtot}$ and for the previously optimized values of the parameters (Eq. 158).

The result is given in Fig. 28. It is now indistinguishable from the stretched cosine profile (and then from the experimentally observed profile by Hussein et al [7]), up to the full average opening angle of the jet $\eta = \alpha \approx 0.2$. It departs from it only in the region of

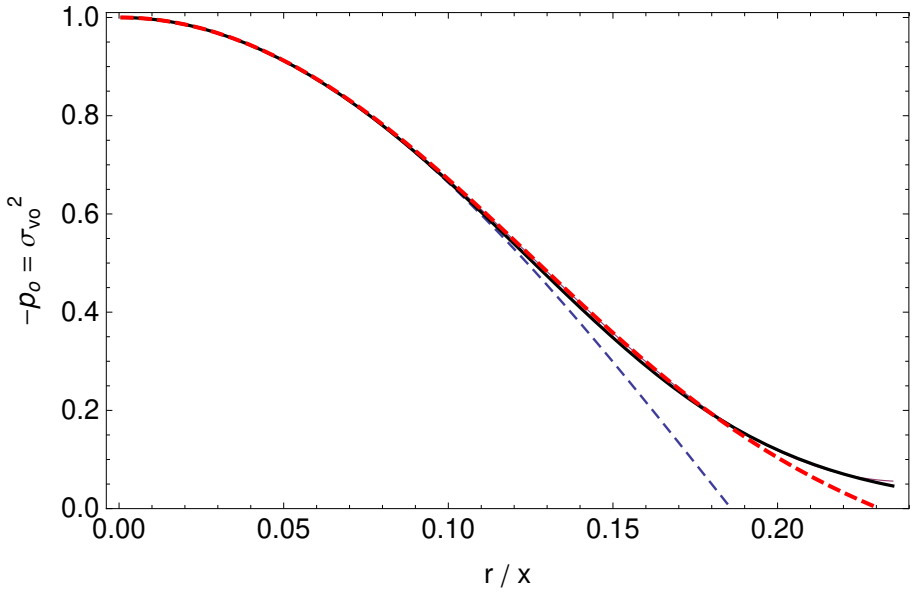

Figure 28: Mean pressure profile in function of the scaled radial distance $\eta = r/x$, derived from the equation $F(\eta) = X + G_s(\eta)\left(\frac{1}{2} - X\right)$ (red dashed curve), compared with the approximate solution $-p_o = \cos(\sqrt{3}\,\eta/\alpha)$ (blue dashed curve), the stretched cosine solution $-p_o = \cos(\sqrt{3}\,Y/\alpha)$ with $Y = \eta/(1 + 0.18(\eta/\alpha)^4)$ (magenta curve), and the experimental curve observed by Hussein et al [7] (black curve, almost identical to the magenta curve). The theoretical and experimental profiles now agree across almost the entire jet, up to $\eta \approx 0.2$.

the interface between the turbulent and the laminar flow, ($\eta = \alpha \to \eta = q\,\alpha \approx 0.235$, the final turbulent-laminar transition). In this region, the experimental data is compatible with the expected full isotropy ($\sigma_u = \sigma_v$) but the precise profile of $-p_o \approx \sigma_v^2 \approx \sigma_u^2$ is badly known (with a relative factor of 3 between the various measurements). Recall also that $\alpha_S = q\,\alpha$ is actually only an average opening angle for a virtual conic shape of the jet, since the true frontier is highly variable, this meaning that there is no real stationary solution around the jet boundary.

Appendix E: estimate of the corrective terms in the k_v equation

The full solution for the Reynolds stress profile $\sigma_v^2(\eta)$ has been obtained without accounting in detail for the corrective terms involving the functions $\rho_F(\eta)$, $R_F(\eta)$ and $h(\eta)$. One may improve this situation and gain some knowledge about their behavior by taking the ratio of the k_V and k_{uv} equations, in which the corrective term $H/H_0 = (1+h)^{-2}$ is cancelled. Setting $K = -k_{uv}/k_v$, one obtains:

$$\frac{\rho_F\,(1 + R_F^2)}{R_F\,(R_F^2 + \rho_F^2)} = K. \tag{160}$$

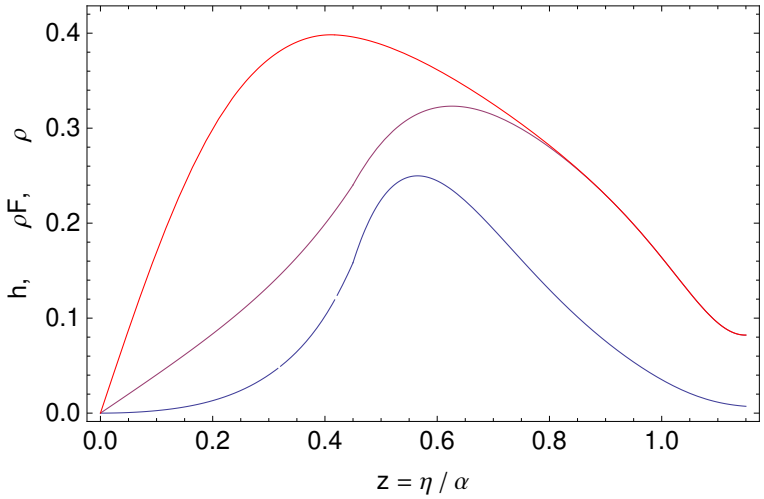

Figure 29: Example of radial profiles obtained for the corrective terms $h(z)$ (lower blue curve) and $\rho_F(z)$ (intermediate magenta curve) under the approximation $R_F(z) \approx 1$ and for $X = 19/80$. The upper red curve is the theoretically obtained radial profile for the correlation coefficient ρ. These expressions account for the various known constraints at the jet center and edge, in particular $\rho_F = \rho$ around the jet edge. They are constructed to yield $F = X + (0.5 - X)G_s$, where G_s is Gaussian (see text).

This equation can be solved in terms of a function $\rho_F(R_F)$:

$$\rho_F = \frac{1 + R_F^2 - \sqrt{1 + 2R_F^2 + (1 - 4K^2)R_F^4}}{2K R_F}. \tag{161}$$

Reversely, the solution can be expressed as $R_F(\rho_F)$. Setting:

$$A = K\,\rho_F \sqrt{27K^2 + 2(2 - 9K^2)\rho_F^2 - K^2\rho_F^4(1 - 4K^2)}, \tag{162}$$

and

$$B = 2^{-1/3}\,(27K^2\rho_F + (2 - 9K^2)\rho_F^3 + 3\sqrt{3}A)^{1/3}, \tag{163}$$

one finds:

$$R_F = \frac{1}{3K}\left(\rho_F + \frac{1 - 3K^2}{B} + B\right). \tag{164}$$

The corrective term to the k_v equation writes:

$$1 + w = \frac{1 + \rho_F^2/R_F^2}{(1 + h)^2(1 - \rho_F^2)^2}. \tag{165}$$

Knowing that $H_0 = 3/\alpha^2$, the k_{uv} equation writes (in terms of pure profiles normalized to unity):

$$k_{uvo} = 3\,\partial_\eta\sigma_{vo}^2 + \eta\,\partial_\eta\partial_\eta\sigma_{vo}^2 = \frac{3}{\alpha^2}\,\sigma_{vo}^2\,\frac{(1 + R_F^2)\,\rho_F}{R_F^3\,(1 + h)^2\,(1 - \rho_F^2)^2}. \tag{166}$$

Another relation derives from the solution to the k_{uv} equation constructed from a Gaussian function:

$$\frac{(1+R_F^2)}{2\,R_F^3}\frac{\rho_F}{(1-\rho_F^2)^2} = \rho\,(1+h)^2\left(1+\frac{21s^2}{4-21s^2}\,G_s\right)^{-2}, \tag{167}$$

with $G_s = \exp(-\frac{1}{2}(\frac{\eta}{s\,\alpha})^2)$.

Since the functions $\rho_F(\eta)$, $R_F(\eta)$ and $h(\eta)$ are expected to vary slowly across the jet radius, we can give them a polynomial form, valid in the center region of the jet $z = \eta/\alpha \ll 1$. We set to order z^4:

$$\rho_F = 2\,\alpha\,z\,(1+a_F z^2+b_F z^4), \quad R_F = 1+A_F z^2+B_F z^4, \quad 1+h = 1+h_2 z^2+h_4 z^4. \tag{168}$$

The relation between R_F and ρ_F implies the following relations between the coefficients of their power series, (valid in the jet central region):

$$A_F = \frac{1}{2}a_F - \frac{3}{8} - 2\alpha^2, \quad B_F = \frac{1}{2}\,b_F - \frac{261}{1280} - 9\,a_4 - a_F\left(\frac{9}{32}+\frac{7}{2}\alpha^2\right) - \frac{1}{16}\,a_F^2 - \frac{3}{8}\alpha^2 - \alpha^4, \tag{169}$$

while the k_{uv} equation yields:

$$h_2 = 6\,\alpha^2, \quad h_4 = 15\,a_4 + \alpha^2\left(\frac{3}{2}+10\,a_F+30\,\alpha^2\right). \tag{170}$$

Around the edge of the jet, i.e. $z \approx 1$, up to the turbulent-laminar transition at $z = q \approx 1.15$, we know several constraints:

- while there is no longer any Schrödinger equation for $z > q$ in the laminar region, we expect the existence of an intermediate region $z_0 < z \approx 1 < q$ in which the various conditions underlying the emergence of a v-Schrödinger equation are fulfilled, while the turbulent energy remains so low that only the ground state solution can manifest itself. Therefore, in this region, $\rho_F = \rho$.

- the function $h(z)$ is built from the parameter $H = H_0(1+h)^{-2}$ which is defined as $H = 1/(4g_v^4 L_v^2)$, where $g_v = \sigma_{vF}/\sigma_v$ and L_v is an integral length in the radial direction (normalized according to the x self-similarity). In the intermediate region where only the ground state solution exists, we expect $\sigma_{vF} = \sigma_v$ so that $g_v = 1$ and then $H = 1/(4L_v^2)$. The L_v profile along the radial direction has been experimentally determined by Wygnanski and Fiedler [24] to be 0.015 in the jet central region and to reach 0.03 around its edge. Then we find $h_B = -0.48$ at the turbulent-laminar transition, while it increases toward the interior of the jet, therefore reaching $h_B \approx 0$ around $z \approx 1$.

- from isotropy around the jet edge, we expect $R_F = \sigma_{uF}/\sigma_{vF} = R = 1$ for $z \approx q$. Experimental data support in a fair way this isotropy: one observes $\sigma_u = \sigma_v$ within uncertainties beyond $z \approx 0.9$ (see Figs. 2 and 3).

Additional constraints across the whole jet are: $0 < \rho_F < 1$ from its very nature of correlation coefficient and $R_F \geq 1$ from the constraint $\sigma_u \geq \sigma_v$ specific to the jet.

We have combined these various constraints into possible solutions for $\rho_F(z)$, $R_F(z)$ and $h(z)$ valid across the whole jet and yielding the Gaussian behavior for the function

$F(z)$, namely:

$$F = X + \left(\frac{1}{2} - X\right) G_s = \sqrt{\frac{6\,\sigma_{uv}}{\alpha^2\,k_{uvo}}} = X\,\sqrt{\frac{\rho}{\rho_F}}\,\left(\frac{2\,R_F^3}{1+R_F^2}\right)^{1/2}\,(1-\rho_F^2)\,(1+h). \quad (171)$$

The combination of these various constraints yield $a_F \approx 1$ and $4.5 < b_F < 13$. We find that R_F remains close to 1 throughout the jet radial distance. This allows us to take the approximation $R_F = 1$, which yields $a_F = 0.91$ and $b_F = 4.5$ in the central region. In the outer part of the jet we have written the fundamental level correlation coefficient as $\rho_F = \rho\,(1 + f_4\,(z-1)^4)$ owing to their equality around the jet edge. Using the identification of the various forms of the solution with a Gaussian function given in Eq. (171) and assuming it to be valid across the whole jet, we can calculate the function $h(z)$ in the center and edge regions, and finally match the inner and outer solutions. We find $f_4 = -4.3$ for a matching point at $z_0 = 0.45$.

We give in Fig. 29 an example of the typical behavior obtained in this way for the corrective terms, using the theoretical solutions $X = 19/80$, $\sigma_{uv} = \sigma_{uvtot}$ and $\sigma_{vo}^2 = -p_o = \cos[\sqrt{3}\,z/(1 + a_4 z^4)]$ with $a_4 = 0.18$ for calculating $\rho(z) = -\sigma_{uv}/(X^2 p_o)$. They remain $\ll 1$, therefore justifying the various approximations which have been initially taken (then relaxed). However, we have not been able to obtain a fully self-consistent solution around the jet edge, since a sign problem remains in the k_{uv} equation in the outer region of the jet (or, in other words, one cannot fulfill all the constraints together). This is discussed in Sec. 8.

References

[1] D.R. Miller & E.W. Comings, "Static pressure distribution in the free turbulent jet", J. Fluid Mech., **3**(1), 1 (1957).

[2] S.B. Pope, *Turbulent Flows*, Cambridge University Press (2000).

[3] H. Tennekes & J.L. Lumley, *A first course in turbulence*, MIT Press, Cambridge, Massachussetts (1972).

[4] U. Frisch, *Turbulence: The Legacy of A.N. Kolmogorov* (Cambridge University Press, 1995).

[5] B. J. Boersma, G. Brethouwer and F. T. M. Nieuwstadt, "A numerical investigation on the effect of the inflow conditions on the self-similar region of a round jet", Physics of Fluids **10**, 899 (1998)

[6] C.L. Lubbers, G. Brethouwer, B.J. Boersma,"Simulation of the mixing of a passive scalar in a round turbulent jet", Fluid Dynamics Research **28** 189 (2001).

[7] H.J. Hussein, S.P. Capp & W.K. George, "Velocity measurements in a high-Reynolds-number, momentum-conserving, axisymmetric, turbulent jet", J. Fluid Mech., **258**, 31 (1994).

[8] B. Cushman-Roisin,"Turbulent jets", Environmental Fluid Mechanics, 1-9 (2014).

[9] L. Landau and E. Lifchitz, *Fluid Mechanics* (Pergamon Press, Oxford, 1980).

[10] L. Landau, "Submerged fluid jet", in L. Landau and E. Lifchitz, *Fluid Mechanics* (Pergamon Press, Oxford, 1980), par. 23,"Exact solutions of the motion equations of a viscous fluid".

[11] V. I. Yatseyev, "On a class of exact solutions of the equations of motion of a viscous fluid", Technical memorandum No. 1349, NACA (1953).

[12] H.B. Squire, "The round laminar jet", The Quarterly Journal of Mechanics and Applied Mathematics, 4(3), 321 (1951).

[13] W.K. George, "The self-preservation of turbulent flows and its relation to initial conditions and coherent structures", Advances in turbulence, **3973**, 39 (1989).

[14] L. de Montera, "A theory of turbulence based on scale relativity", arXiv:1303.3266 (2013).

[15] L. Nottale, "Relativity of Scales, Fractal Space-Time and Quantum Potentials", in *Space-Time Geometry and Quantum Events*, I. Licata Ed., Chap. 5 (2014).

[16] L. Nottale and T. Lehner, "Turbulence and scale relativity", Phys. Fluids **31**, 105109 (2019).

[17] L. Nottale, *Fractal Space-Time and Microphysics: Towards a Theory of Scale Relativity* (World Scientific, Singapore,1993).

[18] L. Nottale *Scale Relativity and Fractal Space-Time: a New Approach to Unifying Relativity and Quantum Mechanics* (Imperial College Press, London, 2011).

[19] N. R. Panchapakesan & J.L. Lumley, "Turbulence measurements in axisymmetric jets of air and helium. Part 1. Air jet", J. Fluid Mech. **246**, 197 (1993).

[20] C. Bailly & G. Comte Bellot, *Turbulence*, Springer, Heidelberg (2015).

[21] C. Bailly, "Physics of turbulent flows", Course given at Ecole Centrale de Lyon (2021).

[22] M. Uhlmann, "Fluid mechanics of turbulent flows", Karlsruher Institut für Technologie, Lecture 4, "Free shear flows" (2011).

[23] A.N. Kolmogorov, "The local structure of turbulence in incompressible viscous fluid for very large Reynolds numbers", C. R. Acad. Sci. URSS **30**, 301 (1941).

[24] I. Wygnanski & H. Fiedler, "Some measurements in the self-preserving jet", J. Fluid Mech., **38**(3), 577 (1969).

[25] M.M. Gibson, "Spectra of turbulence in a round jet", J. Fluid Mech. **15**, 161 (1963).

[26] H. Schlichting, "Laminare Strahlenausbreitung", Z. Angew. Math. Mech. 13, 260-263 (1933).

[27] D.R. Dowling & P.E. Dimotakis, "Similarity of the concentration field of gas-phase turbulent jets", J. Fluid Mech. **218**, 109 (1990).

[28] A. Aiyer and C. Meneveau,"Coupled population balance and large eddy simulation model for polydisperse droplet evolution in a turbulent round jet", Phys. Rev. Fluids **5**, 114305 (2020).

[29] L. Nottale and M.-N. Célérier, "Derivation of the postulates of quantum mechanics from the first principles of scale relativity", J. Phys. A: Math. Theor. **40**, 14471 (2007).

[30] L. Nottale, M.N. Célérier & T. Lehner, "Non-Abelian gauge field theory in scale relativity", J. Math. Phys. **47**, 032303 (2006).

[31] L. Nottale, "Generalized quantum potentials", J. Phys. A: Math. Theor. **42**, 275306 (2009).

[32] M.N. Célérier & L. Nottale L."Electromagnetic Klein-Gordon and Dirac Equations in Scale Relativity", Int. J. Mod. Phys. A25, 4239 (2010).

[33] B. Mandelbrot, *The Fractal Geometry of Nature* (Freeman, San Francisco, 1982).

[34] L. Landau and E. Lifchitz, *Quantum Mechanics: non relativistic theory* (Elsevier, 2013).

[35] N. Mordant, "Lagrangian measurements in turbulence", Ph. D. Thesis, Ecole Normale Supérieure de Lyon (2001).

[36] N. Mordant, P. Metz, O. Michel and J.F. Pinton, "Measurement of Lagrangian Velocity in Fully Developed Turbulence", Phys. Rev. Lett. **87**, 214501 (2001).

[37] N. Mordant, J. Delour, E. Lévèque, O. Michel, A. Arnéodo, and J.-F. Pinton, "Lagrangian Velocity Fluctuations in Fully Developed Turbulence: Scaling, Intermittency, and Dynamics", Journal of Statistical Physics **113**, 701 (2003).

[38] N. Mordant, E. Lévèque and J.-F. Pinton, "Experimental and numerical study of the Lagrangian dynamics of high Reynolds turbulence", New Journal of Physics **6**, 116 (2004).

[39] G.A. Voth, A. La Porta, A.M. Crawford, J. Alexander and E. Bodenschatz, "Measurement of Particle Accelerations in Fully Developed Turbulence", J. Fluid Mech. **469**, 121 (2002) [arXiv: physics/0110027].

[40] L. Landau and E. Lifchitz, *Statistical Physics* (Pergamon Press, Oxford, 1987).

[41] G. K. Batchelor, "Diffusion in free turbulent shear flows", J. Fluid Mech. **3**, 67 (1957).

[42] B. Viggiano et al., "Lagrangian diffusion properties of a free shear turbulent jet", J. Fluid Mech. **918**, A25 (2021)